Moment-based Feature Extraction in SAR Images for Ground Vehicle Recognition

Pouya Bolourchi

Submitted to the
Institute of Graduate Studies and Research
in partial fulfillment of the requirements for the degree of

Doctor of Philosophy
in
Electrical and Electronic Engineering

Eastern Mediterranean University
December 2017
Gazimağusa, North Cyprus

Approval of the Institute of Graduate Studies and Research

Assoc. Prof. Dr. Ali Hakan Ulusoy
Acting Director

I certify that this thesis satisfies the requirements as a thesis for the degree of Doctor of Philosophy in Electrical and Electronic Engineering.

Prof. Dr. Hasan Demirel
Chair, Department of Electrical and Electronic Engineering

We certify that we have read this thesis and that in our opinion it is fully adequate, in scope and quality, as a thesis of the degree of Doctor of Philosophy in Electrical and Electronic Engineering.

Prof. Dr. Hasan Demirel
Co-Supervisor

Prof. Dr. Şener Uysal
Supervisor

Examining Committee

1. Prof. Dr. Gözde Bozdağı Akar
2. Prof. Dr. Hasan Demirel
3. Prof. Dr. Fikret S. Gürgen
4. Prof. Dr. Hüseyin Özkaramanlı
5. Prof. Dr. Şener Uysal
6. Assoc. Prof. Dr. Önsen Toygar
7. Asst. Prof. Dr. Rasime Uyguroğlu

ABSTRACT

Synthetic Aperture Radar (SAR) imaging produces high-resolution images, which are generated independent of any weather condition and solar illumination. These advantages over optical image acquisition systems make the SAR images a reliable source of information. One of the major applications of SAR images is automatic target recognition (ATR) of moving and/or stationary ground vehicles. SAR-ATR images can be characterised to contain background, target, and shadow. There are many problems associated with SAR-ATR image data. Firstly, they have noise especially in the background caused by the interference of returning waves at the transducer aperture. Background removal isolates the foreground, which generates the region of interest (ROI). Other problems are the positional variations of the target, due to changing angles of airborne radar signals, which are generating images that are not scale, translation and rotation-invariant. Typically, the effective recognition is achieved, by utilising many templates for each target at different azimuth angle. Alternatively, scale, translation and rotation invariant feature extraction methods such as moment-based representation can be used to overcome those problems. Moments, which are utilised in this thesis, are scale, translation and rotational invariant and have orthogonal basis, which causes minimum information redundancy. Furthermore, some moments have discrete characteristics, which are beneficial over traditional moments due to having less numerical errors and computational complexity due to normalisation. In comparison to other feature extraction techniques, efficient target recognition can be achieved by adjusting the number of features depending on the information content based on the shape complexity.

In this thesis, we focus on moment based feature extraction techniques and analyse their effectiveness in SAR-ATR images. The main goal of the thesis is to improve the classification performance of the SAR-ATR for the ground vehicles. The contributions of the thesis can be summarised as follows:

The first contribution is to utilise target, shadow, and combined target-shadow regions as separate region of interests (ROIs) for vehicle representation. ROIs in the form of "area", "boundary", and "texture" are used to extract features using Radial Chebyshev Moment. Features extracted from these ROIs are then fused to generate improved classification performance.

The second contribution consists of using feature selection based on Fisher Criterion (FC) followed by data fusion. In this regard, twelve different moment methods are used, and first *k* moments for each feature are selected by ranking all moments based on FC. The selected moments for each feature are fused using different data fusion approaches by utilising feature level fusion and decision fusion.

The third contribution utilises entropy based feature selection. First twelve moment methods are used for feature extraction and a 3D feature matrix is created. Each feature of the 3D matrix contains a row of twelve methods and columns of *s* samples. The entropy calculation of each row is performed to create an entropy vector for that feature. Once entropy for all features is calculated, the entropy matrix (H) is formed, where row of this matrix corresponds to each method and column refers to each feature. For each feature the ranking is performed according to entropy values in descending order and the best *k* moments on each columns are selected.

Finally, ensemble of classifiers is used for improved SAR Image Recognition. Five classifiers are adopted including support vector machine, decision tree, linear discriminant analysis, k-nearest neighbour and random forest. Pseudo Zernike Moment is used to generate the feature vector for the classifiers. The performance of proposed method is calculated by majority voting based on all output labels corresponding to each classifier.

In proposed method of data fusion using Fisher Criterion, the recognition rate is 95.71%, while by utilising entropy the recognition rate reaches to 96.12%. Proposed method of feature fusion of Radial Chebyshev Moments for different ROIs increases the recognition rate up to 98.69%. The highest recognition rate involves ensemble of classifiers by adopting Pseudo Zernike Moment and feature fusion with an accuracy of 99.50%. All proposed methods have either higher or comparable classification performance with the state-of-the-art methods.

Keywords: classification, data fusion, dimensionality reduction, feature extraction, feature ranking, fisher criterion, ensembles of classifiers, entropy, majority voting, moments, support vector machine, synthetic aperture radar.

ÖZ

Sentetik Açıklık Radar (SAR) görüntüleri yüksek çözünürlük kabiliyetine sahip olmaları ile bilinmekte olup her türlü hava koşulları veya güneş ışınlarından bağımsız olarak üretilebilmektedirler. Optik görüntü elde etme sistemleri ile karşılaştırıldıklarında bu avantajları, SAR görüntülerini güvenilir bir veri kaynağı haline getirmiştir. SAR görüntülerinin en önemli uygulamalarından biri, hareket halindeki ve/veya sabit yer araçlarının otomatik hedef tanıması (OHT) olmaktadır. SAR-OHT görüntüleri arka plan, hedef ve gölgeyi içermeleri ile tanımlanabilmektedir. SAR-OHT verileri ile ilgili birçok problem söz konusudur. İlk olarak, özellikle arka planda, dönüştürücü açıklıktan geri gelen dalgaların etkileşimi nedeniyle gürültü oluşmaktadır. Arka planın giderilmesi, ilgi alanı (İA) olarak kabul edilen ön planı izole etmektedir. Diğer problem ise sabit pozlu olmayan görüntülerin meydana gelmesine neden olan yansıyan radar sinyallerinden kaynaklanan hedefin konumsal değişimleridir. Tipik olarak, etkili tanıma, farklı azimut açılardaki her bir hedef için birçok şablon kullanarak başarılır. Alternatif olarak, moment tabanlı gösterim gibi ölçek, çevirme ve dönme değişmez öznitelik çıkarımı yöntemleri bu problemlerin üstesinden gelmek için kullanılabilir. Bu tez çalışmasında kullanılan moment yöntemleri rotasyonel olarak değişken olmamakta ve minimum düzeyde artık bilginin oluşmasına yol açan ortogonal yapıya sahiptir. Buna ek olarak, bazı momentler, normalleştirme sayesinde, sayısal hata ve hesaplama karmaşıklığına sahip olmadıklarından dolayı geleneksel moment yöntemlerine göre avantajları bulunan ayrık karakteristiklere sahiptir. Buna ilaveten, diğer öznitelik çıkarma teknikleri ile karşılaştırıldığında, etkili hedef tanıma, moment özelliklerinin sayısının şekil

karmaşıklığından kaynaklanan bilgi içeriğine bağlı olarak ayarlanabildiği moment bazlı özelliklerin kullanımı ile sağlanabilmektedir.

Bu tez çalışmasında, moment bazlı öznitelik çıkarma teknikleri üzerinde yoğunlaşmakta ve bunların OHT-SAR görüntüleri üzerindeki etkinliği analiz edilmektedir. Tez çalışmasının asıl amacı, SAR-OHT'nin yer araçları konusundaki sınıflandırma verimlerinin geliştirilmesinden ibarettir. Bu tez çalışmasının katkıları aşağıdaki gibi özetlenebilmektedir:

Tez çalışmasının birinci katkısı, araç temsili için hedef, gölge ve birleştirilmiş hedef-gölge alanlarının ilgi alanları (İA) olarak kullanılmasıdır. İA'lar "alan", "sınır" ve "doku" şeklinde ayrılarak Radial Chebyshev Moment yöntemi kullanılarak özelliklerin çıkarılması için kullanılmıştır. Bu İA'lardan çıkarılan özellikler daha sonra sınıflandırma performansını geliştirmek amacıyla kaynaştırılmıştır.

İkinci katkı, Fisher Kriterine (FC) dayalı öznitelik seçimi ve ardından veri kaynaşımından oluşmaktadır. Bu bağlamda, on iki farklı moment yöntemi kullanılmış ve her bir öznitelik için ilk k momentler, tüm momentleri FC'ye göre sıralayarak seçilmiştir. Her öznitelik için seçilen momentler, kaynak kaynaşımı ve karar füzyonu kullanılarak farklı veri kaynaşımı yaklaşımları ile kaynaştırılmıtır.

Üçüncü katkı, entropi temelli öznitelik seçimi kullanmaktadır. Öznitelik çıkarımı için ilk on iki moment yöntemi kullanılır ve bir 3B öznitelik matrisi oluşturulur. 3B matrisin her bir özelliği on iki yöntemden oluşan ve s örneklerinin oluşturduğu sütunlarını içerir. Her satırın entropi hesaplaması, o öznitelik için bir entropi vektörü oluşturularak yapılır. Tüm öznitelikler için entropi hesaplandıktan sonra, bu matrisin

sırası her metoda karşılık gelen entropi matrisi (H) oluşur ve her bir sütun her bir özniteliğe karşılık gelir. Her bir öznitelik için sıralama, azalan düzende entropi değerlerine göre yapılır ve her sütunda en iyi k moment seçilir.

Son olarak, sınıflandırıcıların birleşimi, gelişmiş SAR Görüntü Tanıma için kullanılmıştır. Destek Vektör Makinesi, Karar Ağacı, Doğrusal Ayırtç Analizi, k-En Yakın Komşu Ve Rastgele Orman da dahil olmak üzere beş sınıflandırıcı benimsenmiştir. Pseudo Zernike Moment, sınıflandırıcılar için öznitelik vektörü üretmek için kullanılmıştır. Önerilen yöntemin performansı, her sınıflandırıcıya karşılık gelen tüm çıktı etiketlerine dayalı olarak çoğunluk oyuyla hesaplanmaktadır.

Fisher Kriteri kullanılarak önerilen veri kaynaşım yönteminde tanıma oranı % 95.71 iken, entropi kullanarak tanıma oranı % 96.12'e ulaşmaktadır. Önerilen radyal Chebyshev Momentlerinin farklı İA'ları için kaynaşım yöntemi ile önerilen yaklaşımı, tanıma oranını % 98.69'a kadar arttırmaktadır. En yüksek tanıma oranı, Pseudo Zernike Momenti'ni benimseyerek sınıflandırıcıların toplamını ve %99.50'lik bir doğrulukla öznitelik kaynaşımını içermektedir. Önerilen yöntemlerin tümü, en son çalışmalarla karşılaştırıldığında daha yüksek veya karşılaştırılabilir sınıflandırma performansına sahiptir.

Anahtar Kelimeler: sınıflandırma, veri kaynaşımı, boyutluluk indirgemesi, öznitelik çıkarma, öznitelik sıralaması, fisher kriteri, sınıflandırıcı toplulukları, entropi, oy çokluğu, moment yöntemleri, destek vektör makinesi, sentetik açıklık radarı.

DEDICATION

It is dedicated to:

My Dear Parents, My Lovely Sister and My Sweety Love

ACKNOWLEDGMENT

I would like to thank my supervisors, Prof. Dr. Hasan Demirel and Prof. Dr. Şener Uysal, for their encouragement and support during my Ph.D. studies. I gratefully acknowledge the invaluable guidance and advise they have provided to me throughout this process. I really appreciate the opportunities they have given me and cannot say enough about my gratitude to them.

Special thanks also go to my dear friends Faegheh Yeganli, Mohamad Harastani Masoud Moradi, Moein Jazayeri and Mahmoud Nazzal for sharing the literature and providing invaluable assistance.

I would like to express my deepest gratitude to my lovely family: Hossein Bolourchi, Nasrin Tahami and Pouneh Bolourchi; they gave me a chance for completing my higher education in Cyprus. Without their support, both in financial and emotional matter, achievement of this level was impossible.

Finally yet importantly, I would like to express my deepest appreciation to my love Narjes Azimi who has always been the source of my motivation. Without her patience, I would not have been able to complete my Ph.D. degree.

TABLE OF CONTENTS

LIST OF TABLES

LIST OF FIGURES

LIST OF SYMBOLS AND ABBREVIATIONS

α	Tuning factor for Jacobi moments
β	Tuning factor for Jacobi moments
$\delta(.)$	Dirac delta
$\delta(s)$	Sum rule
ξ	Threshold value for shadow
$\eta(s)$	Max rule
λ	Eigen value
μ	Mean
$\mu(s)$	Mean rule
ς	Localization factor
$\rho(p,N)$	Squared norm
σ	Standard deviation
τ	Threshold value for target
Φ	Feature matrix
$\varpi(s)$	Median rule
$(a)_k$	Pochhammer
${}_pF_q$	Generalized Hyper-geometric series
a	Weight constant
A	Feature of train
ACC	Accuracy
ATR	Automatic Target Recognition
AUC	Area Under a Curve

b	Bias
B	Feature of test
CFM	Chevyshev Fourier Moment
C_i	Class number
CM	Chebyshev Moment
CM #1	Chebyshev Moment (of the first kind)
CM #2	Chebyshev Moment (of the second kind)
Cov	Covariance matrix
D	Database
D (a,b)	Normalised Euclidean metric
DCCF	Distance Correlation Classifier Filter
DF	Decision Fusion
DT	Decision Tree
EFS	Elliptical Fourier Series
$e^{-iq\theta}$	Angular part of polynomial
EMACH	Extended Maximum Average Correlation Height
F	Feature ranking
f (x,y)	Digital SAR image
FC	Fisher Criterion
FF	Feature Fusion
FMM	Fourier Merlin Moment
FN	True Negatives
FNR	False Negative Rate
FP	False Positive
FPR	False-Positive Ratio

FRV	Feature Ranked Vector
FV	Feature Vector
g	Dimension of feature space
g_c	Centre pixel's intensity
GI	Gini Index
GM	Gegenbauer Moment
GOM	Geometric Moment
g_p	Neighbour pixel's intensity
H	Entropy score matrix
HOG	Histogram of Oriented Gradients
h^{all}	Entropy of all samples in the training set
H_{rank}	Ranked entropy matrix
h^s	Entropy score
h^w	Within-class entropy
HWT	Haar Wavelet Transform
ICA	Independent Component Analysis
I_{avg}	SAR image after using averaging filter
I_{hist}	Histogram equalised image
I_{Thresh}	Gray level threshold
J	Interclass separation
JM	Jacobi Moment
K	Fold
$K(.,.)$	Kernel function
KLDA	Kernel Linear Discriminant Analysis
KM	Krawtchouk Moments

k-NN	k- Nearest Neighbour
KPCA	Kernel Principal Component Analysis
LBP	Local Binary Pattern
LDA	Linear Discriminant Analysis
LGRPH	Local Gradient Ratio Pattern Histogram
LM	Legendre Moment
LPP	Locality Preserving Projections
MACH	Maximum Average Correlation Height
MID	Maximum Interclass Distance
MINACE	Minimum Noise and Correlation Energy
MLGRPH	Multiscale Local Gradient Ratio Pattern Histogram
MMSE	Minimum Mean Square Error
$M_{p,q}$	Moment sequence
MSE	Mean Square Error
MSTAR	Moving Stationary Target Acquisition and Recognition
NMF	Nonnegative Matrix Factorization
NN	Neural Network
OM	Orthogonal Moments
p	Order
P	Polynomial basis
PBF	Polynomial Basis Function
PCA	Principal Component Analysis
PDCCF	Polynomial Distance Correlation Classifier
$P_{i,j}$	Class probability
PLS	Partial Least Squares

PZM	Pseudo Zernike Moment
q	Repetition
R	Neighbor radius
RBF	Radial Basis Function
RCM	Radial Chebyshev Moment
RCS	Radar Cross Section
RF	Random Forest
RHFM	Radial Harmonic Fourier Moment
ROC	Receiver Operating Characteristic
ROI	Regions of Interest
$R_{pq}(r)$	Radial part of polynomial
RT	Radon Transform
S	Sample
SA	Shadow-Area
SAR	Synthetic Aperture Radar
S_B	between-class scatter matrix
SB	Shadow-Boundary
SEN	Sensitivity
SF	Feature level fusion
S_i	Support Vector
SPE	Specificity
SRC	Sparse Representation Classifier
ST	Shadow-Texture
SVM	Support Vector Machine
S_W	within-class scatter matrix

TA	Target-Area
TB	Target-Boundary
TT	Target- Texture
TN	True Negative
TNR	True Negative Rate
TP	True Positive
TPR	True Positive Rate
TSA	Combined Target-Shadow-Area
TSB	Combined Target-Shadow-Boundary
TST	Combined Target-Shadow-Texture
w^*	Optimal projection
$\overline{x}$	Global mean
y	Label
Z	Number of neighbor pixel
ZM	Zernike Moment

Chapter 1

INTRODUCTION

1.1 Introduction

Synthetic Aperture Radar (SAR) images have a very high resolution with the capability to work independently from any weather condition and solar illumination. These advantages over optical systems make the SAR images a reliable source of information for many applications in natural hazards and environmental monitoring, such as fire [1], flood [2] and earthquake detection [3] on land; and ship detection [4], wave forecasting and marine climatology [5] on the oceans. SAR images are also used in agricultural industry [6], homeland security applications [7] and military surveillance systems [8].

In this thesis, the focus is on the detection, discrimination, feature extraction and classification of different targets in military surveillance systems. Moving stationary target acquisition and recognition (MSTAR) database is provided by the United States Air Force to the public for research purposes. It is a standard SAR-ATR database [9], which is widely used by many researchers in this field. Since MSTAR data-set contains noise and radar reflections are not scale, translation and pose-invariant, many algorithms are introduced in the pre-processing for finding the region of interest (ROI) after noise removal and segmentation, which is to be considered in the post processing. The post processing includes feature extraction, feature selection for dimensionality

reduction and increasing the class separation. The final phase is the classification stage with data fusion.

1.2 Synthetic Aperture Radar

Synthetic Aperture Radar (SAR) images refer to images that are captured by an active illumination system. An antenna, attached on a platform (which is either airborne or spaceborne) in the direction of the flight path, transmits a radar signal towards the target to simulate an extremely large antenna or aperture electronically [134]. The signal processing uses magnitude and phase of the received signals over successive pulses. After a given number of cycles, the stored data is recombined to form a finer resolution [10]. The side-looking viewing geometry of imaging radar systems is illustrated in Fig1.1. Slant range refers to the distance measured along a line between the radar antenna and the center of illuminated target. Ground Range is the perpendicular distance from the ground track to a given object on the Earth's surface. Cross range refers to the across-track dimension perpendicular to the flight direction. Depression angle refers to the angle between the line of sight from the radar to the center of illuminated object and horizontal plane at the radar. Altitude is the straight line from radar to the ground track, which measures height of a target over the earth's surface, Azimuth direction or along range is the direction parallel to the radar flight path and azimuth angle refers to the angle between the heading of the vehicle and the azimuth direction. Figure 1.2 shows a sample MSTAR target at different azimuth poses.

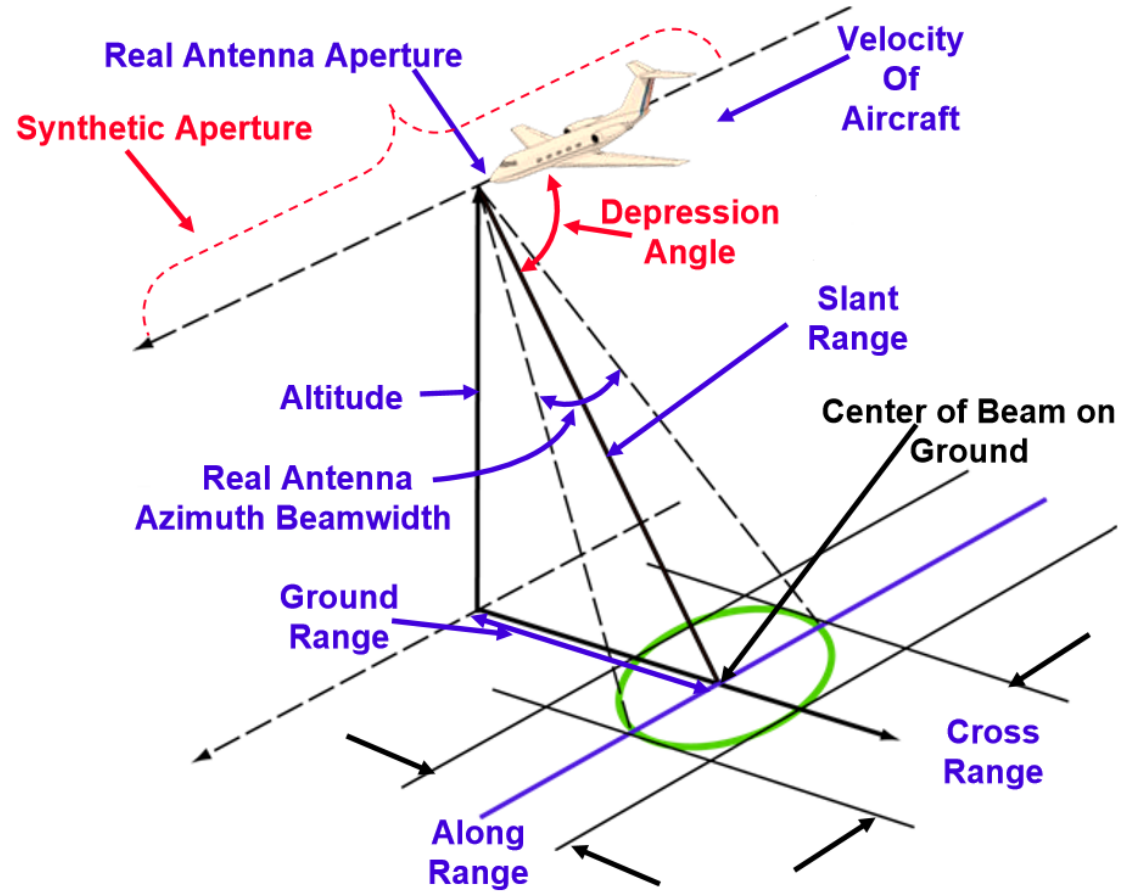

Figure 1.1: Synthetic Aperture Radar glossary [11]

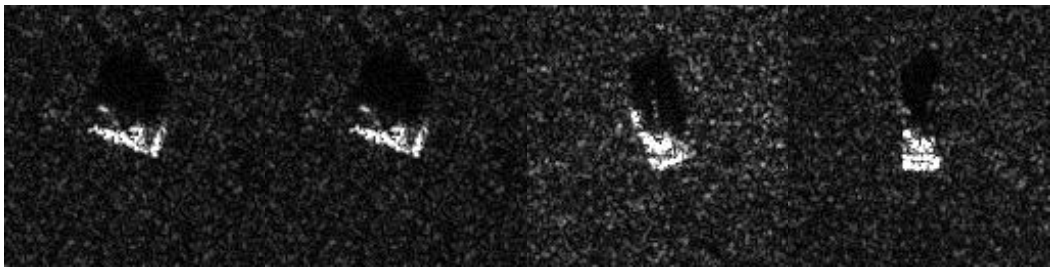

Figure 1.2: Different azimuth angle of the same target

Moments are estimation of population parameters used in the statistic. Moments are specific quantitative measure of the shape of a set of points. They can also be utilised for feature extraction by capturing significant information of an image. In this regard, moments as shape descriptors present powerful techniques for extracting shape-based features in SAR images.

Various types of moments are introduced in the literature [125] [132]. Some moments are defined in the Cartesian coordinate with continuous form. Legendre Moments [12], Chebyshev Moments, Gegenbauer Moments [13] and Jacobi Moments [14] are an example of this type. They are simplest orthogonal moments. Jacobi is the general form of this type in which other moments can be obtained from it.

Other types of moments, which are defined in the Cartesian coordinate with discrete form are Krawtchouk Moments [15], Racah Moments [16], Meixner Moments [17], Charlier Moments [18] and Hahn Moments [19]. Racah Moments are the general form of this type from which other moments of this type can be obtained. Although both types of these moments (continuous and discrete moments in Cartesian coordinate) are scale and translation invariant, obtaining rotational invariance [20] from them is difficult. In addition, computational complexity of these types of moments is extremely high.

Zernike Moments [21], Pseudo Zernike Moments [22] [129], Radial Harmonic Fourier Moments [23] [131], Chebyshev-Fourier Moments [24] [128], Fourier Merlin Moments [25] [130] and Jacobi Fourier Moments [26] are defined in the polar coordinate that has the property of being scale, translation [126] and rotational invariance [127]. The experimental results show a drastic improvement in performance by utilising moments in polar coordinates.

All aforementioned moments in polar coordinate are in continuous function. Hence, for a digital image, approximation by discrete summation is utilised. However, this process leads to numerical errors in computation of moments. To reduce this problem,

Radial Chebyshev Moments [27] are introduced reducing both computational complexity and computational errors caused by approximations. More details about moments are offered in Chapter 4.

Moments have been used in feature extraction for the SAR images. Amoon and Rezai addressed optimal selection of Zernike moments features [28]. Clemente et al. used Krawtchouk Moments for effective feature extraction [29]. Bolourchi et al. utilised Radial Chebyshev moment for extracting features [27]. In [30] they also used Geometric moments, Legendre moments, Zernike moment and Pseudo Zernike moment. Further discussion of using moments in SAR images is given in Chapter 4.

1.3 Problem definition

Basically, there are many problems associated with SAR images and specifically with images provided in MSTAR database. First, SAR images consist of high-resolution imagery, which means high amounts of data. Analyzing the enormous amount of data requires high computational cost; therefore, there is a need to adopt algorithm(s) for dimensionality reduction in the form of feature extraction followed by feature selection.

Second, images in MSTAR data-set are contain noisy background. This causes false alarm and miss rate to be increased in the classification stage and poor recognition rate to be achieved. Thus one problem to isolate the ROIs by segmentation techniques after background removal.

Third, SAR images are sensitive to the changes in scale and translation. Therefore, it is required to utilize feature extraction technique (s) that are scale and translation

invariant. Furthermore, radar reflections are not pose-invariant in MSTAR images, and therefore for effective recognition rate many templates are required for each target at different azimuth angle, which in turn raises the computational complexity. Due to this problem, a pose invariant feature extraction process is required to provide effective representation of the pose varying targets.

Fourth, the redundancy brought by the correlation of features influence the classification performance. To address this problem an algorithm that can represent the properties between the features with no redundancy or overlap of information is required.

Finally, in the case of target recognition, it is vital to detect a target with the highest recognition rate. In this regard, for improving recognition rate we should use a form of data fusion.

1.4 Thesis objectives

The main objectives of this thesis are listed as follows:

1- Using moment-based methods for feature extraction. This process tries to extract dominant features in ATR. Moments are scale, translation and rotation invariant [126] [127] with their robustness to noise and having a minimum information redundancy. Furthermore, some moments are defined in discrete domain, which reduce computational complexity, due to normalisation and computational error caused by approximations in the continuous domain.

2- Applying feature ranking approaches as a feature selection method in SAR ATR. We propose novel approches based on feature ranking to choose dominant features. In this regard, two feature-ranking approaches based on

entropy, and Fisher's criterion (FC) are proposed. It is critical to determine the number of top features for effective classification and dimensionality reduction.

3- Applying data fusion, which involves feature level fusion, decision fusion and feature fusion for improvement in the recognition rate. Regarding decision fusion, many rules such as sum rule, max rule and median rule are used to improve the overall classification performance.

4- Applying ensemble of classifiers including support vector machine (SVM), random forest (RF), decision tree (DT), k-nearest neighbour (k-NN) and linear discriminant analysis (LDA). Since the classification based on one classifier may be considered to be biased, majority voting (MV) among classifiers are used for accuracy enhancement in ATR.

1.5 Thesis contributions

In this thesis, several methods are proposed to improve the classification performance. Main contributions of this thesis can be summarised as follows:

1- Utilising different segmented sections as informative/discriminative parts of ROI and combining different segmentation parts with different ROI (target, shadow, combined target-shadow). Extracting features of each segmented part by RCM and finally fusing all features.

2- Introducing Fisher Criterion based feature selection method for feature ranking. Twelve moment based feature extraction methods are used for capturing important information of SAR images. For each method, 100 features are extracted. Ranking among each moment was achieved by using Fisher Criterion. The selected k moments are fused using different data fusion approaches by utilising feature level fusion or decision fusion. In the case of

feature level fusion, feature vectors coming from the selected moments are concatenated, whereas in the decision fusion, the class probabilities are combined by using sum, median and max rules.

3- Introducing entropy based feature selection method for feature ranking. For each SAR image, first a 3D feature matrix ($\phi_{i,j,s}$) is created where *i* refers to each method of moment for *i=1,2,…,12. j* represents each feature(*j=1,2,…,100)* and *s* is the number of samples in the training set for *s=1,2,…,1622.* For each feature, *j*, entropy of sub-feature matrix ($F_{i,k}$) is evaluated. Once entropy for all features is performed, the entropy score matrix ($H_{i,j}$) is created. Then the columns of matrix H is ranked based on its entropy values in the descending order. Feature selection is performed by choosing top *k* moments associated with highest ranked entropies of all methods. After feature selection, the most discriminant features are grouped to represent an image, which in turn increases the classification performance.

4- Introducing ensemble of the classifiers. Extracted features using PZM from target, shadow and combined target-shadow regions are fused using feature fusion and are fed to different classifiers. Five classifiers are adopted including support vector machine, decision tree, a linear discriminant analysis, k-nearest neighbour and random forest. Finally, the performance of the proposed method is calculated by majority voting based on all output labels corresponding to each classifier method.

All proposed methods have either higher or comparable classification performance in comparison with the state-of-the-art.

1.6 Thesis overview

The remainder of this thesis is as follows. Chapter 2 presents state-of- the-art including feature extraction, dimensionality reduction and classification in SAR images. Chapter 3 provides the methodology, which is used in this thesis: MSTAR data type, segmentation, feature extraction, ranking, feature selection, data fusion, and classifiers. Chapter 4 describes the different types of moments in Cartesian and polar coordinates. In Chapter 5, we introduce a new approach for target recognition based on the fusion of different segmentation parts and region using RCM. In Chapter 6 and 7, we introduce a novel feature selection method based on FC and entropy respectively to determine the optimal number of top features by feature ranking. Furthermore, data fusion techniques are introduced to improve the recognition rate. In Chapter 8, we present a novel approach by calculating the PZM feature vectors for different segmented parts and regions of SAR images. The PZM feature vectors are fed to ensemble of classifiers and the performance of the proposed method is calculated by majority voting based on all output labels corresponding to each classifier. Finally, Chapter 9 presents thesis conclusions and future work.

Chapter 2

STATE-OF-THE-ART IN SAR TARGET RECOGNITION

2.1 Introduction

Several methods have been proposed for Automatic Target Recognition (ATR) in Synthetic Aperture Radar (SAR) Images. Moving Stationary Target Acquisition and Recognition (MSTAR) database [9] is most widely used database in the literature. In a standard SAR-ATR method; feature extraction, dimensional reduction, feature selection, and classification are used as the standard phases. In this chapter, we have an overview on the available methods of state-of-the-art for SAR-ATR.

2.2 Feature extraction

Feature extraction of SAR images is the main step in SAR ATR. Recently various types of features have been adopted in the literature. Roughly, feature extraction techniques can be categorised into four distinct types, namely transformed images techniques, template-matching techniques, pixel based techniques and feature based techniques.

2.2.1 Transform domain approaches

In [31] Zhao and Principe used the whole image vector as the feature vector. In [32] Radon Transform (RT) is successfully adopted for feature extraction and classification, where RT for a SAR image $f(x,y)$ can be defined as:

$$T_R(r,\theta) = \int_{-\infty}^{\infty}\int_{-\infty}^{\infty} f(x,y)\delta(xcos\theta + ysin\theta - r)dxdy \quad (2.1)$$

where $\delta(.)$ is the Dirac delta-function defined as:

$$\delta(x) = \begin{cases} 1 & if\ x = 0 \\ 0 & otherwise \end{cases} \quad (2.2)$$

and r and θ in the polar coordinates which are defined as:

$$r = (x^2 + y^2)^{\frac{1}{2}}, and \quad \theta = tan^{-1}(\frac{y}{x}) \quad (2.3)$$

For a SAR image with size 128×128, 16384 features should be considered for both methods. Different wavelet transforms [33] such as Haar wavelet transform (HWT) [32] are also used for feature extraction. The monogenic signal is used in [34] for capturing the characteristics of the SAR images. Due to the extraction of many features, the computational complexity of all techniques mentioned above is very high which implies an extremely large requirement of memory and computational cost.

2.2.2 Template matching approaches

Templates refer to any reference images, which are constructed from the geometrical characteristics of the samples in the training set. Due to the variation of MSTAR images in pose and illumination for a successful target recognition, a large database of template for each sample is required. The accuracy depends on how well features are matched to the template. There are two disadvantages associated with template matching. First, many template models are required which would increase the computation complexity. Another drawback is backgrounds of MSTAR images, which include no useful information and increase the computational complexity of the system, therefore it is necessary to design a filter template to reduce huge number of features to be used for feature extraction. Maximum average correlation height (MACH) [35], distance correlation classifier filter (DCCF) [35], a combined

MACH/DCCF [35], extended maximum average correlation height (EMACH) [36], polynomial distance correlation classifier filter (PDCCF) and minimum noise and correlation energy (MINACE) [37] are applied to SAR images. Mahalanobis, et al, [35] are deployed the combined MACH/DCCF, by averaging all training samples, which belongs to each class to create a class template. DCCF, which maximises the interclass distance, is applied to all templates. MACH/DCCF are applied on the test. Mean squared error (MSE) of MACH/DCCF filtered and templates are calculated. Test image belongs to the class in which the MSE is minimised. MSTAR data-set is commonly used as 3-class and 10-class recognition problems. MACH, DCCF or combination of them successfully applied on 3-class recognition problems. However, it fails for a 10-class recognition problem. EMACH and PDCCF are the improved versions of MACH and DCCF respectively which is used for 10-class problem cases.

MINACE filters have the different mechanism in which the number of training set involved to construct the filter depends on the correlation scores of each image in the training set. In the first iteration, only one image is utilised to form a filter. All correlation scores are calculated by created filter. If all scores are above the predetermined threshold, the algorithm is terminated. Otherwise, the filter is updated by a combination of previous images used to create the filter with the lowest correlation score. The filter is updated, score is calculated, and the process is continued for the next iterations till all training images satisfy the threshold conditions.

Quarter power, log magnitude and conditionally Gaussian classification models are techniques using distance metrics that are based on minimum squared error or maximum likelihood scores and are studied in [38].

The conditionally Gaussian uses maximum likelihood estimator with complex normal distribution while quarter power and log magnitude uses MSE estimator with gamma and log normal model distribution respectively. Quarter power has high performance [39-40] while log magnitude has poor performance since background noise is not well presented in log magnitude technique.

2.2.3 Texture based approaches

Some feature extraction techniques are applied to all pixels of SAR images. Local Binary Pattern (LBP), local gradient ratio pattern histogram (LGRPH) and Multiscale local gradient ratio pattern histogram (MLGRPH) are surveyed in [41]. LBP is used for extracting the most useful information of an image. The original LBP with 3-pixel block operator is defined as:

$$LBP_{Z,R} = \sum_{p=0}^{z-1} s(g_p - g_c)2^p \tag{2.4}$$

where Z is the number of neighbour pixels, and R is the neighbour radius. A most common choice for Z and R is 8 and 1 respectively. g_c is centre pixel's intensity, and g_p is the neighbour pixel's intensity, and term s should satisfy the following condition:

$$s(x) = \begin{cases} 1, & x \geq 0 \\ 0, & x < 0 \end{cases} \tag{2.5}$$

In LBP the area is divided into k small non-overlapping regions. The LBP histograms are extracted for each sub-region and are concatenated to form a single vector. LGPRH and MLGPRH are the improved versions of LBP. Histogram of oriented gradients (HOG) is studied in [42].

2.2.4 Geometry based approaches

Geometry based approaches refer to the approaches that captures important information about a target class and therefore significantly decreases the number of

features to be extracted. These approaches are preferred by many researchers because of reducing the computational complexity. Some approaches such as elliptical Fourier series (EFS) [43] and Hu moments [44] are studied for target recognition in SAR images. Some feature such as edges and corners have been studied in [45]. In [46] the approximate length and width of the target, the average radar cross section (RCS) and log standard deviation have been surveyed. Having prior knowledge about target pose in [46], only few features are used to evaluate recognition rate. Moments are an alternative method that are successfully adopted in many SAR image applications such as Zernike moment [28] and Krawtchouk [29] moment. Moments are rotation, scale and translate invariant [126] [127], which cope with the MSTAR images due to variation in target pose, also fewer features are needed for target recognition. More details about moments are provided in chapter 4.

2.3 Dimensionality reduction

The number of raw features extracted from MSTAR images data-set is extremely high (16384 features) compared with the number of sample sets. Data reduction is required either directly after preprocessing or after feature extraction (especially for the methods in section 2.2.1 and 2.2.2). Feature selection is made to produce new feature vectors to be used for generating a low-dimensional representation of the original MSTAR data-set. Many previous research have proposed feature selection and dimensionality reduction (linearly and nonlinearly) such as linear discriminant analysis (LDA) [47], principal component analysis (PCA) [47], independent component analysis (ICA) [48] and nonnegative matrix factorization (NMF) [49] for linear approaches and kernel linear discriminant analysis (KLDA) [50], kernel principal component analysis (KPCA) [51], Locality Preserving Projections (LPP) [52] and Maximum Interclass Distance (MID) [53] for nonlinear dimensionally

reduction in MSTAR. In the following subsection a brief explanation of PCA, which is used for dimensionality reduction.

2.3.1 Dimensionality reduction based on PCA

PCA is a method of dimensionality reduction, which is utilised to extract a set of orthogonal basis from the MSTAR data-set [54]. Linear combinations of basis are used to show high-dimensional original data. Suppose X be a matrix of original data with a size of $n \times m$ with n number of sample and m number of features as:

$$X_{n,m} = \begin{bmatrix} x_{1,1} & \cdots & x_{1,m} \\ \vdots & \ddots & \vdots \\ x_{1,n} & \cdots & x_{n,m} \end{bmatrix} \tag{2.6}$$

Basically, the following steps are required for dimensionality reduction using PCA. First, we compute the mean, μ_j, of the training set as:

$$\mu_j = \frac{1}{m} \sum_{k=1}^{m} x_{k,j} \tag{2.7}$$

and then we evaluate covariance matrix, $Cov_{i,j}$, of the training set as:

$$Cov_{i,j} = \sum_{k=1}^{m} \frac{(x_{k,i} - \mu_i)(x_{k,j} - \mu_j)^T}{m-1} \tag{2.8}$$

$\lambda_1 > \lambda_2 > \cdots \lambda_n > 0$ are ordered eigenvalues of covariance matrix. All eigenvalues and eigenvectors (v) of covariance matrix are defined as follows:

$$\sum Cov\, v = \lambda v \tag{2.9}$$

Next, we choose V eigenvectors of corresponding to the k largest positive eigenvalues ($\lambda_1 > \lambda_2 > \cdots \lambda_k > 0$). Finally, the reduction can be made by evaluating $y=V.X$.

2.4 Classification methods

The final step in SAR-ATR is classification. Classification in MSTAR data refers to

supervised classification. Several classifiers are introduced in MSTAR classifications such as SVM, neural network (NN), decision tree (DT), a linear discriminant analysis, (LDA) k-nearest neighbour (k-NN) and random forest (RF). In [55] sparse representation classifier (SRC) has adopted to MSTAR images. However it is not optimal for solving classification problems as mentioned in [56].

Numerous dictionary-learning algorithms also have been proposed for classification techniques such as K-SVD [57] and online dictionary learning [58]. A survey of supervised dictionary learning and sparse representation can be found in [59].

In this thesis, SVM classifier for target recognition in SAR images based on supervised learning is deployed. More details associated with SVM classifiers are given in section 3.7.1. In addition to SVM, an ensemble of classifiers is applied by majority voting among many classifiers, which will be seen in chapter 8. Table 2.1 shows a summary of some studies in SAR automatic target recognition focusing into feature extraction, feature selection and classification methods. Yuan et al [36] used MLGRPH as a feature extraction followed by SVM classifier using 3-class MSTAR data and has the highest performance in the literature. For 10-class problem, the best approach is achieved by DeVore, & O'Sullivan, [38] that extracts 2304 features by utilising normalized image feature extraction followed by k-NN classifier.

Table 2.1: Review of state-of-the art studies in MSTAR images

Author(s)	Feature Extraction	Feature Selection	Classifier	Class	Number of Features	ACC (%)
Zhao, Q., et al (2001). [31]	Template Matching	-	SVM	3	-	90.40
Srinivas, U., et al (2014). [33]	Wavelet	-	SVM	3	-	86.33
Liu, M., et al. (2013). [52]	-	LLP	k-NN	3	48	83.52
Liu, M., et al (2013). [52]	-	PCA	k-NN	3	49	72.31
Liu, M., et al (2013). [52]	Gaussian Distribution	LLP	k-NN	3	48	91.06
Anagnostopoulos, G. C. (2009). [43]	Region Descriptor	-	SVM	10	2304	94.10
Song, S., et al (2016). [42]	SAR-HOG	-	SVM	10	-	93.87
Song, S., Xu, B., & Yang, J. (2016). [42]	SAR-HOG	-	k-NN	10	-	94.27
Patnaik, R., & Casasent, D. (2005). [37]	MINACE	-	Max Value	3	4096	90.6
Bryant, M. L., & Garber, F. D. (1999). [60]	80x80 Normalized Image	-	SVM	3	6400	90.99
DeVore, M. D., & O'Sullivan, J. A. (2002). [38]	Normalized Image	-	k-NN	10	2304	95.50
Yang, Y., Qiu, Y., & Lu, C. (2005). [44]	Hu	-	k-NN	7*	-	76.85
Yang, Y., Qiu, Y., & Lu, C. (2005). [44]	Hu	-	SVM	7*	-	73.69
Yuan, X., et al (2014). [36]	MLGRPH	-	SVM	3	-	93.88
Yuan, X., et al (2014). [41]	-	PCA +LDA +ICA	SVM	3	-	90.57
Yuan, X., et al (2014). [41]	-	MID	SVM	3	-	93.49

* In this paper they did not consider BMP2, T72 and BRT70

Chapter 3

METHODOLOGY

3.1 Introduction

We present the methodology that is used in this thesis, which includes segmentation methods, feature extraction, ranking, data fusion, and classifiers. However before we start with methodology, we briefly introduce the MSTAR databases which are used in the whole thesis.

3.2 Database

Two types of MSTAR database used throughout this thesis, for feature extraction and classification namely, three-class database and ten-class database.

3.2.1 Three-class database

Three-class database type is widely used in many research areas. In this thesis, all proposed methods are tested by utilising three-class database. In Chapter 5 and 8we also include comparisons of ten-class database with some of the state-of-the-art MSTAR images.

In three-class database, each image has a target vehicle from three different types of ground vehicles with 7 serial numbers. The first type of ground vehicle is an armoured personnel carrier (BTR70) with only one serial number (SN_C71). The second type of vehicle belongs to the infantry-fighting vehicle (BMP2) with 3 different serial numbers as SN_5663, SN_9566 and SN_C21. The last vehicle type is a tank (T72) with three

different serial numbers as SN_132, SN_812 and SN-S7. All MSTAR images have 128 × 128-pixel size. X-band SAR sensor is used for data collection by Sandia National Laboratory (SNL). The samples are collected either at 15° or 17° depression angle. Totally 429, 1285 and 1274 samples are gathered for classes BTR70, BMP2 and T72 respectively with consideration of depression angle and serial numbers. Total samples of MSTAR data are 2987. The summary of data utilised for classification is shown in Table 3.1.

Table 3.1: SAR database (three-class database)

		For each serial		**For each class**		
Type/ Class	**Serial Number**	**Samples 17°Angle**	**Samples 15°Angle**	**Samples 17°Angle**	**Samples 15°Angle**	**Number of Samples**
BTR70	SN_C71	233	196	233	196	429
BMP2	SN_9563	233	195	698	587	1285
	SN_9566	232	196			
	SN_C21	233	196			
T72	SN_132	232	196	691	582	1274
	SN_812	231	195			
	SN_S7	228	191			
Total				**1622**	**1365**	**2987**

3.2.2 Ten-class database

This type of vehicle contains the previous three types (BTR70, BMP2, and T72) and the other seven types of vehicles includes: D7 a bulldozer, BDRM2, ZIL131 two types of trucks, 2s1, ZSU-23-4 two types of cannon, BTR60 an armoured car and T62 a tank. A summary of data type of 10-class recognition is given in Table 3.2. Also the Optical images of all 10 types of vehicles and their corresponding SAR representation are illustrated in Fig.3.1.

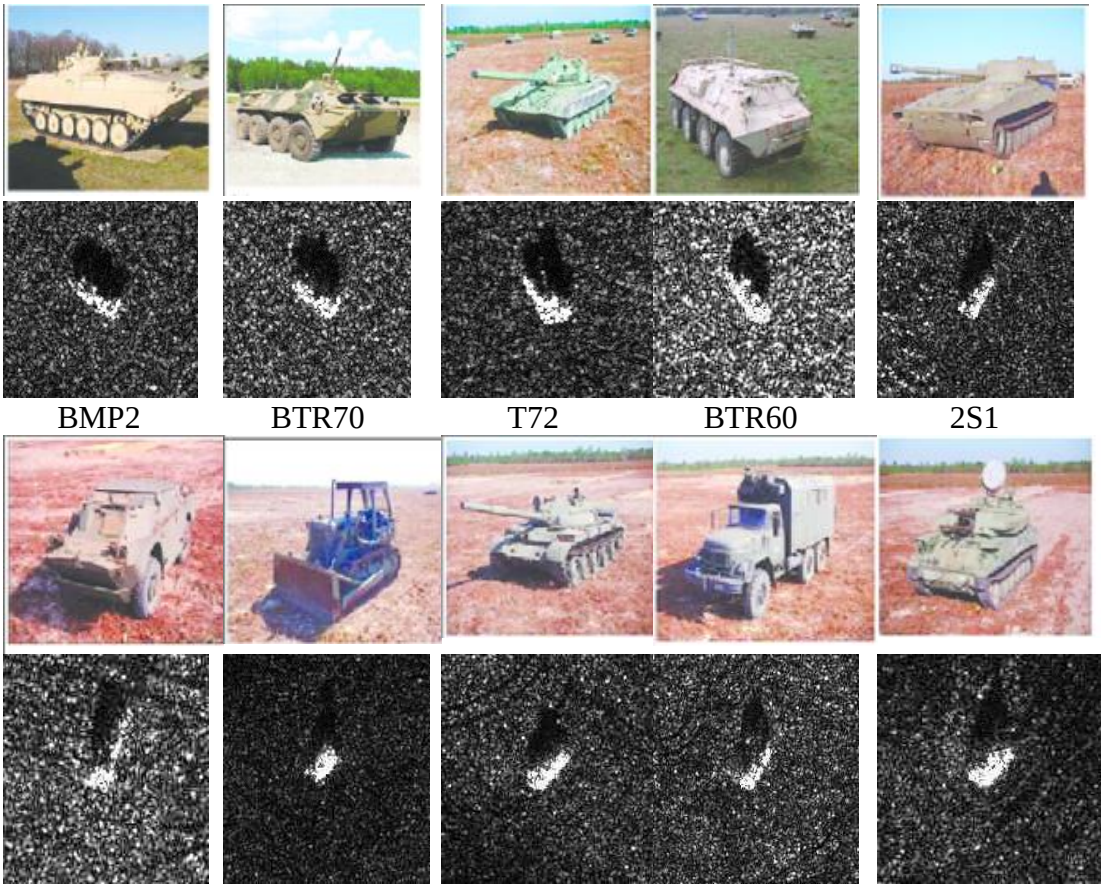

Figure 3.1: Optical images and SAR images of different vehicles

Table 3.2: SAR database (ten-class database)

Vehicle Class	Number of sample at 17° of depression Angle	Number of samples at 15° of depression angle
BMP2	698	587
BTR70	233	582
T72	691	196
BTR60	256	195
2S1	299	274
BRDM2	298	274
D7	299	274
T62	299	273
ZIL131	299	274
ZSU-23-4	299	274

3.3 ROI segmentation

MSTAR images consist of background, shadow and target regions. For effective classification, it is essential to remove noises associated with each image. However,

since the intensity level of shadow and background from one SAR image to another one is changing drastically concerning the angle as it is shown in Fig. 3.2, it requires more advanced methods for thresholding rather than traditional methods. Many approaches for preprocessing introduced in the literature. Soh and Tsatsoulis [61] suggest calculation of optimal thresholds. Schumacher and Schiller [62] used clustering for effective segmentation. The Bayesian approach could also be used to obtain results on the MSTAR database images [63].

Our aim is to define an algorithm for extracting target, shadow, and combined target-shadow regions as ROIs. For each region further, we define ROIs as an area, boundary and texture. It means for each input of SAR images we produce nine regions of interests (ROIs) as Target-Area (TA), Target-Boundary (TB), and Target- Texture (TT) for the target region, Shadow-Area (SA), Shadow-Boundary (SB) and Shadow-Texture (ST) for shadow region and combined Target-Shadow-Area (TSA), combined Target-Shadow-Boundary (TSB) and combined Target-Shadow-Texture (TST) for combined target-shadow regions.

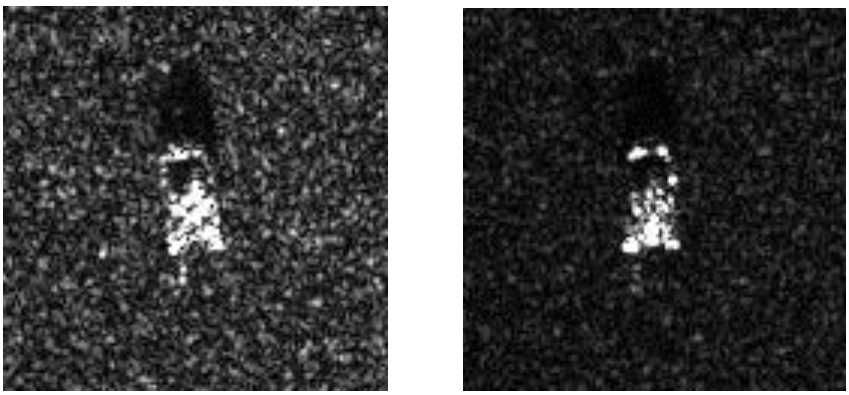

Figure 3.2: SAR images of BMP2 illustrating different intensity

To do so, effective preprocessing consists of five stages as histogram equalisation, average filtering, thresholding, Sobel filtering and dilation. In the following subsection, we use an image (hb03787.004) captured at 17° depression angle form BRT70 group (armoured personnel carrier) with serial number SN-C71 to find all nine ROIs mentioned above.

3.3.1 Histogram equalisation

Histogram equalisation is applied to the original input SAR image (hb03787.004). The aim of using histogram equalisation is to produce the output that has pixel values distributed equally on the interval [0, 1]. The output is defined as:

$$I_{hist} = \sum_{j=0}^{k} \frac{n_j}{n}, k = 0,1,2, \dots, L-1 \quad (3.1)$$

where n_j be the number of occurrences of grey level j, n is being the total number of pixels in the image and L is the number of possible intensity value which is 256 in this study. The mapping from original SAR image to histogram equalisation is shown in Fig. 3.3.

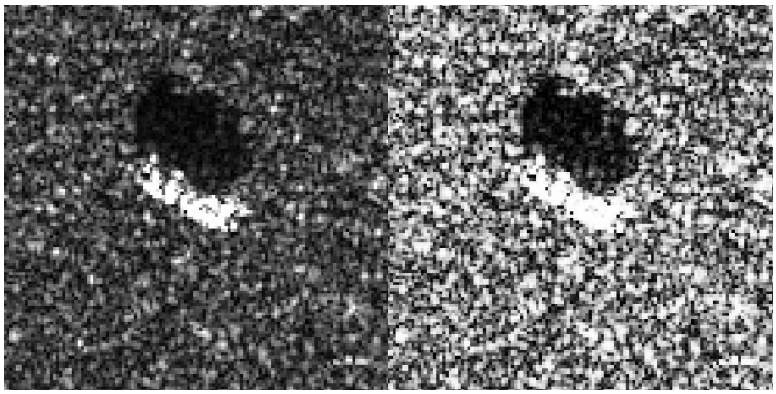

(a) (b)

Figure 3.3: a. Original SAR image, b. Histogram equalised image

3.3.2 Averaging filtering

Since the variance of noise in the average is smaller than the variance of the pixel noise, averaging filters are a good choice to reduce noise artefacts. Equalised image is smoothened by the averaging filter as it is illustrated in Fig. 3.4. The filter mask size of the average filter was chosen to be 11×11.

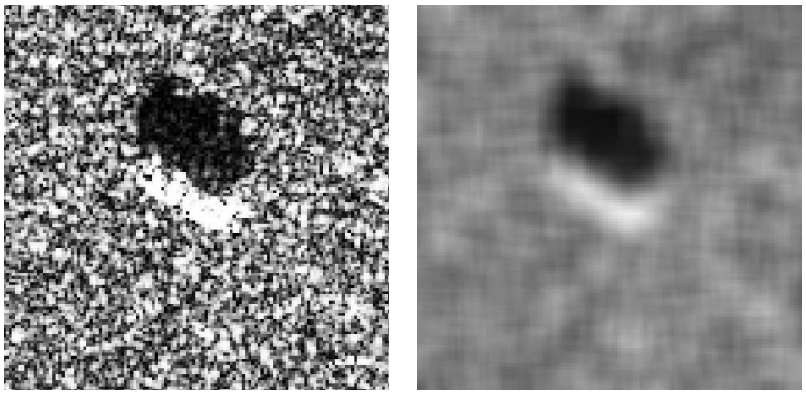

(a) (b)

Figure 3.4: a. Histogram equalised image, b. Averaging filter

3.3.3 Thresholding

Next step of preprocessing is to detect target, shadow and combined target-shadow. The detected regions are called area of target (TA), shadow (SA) and combined target-shadow (TSA). For detecting both target and shadow regions, it is necessary to apply different threshold levels for obtaining both parts. The grey level threshold is defined as a constant between 0 and 1:

$$I_{Thresh}(i,j) = \begin{cases} 0 & I_{avg}(i,j) \leq \tau \\ 1 & I_{avg}(i,j) > \tau \end{cases} \tag{3.2}$$

where τ is the threshold value for target and I_{avg} is the processed SAR image after using averaging filter. In order to detect the target, which is brighter in the image as illustrated in Fig. 3.5-a, it is required to choose the constant nearest to 1. In [64], it was

suggested to have 0.8 to be a threshold pixel value for target regions. The experimental results validate the effectiveness of τ at 0.8 for efficient segmentation.

Shadow regions are areas on the ground that are not scanned by the radar signals due to reflections. The natural result of this process is that no returned signal is received and these areas appear dark in the SAR images. Therefore, for detecting shadow regions, which cover darker area in the image, a constant, ξ, is defined as the threshold for shadow region that is closer to zero should be chosen. In this context, ξ is chosen to be 0.2 for effective shadow segmentation. The thresholded images at this stage can be considered to be an area (TA) (or mask) of target, shadow (SA) and combined target-shadow (TSA) as it is shown in Fig. 3.5.b, 3.5.c and 3.5.d respectively. Besides area, another ROI is called texture.

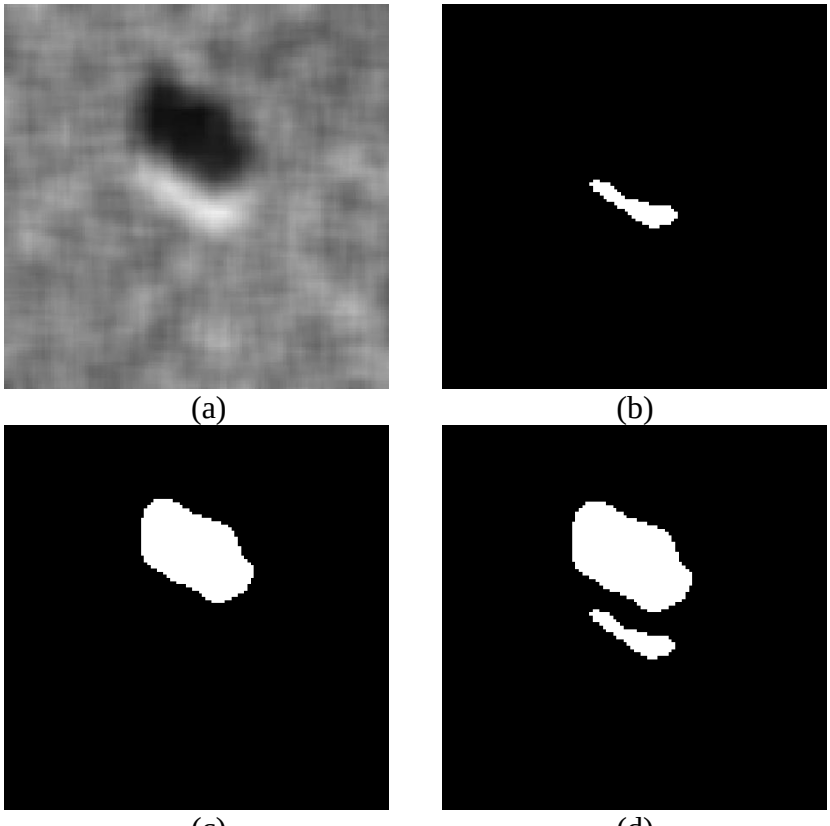

Figure 3.5: a. Averaging filter, b. area of target (TA), c. area of shadow (SA), d. area of combined target-shadow (TSA)

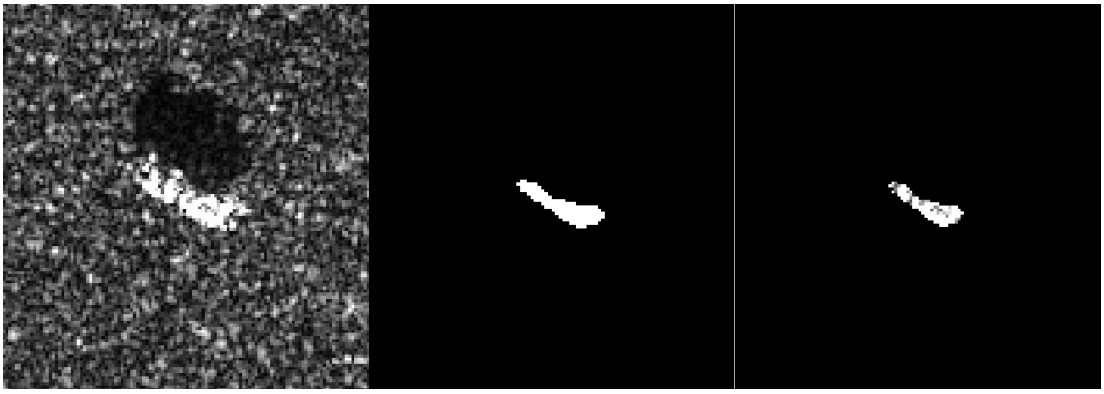

(a) (b) (c)

Figure 3.6: The procedure to produce texture for target region a. Original SAR image, b. TA C. Texture of target (TT -by multiplying Fig. 3.6-a by Fig. 3.6.b)

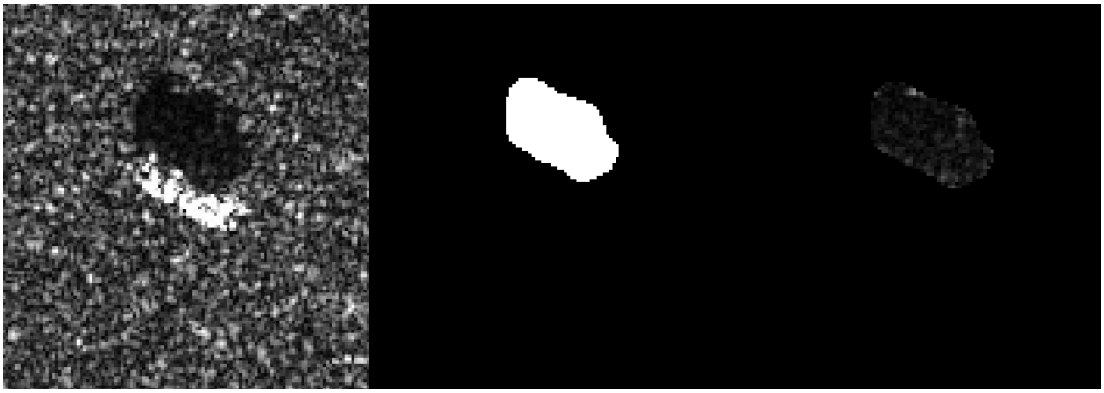

(a) (b) (c)

Figure 3.7: The procedure to produce texture for shadow region a. Original SAR image, b. SA, C. Texture of shadow (ST-by multiplying Fig. 3.7-a by Fig. 3.7.b)

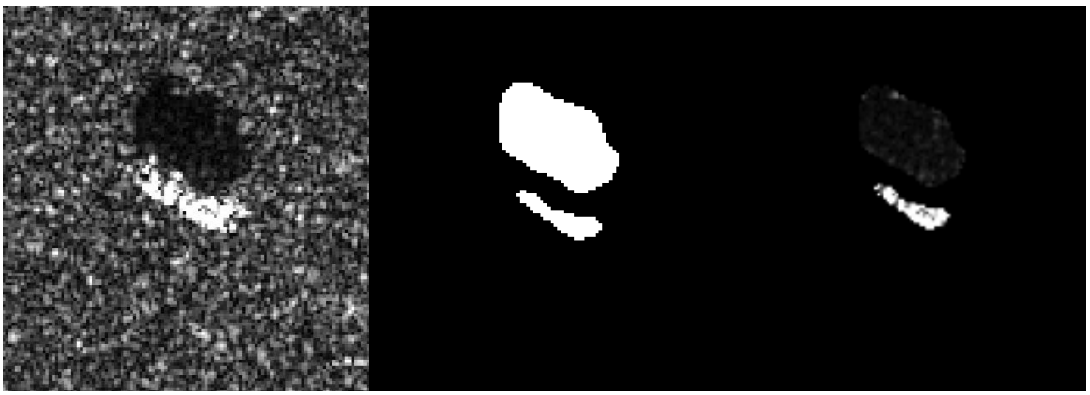

(a) (b) (c)

Figure 3.8: The procedure to produce texture for combined target-shadow region a. Original SAR image, b. TSA, C. Texture of combined target-shadow (TST by multiplying Fig. 3.8.a by Fig. 3.8.b)

Taking the area (or mask), it is multiplied with the input image to generate the texture containing texture of the target (TT), shadow (ST) and combined target shadow (TST) as it is illustrated in Fig. 3.6, Fig. 3.7 and Fig. 3.8 respectively.

3.3.4 Sobel filter followed by dilation

Sobel filter [64] is employed to perform edge detection on the mask image to detect the boundaries. In this regard, the edge boundaries of the target, shadow, and combined target-shadow regions are extracted. Dilation by 2×2 structuring element is used to connect the disconnected edges and emphasise the boundaries. The product image at this stage is called boundary. (The procedure to produce boundary from area for target (TB), shadow (SB), and combined target-shadow (TSB) are illustrated in fig 3.9, fig 3.10 and fig 3.11 respectively.

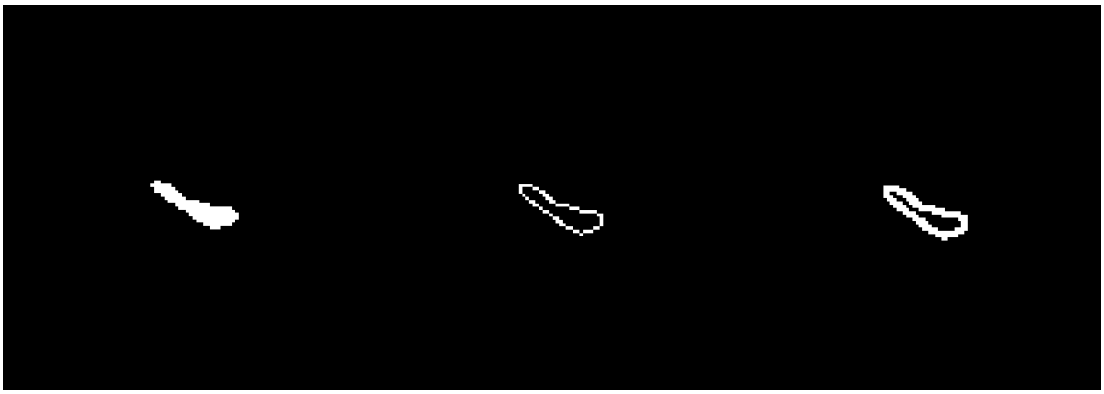

(a) (b) (c)

Figure 3.9: The procedure to produce boundary from area for Target region a. TA, b. Sobel filter, c. TB

(a) (b)

Figure 3.10: The procedure of produce boundary from area for shadow region a. SA, b. SB

(a) (b)

Figure 3.11: The procedure of produce boundary from area for combined target-shadow region a. TSA, b. TSB

In order to justify that preprocessing approach is good enough that not affect the overall performance significantly, we randomly selected few samples of different vehicles at different azimuth and depression angles. Manually we extracted region of interest of those samples. Then we compared the accuracy (ACC), True Positive Rate (TPR) /sensitivity, True Negative Rate (TNR)/specificity, and False Negative Rate (FNR)/miss of proposed preprocessing approach with alternative preprocessing in the literature respect to the manual segmentation.

Original Image	Threshold Manually	Threshold Automatically	Red color indicates false negative and green color indicated false positive

Figure 3.12: Comparison of Manual and Automatic thresholding

Figure 3.12 shows the manual and automatic theresholding. By comparing two methods we evaluated the false negative (FN) and false positive (FP) of automatic thresholding. FN and FP are shown in red and green respectively. Then ACC, TPR, TNR and FNR are evaluated as shown in Table 3.3:

Table 3.3: ACC, TPR, TNR and FNR of one sample

Sample Name	ACC (%)	TPR (%)	TNR (%)	FNR (%)
hb03799.000	99.14	89.53	99.27	14.47

We also considered more samples randomly and we evaluated ACC, TPR, TNR and FNR of each sample. Finally, we took the average as it shown in Table 3.4.

Table 3.4: Average of ACC, TPR, TNR and FNR of 20 samples

Method	Number of samples	ACC (%)	TPR (%)	TNR (%)	FNR (%)
Method introduced	20	98.88	92.51	99.44	21.26
Alternative Method [139]	20	98.01	93.11	97.30	24.42

As we observe the accuracy of automatic thresholding, which plays a critical role in this thesis, is high and it is close to the manual segmentation. Also in Table 3.4, we compared our method with alternative method [138] in which they adopt Logarithmic transformation followed by Morphological filter and geometric clustering operation. The comparison shows that preprocessing approach is comparable to alternative method.

3.4 Moment based feature extraction

Feature extraction algorithms extract unique target information from each image. Identifiability, translation, rotation and scale invariance [126] [127], affine invariance [133] and noise resistance [65] must be considered for the adopted algorithm. For those items, moment-based descriptors can be utilised as an effective region-based shape descriptor. In this thesis, twelve moment-based methods introduced both in Cartesian and polar coordinates as a robust feature extraction method. The details of the moment-based method are given in chapter 4. In chapter 5 two feature extraction techniques as Zernike Moment and Radical Chebyshev Moment are used, and their results are compared with respect to different ROIs as we studied in the previous subsection. In chapter 6 and 7, twelve moment-based methods are utilised as Legendre Moments, Chebyshev moment of first and second kind, Gegenbauer Moments, Jacobi Moments, Krawtchouk Moments, Zernike Moments, Pseudo Zernike Moments, Fourier Merlin Moments, Chebyshev Fourier Moments, Radial Harmonic Fourier Moment, and Radial Chebyshev Moments for feature extraction. Then different ranking methods used for selection of best features, which in turns improve the recognition rate. In chapter 8, Pseudo Zernike Moments are used by applying different ROIs. The improvement is made by an ensemble of classifiers.

3.5 Ranking

Twelve-moments are used for evaluating the accuracy of classification. These methods are then ranked according to 2 different approaches as Fisher criterion and entropy.

The aim of ranking features is to measure the relevance of features to select the most discriminative features which reduce the dimensionally of data-set, speeding up the learning process, and improving classification performance. Many approaches for feature ranking are introduced in the literature [66-70].

Let *D* represents a *n*×*m* matrix, where $D = [X_1, X_{2,} \dots, X_n]^T$ is the data-set containing of *n* samples, and $X_i = (x_{i1}, x_{i2,} \dots, x_{im})$ is a vector of *m* features. Let *f* be a vector of values of a feature defined as:

$$f_j = (x_{1j}, x_{2j}, \dots, x_{nj})^T \tag{3.3}$$

Let *F* be feature ranking applied on the database *D* as:

$$F = [f_r^1, f_r^2, \dots, f_r^n] \tag{3.4}$$

where the superscript denotes the position in the ranked list of a feature f_r and this list is ranked in descending order. Top *k* ranked features is selected; where *k* can be tuned experimentally [71].

3.6 Data fusion

Data fusion of SAR images used for the improvement of recognition rate by increasing the feature information of the images and for reducing the complexity of training by integrating various features. Three types of fusion are utilised in this thesis, feature level fusion, decision fusion and fusion among classifiers which is called ensemble of classifiers.

3.6.1 Feature level fusion

Fusion divided into different kinds [72]. One, which is used in this thesis, is called feature level fusion, which is a method of combining all features [73] or selected features [74] in series for obtaining a new feature vector.

In this study, all features introduced in chapter 5 are concatenated into a single feature vector. In chapter 5, features coming from different ROIs are fused. Feature fusion (FF) is defined as:

$$FF = [FV_1\ U\ FV_2\ U\ \dots U\ FV_n\ ] \tag{3.5}$$

where FV refers to the feature vector of each ROI (for example all features for texture in target regions form a feature vector) or feature vector of each method.

In chapter 6 and 7, the features are coming from 12 different moments. The first top *k* highest ranked methods are chosen and fused to form a data with *k×100* features.

In this thesis, avoiding the ambiguity among concatenated features, feature concatenation in chapter 5 (coming from different ROIs) is called feature fusion and feature concatenation in chapter 6 and 7 (coming from different moments) is called feature level fusion. Suppose that $frv_1, frv_2, \dots, frv_n$ are feature ranked vectors (FRV) then feature level fusion is defined as:

$$SF = [FRV_1\ U\ \ FRV_2\ U\ \dots U\ FRV_n]_{1\times s} \tag{3.6}$$

where *s* is the length of the vector for SF, *n* is the number of ranked methods such that $s \leq n$.

3.6.2 Decision fusion

The second type of fusion refers to decision fusion. The aim of decision fusion is to find the output label of each sample after different methods of moments are applied. In this regard, for any sample, first top *k* highest ranked methods are chosen and the class probability for each selected moment is evaluated. Four rules are associated with decision fusion as a max rule, sum rule, mean rule and median rule. The following example shows how decision fusion works with each rule. In this example one sample (sample number 10 belongs to BTR70) is chosen. The top 3 moment-based methods are applied and the class probability of each moment is calculated, summarised in Table 3.5.

Table 3.5: Class probability of top 3 moments of given sample

	First Moment			**Second Moment**			**Third Moment**		
Rules	**C 1**	**C 2**	**C 3**	**C 1**	**C 2**	**C 3**	**C 1**	**C 2**	**C 3**
Sample 10	0.899	0.097	0.004	0.969	0.030	0.001	0.629	0.356	0.015

3.6.2.1 Max rule

For each sample the class probability ($P_{i,j}$) is evaluated, where i = 1, 2, 3 refer to each class and j = 1, 2, …,12 refer to each selected moment. In max rule first, the maximum probability of each class for all of the selected moments is evaluated. Then for each sample (s), the label of the class with the highest probability is selected as follows:

$$\eta(s) = \{i|arg_i \max(\max_j(P_{i,j}))\} \quad (3.7)$$

The summary of an evaluation of max rule is given in Table3.6.

Table 3.6: Evaluation of max rule

	Class 1			Class 2			Class 3		
Rules	**M 1**	**M 2**	**M 3**	**M 1**	**M 2**	**M 3**	**M 1**	**M 2**	**M 3**
Probability	0.899	0.969	0.629	0.097	0.030	0.356	0.004	0.001	0.015
Maximum of Each class	0.969			0.356			0.015		
Maximum of Max	0.969			-			-		
Correspond-ing label	1			-			-		

3.6.2.2 Sum rule

In sum rule, the accumulated probability of the selected method of moments for each class is calculated. For each sample, the label corresponding to the maximum accumulated probability, $\mu(s)$ is reported to be the selected label for this technique, which is defined as:

$$\delta(s) = \{i | arg_i \max(\sum_{j=1}^{k} P_{i,j})\} \tag{3.8}$$

The summary of an evaluation of max rule is given in Table 3.7.

Table 3.7: Evaluation of sum rule

	Class 1			Class 2			Class 3		
Rules	**M 1**	**M 2**	**M 3**	**M 1**	**M 2**	**M 3**	**M 1**	**M 2**	**M 3**
Probability	0.899	0.969	0.629	0.097	0.030	0.356	0.004	0.001	0.015
Summation Each class	2.497			0.4830			0.02		
Max of Summation	2.497			-			-		
Correspond-ing label	1			-			-		

3.6.2.3 Mean rule

An alternative method is the mean rule, which can be considered as the normalised sum rule, defined as:

$$\mu(s) = \{i|arg_i \max(\frac{1}{k}\sum_{j=1}^{k} P_{i,j})\} \quad (3.9)$$

Table 3.8 shows the calculation procedure of mean rule.

Table 3.8: Evaluation of mean rule

	Class 1			**Class 2**			**Class 3**		
Rules	**M 1**	**M 2**	**M 3**	**M 1**	**M 2**	**M 3**	**M 1**	**M 2**	**M 3**
Probability	0.899	0.969	0.629	0.097	0.030	0.356	0.004	0.001	0.015
Mean Each class	0.832			0.161			0.007		
Max of Mean	0.832			-			-		
Correspond-ing label	1			-			-		

3.6.2.4 Median rule

Median probability of the selected method of moments for each class can be presented as:

$$\varpi(s) = \{i|arg_i \max(median(P_{i,j}))\} \quad (3.10)$$

Table 3.9 indicates the procedure for evaluation of the Median rule.

Table 3.9: Evaluation of median rule

	Class 1			**Class 2**			**Class 3**		
Rules	**M 1**	**M 2**	**M 3**	**M 1**	**M 2**	**M 3**	**M 1**	**M 2**	**M 3**
Probability	0.899	0.969	0.629	0.097	0.030	0.356	0.004	0.001	0.015
Median Each class	0.899			0.097			0.015		
Max of Median	0.899			-			-		
Correspond-ing label	1			-			-		

3.6.3 Ensemble of classifiers

In this thesis, the majority voting approach is utilised for determining the output label amongst different classifiers namely as SVM, k-NN, decision tree, random forest and LDA. Due to simplicity and acceptable performance, majority voting is one of the most useful combination methods [75]. In majority voting [76], the ensemble chooses a label of a class when either all classifiers agree on the specific class or one label receives the highest number of votes. If two labels have the same vote, the selection is made randomly between this two specific classes.

3.7 Classifiers

In this thesis, support vector machine is used for evaluating the accuracies of many algorithms. Additionally, in chapter 8, we deployed another four classifiers as a k-nearest neighbour, decision tree, random forest and LDA for improvement in accuracy by fusion among them. In the following subsection, we briefly represent each classifier and validation techniques, which are used in this study.

3.7.1 SVM classifier

The SVM is the most powerful classifier based on statistical learning principles. The SVM algorithm has been successfully adapted to various types of applications in MSTAR studies [77-81]. In the training stage, SVM tries to find the optimal class-separation hyperplane in the maximal margin, which is the distance between the support vectors on the boundary. Support vectors are located on the two parallel hyperplanes as shown in the Fig. 3.13 and the distance between them is $\frac{2}{\|w\|}$.

SVM was first adopted for pattern recognition in [82]. SVM Considers a set of samples which contains X (train set vector) and Y (corresponding labelled set vector) and the decision surface is defined as:

$$f(x) = \sum_i a_i y_i K(x_i, x_i') + b \tag{3.11}$$

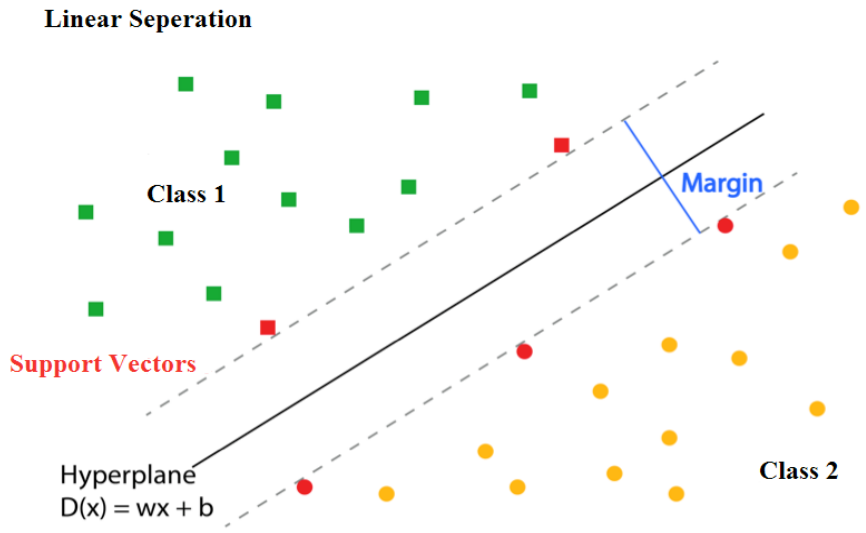

Figure 3.13: Illustration of the linear separation of the SVM hyper plane [83]

where a_i is weight constant which is optimised during the training process., *K(.,.)* is kernel function, x_i are support vectors, and *b* is bias and $y_i = \pm 1$ is the label of sample x_i . *K(.,.)* describes the behaviour of support vectors as the kernel function. Various kernels can be used during SVM training, such as linear, polynomial (cubic, quadratic) and radial basis function (RBF). In this thesis, we wildly used SVM classifier with a linear kernel. The Linear kernel is a good approximation and fast in comparison to nonlinear kernels (RBF, Cubic, etc.). Since solving the optimisation problem for a linear kernel is much faster it is often suggested to start with a linear kernel. The kernel function used in this thesis are listed in Table 3.10.

Table 3.10: Different kernel functions used in SVM

Method	Kernel Function
Linear	$k(x, x') = x^T x'$
Polynomial	$k(x, x') = (1 + x^T x')^d, \ for\ any\ d > 0$
RBF	$k(x, x') = e^{\frac{-\|x^T x'\|}{2\sigma^2}}\ for\ \sigma > 0$

3.7.2 k-NN classifier

k-Nearest Neighbour (k-NN) classification is the simplest classifier and is deployed in many MSTAR images applications [84-87]. Data split into a training set and a test set. The *k* nearest (usually *k=3*, *k=5*) training set objects are found, and then the distance between the test object and all the training objects are evaluated using a normalised Euclidean metric that is generated by:

$$D(A, B) = \sqrt{\frac{\sum_{i=1}^{g}(x_i - y_i)^2}{g}} \tag{3.12}$$

where g is the dimension of feature space and $A = (x_1, x_2, \dots, x_m)$ and $B = (y_1, y_2, \dots, y_m)$ are the features of train and test respectively.

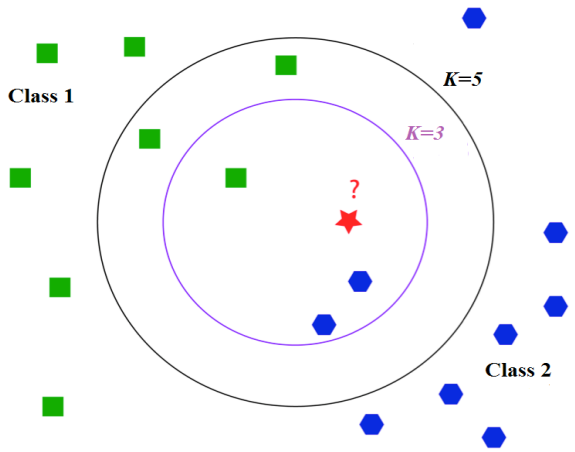

Figure 3.14: Illustration of the separation of the k-NN with different *k* value [83]

The classification is determined by majority vote of the *k* nearest neighbours. A simple example provided in Fig. 3.14. Different *k* value can affect the assigned class of the star. When *k = 3* the star corresponds to class 2 because the three closest neighbours involve two polygons (class 2) and a rectangle (class 1). However, by choosing *k= 5*, star corresponds to class 1, because the five closest neighbours include three rectangles (class 1) and two polygons (class 2).

3.7.3 Decision tree classifier

A decision tree is another classifier that used in some SAR images application [88-89]. Some few terms are used to design the decision tree algorithm are as follows [90]:

- Root node: It characterises whole sample, and gets further divided into two or more homogeneous sets.
- Splitting: This is a process of dividing a node into two or more sub-nodes.
- Decision node: When a sub-node splits into further sub-nodes, then it is called decision node.
- Leaf (Terminal node): Nodes do not split is called Leaf or Terminal node.

In the decision tree, firstly we choose the best feature of the data-set at the root of the tree. Then we divide the training set into subsets. Subset must contain data with the same value for a feature. The procedure above continues until we find terminal nodes in all the branches of the tree [89] as it is illustrated in Fig. 3.15.

For finding the best feature, many algorithms exist such as entropy, Chi-Square, and Gini Index (GI). In this study, GI is used for finding the best feature. GI measure frequency of detecting a random element incorrectly, it means a feature with lower GI, should be preferred. The GI for each feature is calculated as:

$$GI = 1 - \sum_{i=1}^{M} [p(i|C)]^2 \tag{3.13}$$

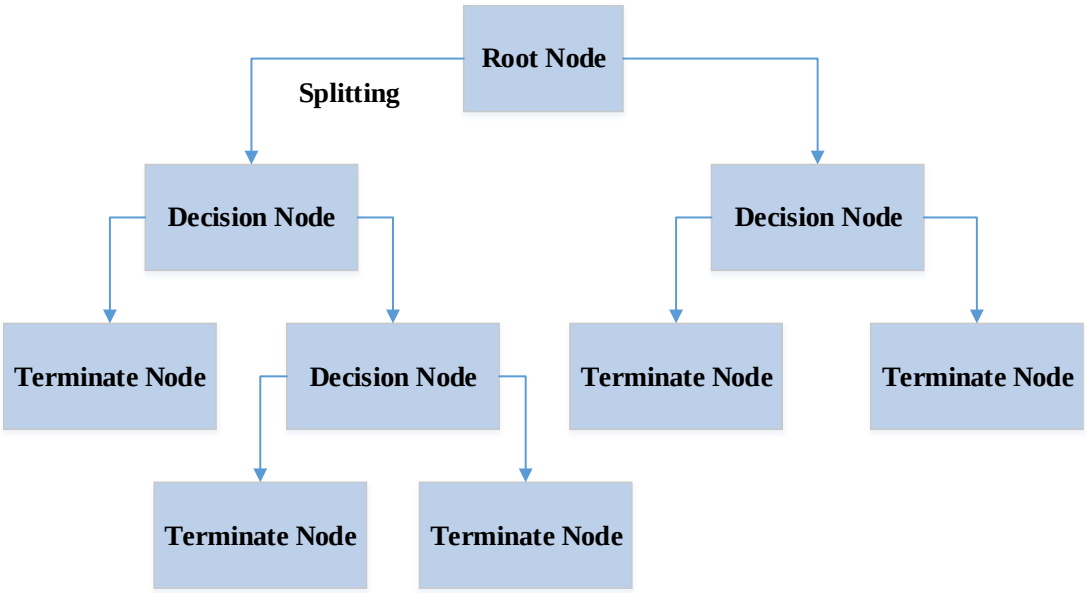

Figure 3.15: Decision tree algorithm

In each node, a feature with a lower value than other should position, as root and a branch with GI one should be converted to a terminal node. A branch with GI less than one needs further splitting.

3.7.4 Random forest classifier

Random forest [92] is another classifier, which is used in this study. RF is an ensemble technique in which the final prediction is based on the majority voting among decision trees. A final prediction is computed based on the results of the individual predictions. Figure 3.16 displays *n* decision trees and a classification obtained from each of them. In this example only 3 trees are shown. Tree 1 votes for label 1, while tree 2 and tree *n* vote for 2. The final prediction is based on majority voting among trees, which clearly will be 'Class 2'.

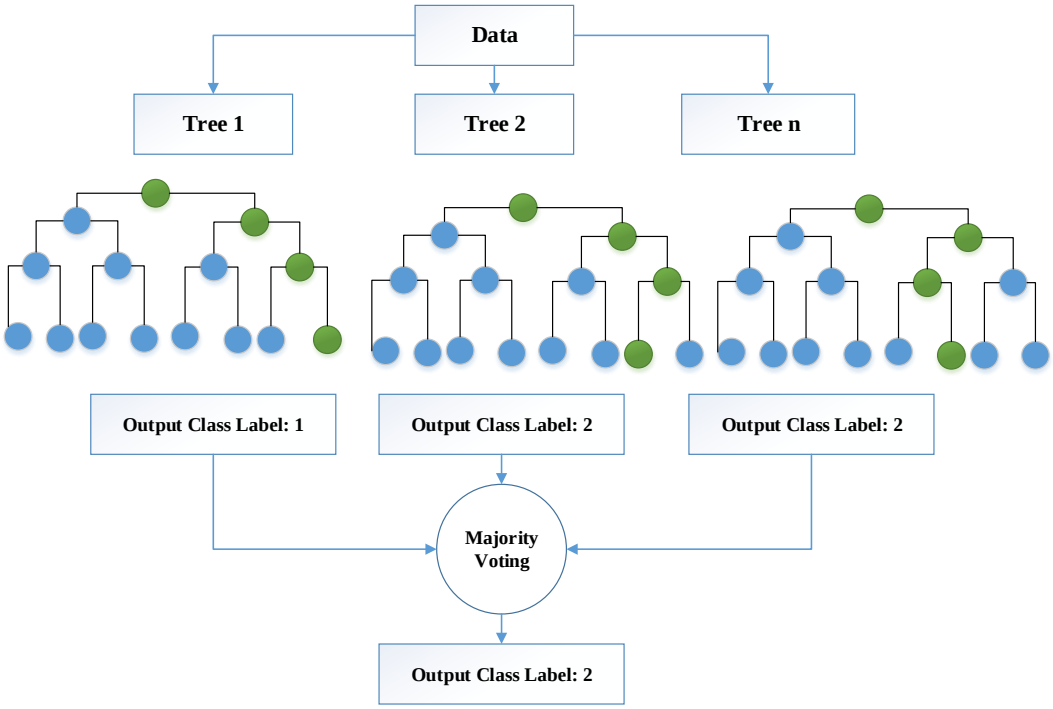

Figure 3.16: Random forest decision [93], tree 1 votes for label 1, while tree 2 and tree *n* vote for 2

3.7.5 Linear discriminant analysis classifier

Linear discriminant analysis (LDA) is also used in many MSTAR database as a classifier [94-96]. The aim of deploying LDA is to find a linear combination of features that separates two or more classes of objects. The resulting combination may be used as a linear classifier. Finding the linear discriminant among classes, the following algorithm is applied to a data matrix $X \in R^{M\times N}$, $x_i \in R^{M\times 1}$. Calculate the mean of each class as:

$$\mu_c = \frac{1}{N_c}\sum_{i=1}^{N_c} x_i \tag{3.14}$$

where N_c is the number of sample of each class.

Compute the global mean as:

$$\mu = \frac{1}{N}\sum_{i=1}^{N} x_i \tag{3.15}$$

Compute within-class scatter:

$$S_w = \sum_{i=1}^{c} S_i \tag{3.16}$$

where S_i

$$S_i = \sum (x - \mu_c)(x - \mu_c)^T \tag{3.17}$$

Compute between class scatter

$$S_B = \sum_{i=1}^{C} N_c(\mu_c - \mu)(\mu_c - \mu)^T \tag{3.18}$$

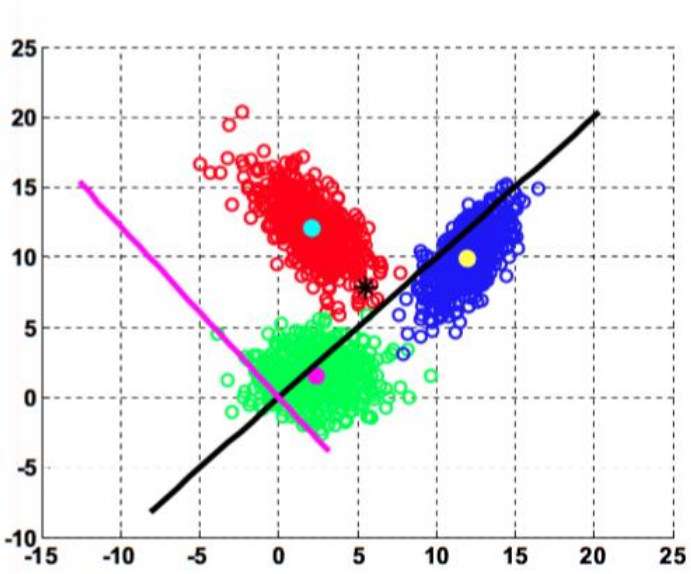

Figure 3.17: Illustration of the separation of the LDA [97]

Compute eigenvalues and eigenvectors of $S_w^{-1}S_B$ and sort them in descending order and. For C class problem, we have C-1 projection vectors. Hence optimal projection matrix W^* is the ones whose columns are the C-1 eigenvectors corresponding to the C-1 largest eigenvalues of:

$$S_w^{-1} S_B W^* = \lambda W^* \tag{3.19}$$

Figure 3.17 shows two optimal linear discriminant vectors that separate three different classes.

3.7.6 Validation approaches

Two validation approaches are used in this thesis as leave-one-out and *k*-fold cross validation techniques. In leave-one-out class validation, technique *s-1* samples are used as train set and remaining one is used as a test set. The algorithm is repeated *s* times and the total accuracy is the average of all accuracy in each iteration.

In the classification stage, *k*-fold class validation technique is applied. In this model, whole dataset is divided to *k* equal subsets. The algorithm is then repeated *k* times. Each time *k−1* subsets are chosen as a training sample set, and the remaining sample set is used for testing. In each fold, accuracy is calculated, and at the end of k-fold, the average accuracy is calculated [98]. In this thesis *k* is chosen to be 10.

3.8 Performance metrics

In this thesis, we compare the performances of the proposed methods using True Positive Rate (*TPR*) /sensitivity, True Negative Rate (*TNR*)/specificity, False Negative Rate (*FNR*)/miss rate and Accuracy to generate different metrics for performance analysis. They are defined as [99]:

$$Sensitivity = TPR = \frac{TP}{TP + FN} \tag{3.20}$$

$$Specificity = TNR = \frac{TN}{TN + FP} \tag{3.21}$$

$$Miss\ Rate = FNR = \frac{FN}{FN + TP} \tag{3.22}$$

$$Accuracy = \frac{TP + TN}{TP + FP + FN + TN} \tag{3.23}$$

where *TP*, *FN*, *TN* and *FP* denote true positive, false negative, true negative and false positive results respectively that are defined in the interval [0, 1].

3.9 Receiver operating characteristic curve

The ROC curve is generated by plotting the sensitivity against 1- specificity or the false positive rate (FPR) at various threshold settings. As it is illustrated in Fig. 3.18 it shows how well the recognition rate is. As the area under the curve is larger, then the recognition rate is higher.

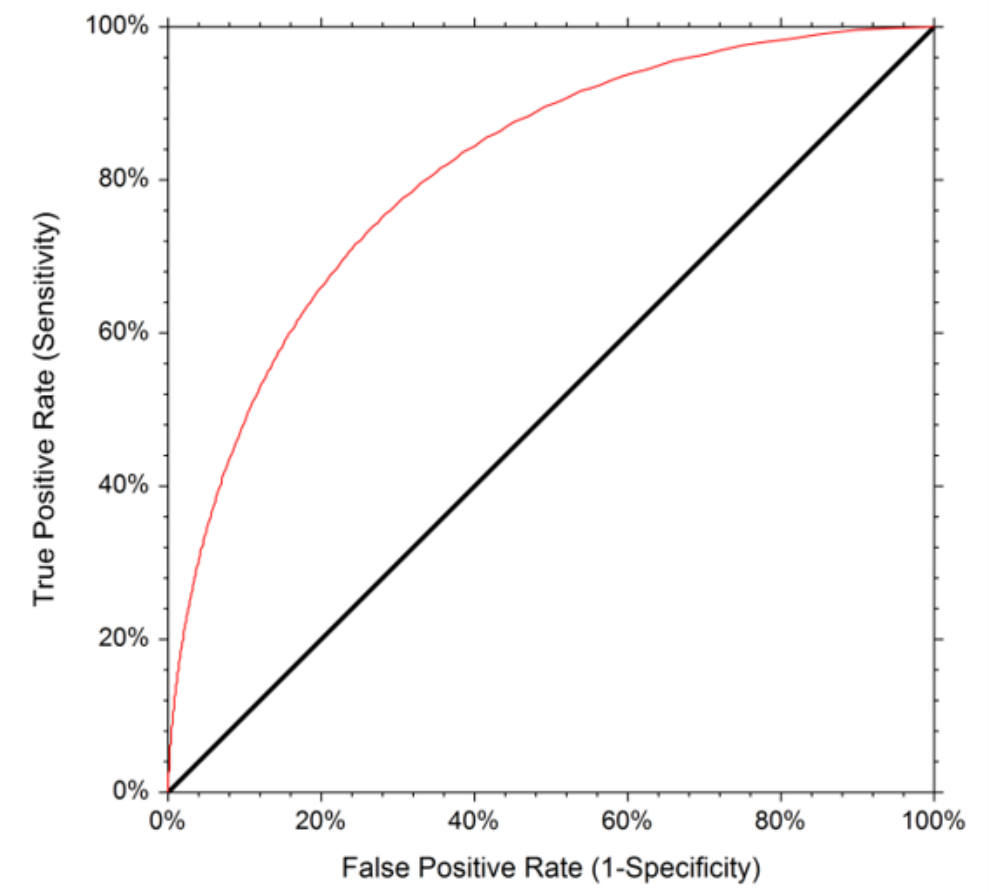

Figure 3.18: ROC curve analysis [100]

Chapter 4

MOMENTS AS 2D SHAPE DESCRIPTORS

4.1 Introduction

In this chapter, we have an overview of Moment Methods. Different types of moments are introduced, their properties are studied, and the pros and cons of those methods are discussed.

4.2 What are moments?

Moments are scalar quantities, which are used to capture dominant features of an Image [20] and are widely used in many applications such as image enhancement, object recognition, edge detection, texture analysis and image reconstruction [101-104]. Moments mathematically can be defined as the projection of a function onto a polynomial basis. For a digital SAR image *f (x,y)* general form of moments can be written as:

$$M_{p,q} = \int \int P_p(x) P_q(y) f(x,y) dxdy \tag{4.1}$$

where p and q are called the order and repetition of the moment respectively with $p,q=0,1,\ldots$. P_p and P_q are Polynomial Basis Function (PBF). The simplest moment is called Geometric Moment with the PBF, which is defined as the product of pixel coordinates ($x^p \times y^q$) [30] as:

$$M_{p,q} = \int_{-\infty}^{\infty} \int_{\infty}^{\infty} x^p y^q f(x,y) dxdy \tag{4.2}$$

Geometric Moments are widely used in image analysis and pattern recognition techniques due to their simplicity and invariance. As Hu states in [105] moment sequence $(M_{p,q})$ is uniquely determined by digital SAR image $f(x,y)$ in a limited part of the xy plane as:

$$M_{p,q} = \sum_{x} \sum_{y} x^p \, y^q f(x,y) \tag{4.3}$$

Each low order moment has a meaning. For the binary SAR image, $M_{0,0}$ is a mass of image. $\frac{M_{1,0}}{M_{0,0}}$, $\frac{M_{0,1}}{M_{0,0}}$ describe the centroid of an image in horizontal and vertical projection respectively. $M_{2,0}$ and $M_{0,2}$ is distribution of mass in x and y axis. Furthermore, if we normalize the image such that $M_{0,0}$ =1, then $M_{1,0}$ and $M_{0,1}$ are the mean value. For zero mean $M_{2,0}$ and $M_{0,2}$ are variances in x and y direction respectively and $M_{1,1}$ is the covariance. The horizontal and vertical skewness which measure the deviation of projection from symmetry are $\frac{M_{3,0}}{\sqrt{M_{2,0}^3}}$ and $\frac{M_{0,3}}{\sqrt{M_{0,2}^3}}$ respectively. The horizontal and vertical Kurtosis which measure the peak of the pdf are $\frac{M_{4,0}}{M_{2,0}^2}$ and $\frac{M_{0,4}}{M_{0,2}^2}$. However, unfortunately, the basis set $\{x_p, y_q\}$ is not orthogonal and it suffers from a high degree of information redundancy; therefore, orthogonal moments are introduced in the literature [11-25].

4.3 Orthogonal moments

Orthogonal Moments (OM) are introduced due to their stability, fast numerical implementation, avoiding a high degree of information redundancy, which in turn leads to a high classification rate and a greater robustness to random noise. Two groups of moments are defined in Cartesian and polar coordinates. In the following subsection, we have an overview about each group of OM and their properties.

4.3.1 Moments in Cartesian coordinates

This group of OM are further divided into two types namely continuous or discrete moment. The main motivation to define Moments in Cartesian is that they preserve orthogonality even on the sampled image [106]. The general form of moments in Cartesian form is given in Equation 4.1.

Some moments like Legendre moments are continuous while others such as Krawtchouck moments are discrete. However, for a digital SAR image, all moments can be approximated and viewed in the discrete domain as:

$$M_{p,q} = \sum\sum P_p\,(x) P_q(y) f(x,y) \tag{4.4}$$

To extract features, polynomial basis $P_p(x)$ and $P_q(y)$ should be evaluated for each method. Table 4.1 shows polynomial basis function of different method of moments in Cartesian coordinates. Using Equation 4.4, the first 100 features for each moment are extracted for any p = 0,1, ..., 9 and q = 0, 1, ..., 9. For a digital SAR image with size $N \times N$, variables x and y are normalized by mapping their values between -1 and 1 as follows:

$$x = -1 + 2\frac{x}{N-1} \qquad , \qquad y = -1 + 2\frac{y}{N-1} \tag{4.5}$$

4.3.1.1 Continuous moments in Cartesian

Legendre moments, Chebyshev moments, Gegenbauer moments and Jacobi moments are continuous moments which are defined on the Cartesian coordinate. Generalized Hyper-geometric series should be determined first before any further processing as:

$${}_pF_q\left(a_1, a_2, \dots, a_p; b_1, b_2, \dots, b_q; z\right) = \sum_{k=0}^{\infty} \frac{(a_1)_k (a_2)_k \dots (a_p)_k}{(b_1)_k (b_2)_k \dots (b_q)_k} \frac{z^k}{k!} \tag{4.6}$$

where $(a)_k$ is called pochhammer symbol and it is defined as:

$$(a)_k = a(a+1)\ldots(a+k-1) = \frac{(a+k-1)!}{(a-1)!} = \frac{\Gamma(a+k)}{\Gamma(a)} \tag{4.7}$$

In Equation. 4.6, *(i)* terms are defined in the numerator for any indexes up to *p* and *(ii)* terms in the denominator for any indexes up to *q*.

Table 4.1: Polynomial basis functions of different moments on Cartesian coordinate

Method	Polynomial Basis Function
LM	$P_p(x) = {}_2F_1(-p, p+1; 1; \frac{1-x}{2})$
CM #1	$P_p(\mathrm{x}) = {}_2F_1(-\mathrm{p}, \mathrm{p}; \frac{1}{2}; \frac{1-x}{2})$
CM #2	$P_p(\mathrm{x}) = (\mathrm{p}+1)\,{}_2F_1(-\mathrm{p}, \mathrm{p}+2; \frac{3}{2}; \frac{1-x}{2})$
GM	$P_p^{(\lambda)}(x) = \frac{\Gamma(\mathrm{p}+2\lambda)}{p!\,\Gamma(2\lambda)}\,{}_2F_1(-p, p+2\lambda; \lambda+\frac{1}{2}; \frac{1-x}{2})$
JM	$P_p^{(\alpha,\beta)}(x) = \binom{p+\alpha}{p}\,{}_2F_1(-p, p+\alpha+\beta+1; \alpha+1; \frac{1-x}{2})$

Although the aforementioned general form is valid for evaluating different moments, practically for efficient calculation with minimum computational complexity, a recurrence formula is also suggested in [20]. In the processing section, we briefly introduce moments that have been used for feature extraction in Cartesian coordinates with their recurrence formula.

4.3.1.1.1 Legendre Moments (LMs)

LMs are widely applied in different applications in image processing. In comparison to Geometric moments [107], they have a more efficient representation of an image with less amount of information redundancy. LMs with a complete orthogonal basis set is defined over the interval [-1, 1]. The recurrence relation can be defined as:

$$P_0(x) = 1$$
$$P_1(x) = x \tag{4.8}$$
$$P_{p+1}(x) = \frac{2p+1}{p+1} x P_p(x) - \frac{p}{p+1} P_{p-1}(x)$$

4.3.1.1.2 Chebyshev Moments (CMs)

Two types of CMs are introduced in the literature [107]: CM#1 (the first kind) and CM #2 (the second kind). They only differ by initial value of $P_1(x)$ term. This value is *x* for CM #1 while the value for CM #2 is *2x*. CM #2 is more often used in image processing applications. The recurrence formula for the second kind (CM #2) is defined as:

$$P_0(x) = 1$$
$$P_1(x) = 2x \tag{4.9}$$
$$P_p(x) = 2x P_{p-1}(x) - P_{p-2}(x)$$

The graph of the CM #1 are shown Fig. 4.1. This graph shows different polynomials up to order 6. The kernel functions of the 2-Dimensional CM #1 on $\langle -1, 1\rangle \times \langle -1, 1\rangle$ is illustrated in Fig. 4.2.

4.3.1.1.3 Gegenbauer Moments (GMs)

GMs have the extra parameter λ. The recurrence formula is defined as:

$$P_0^{(\lambda)}(x) = 1$$
$$P_1^{(\lambda)}(x) = 2\lambda x \tag{4.10}$$
$$P_{p+1}^{(\lambda)}(x) = \frac{2(p+\lambda)x}{p+1} P_p^{(\lambda)}(x) - \frac{p+2\lambda-1}{p+1} P_{p-1}^{(\lambda)}(x)$$

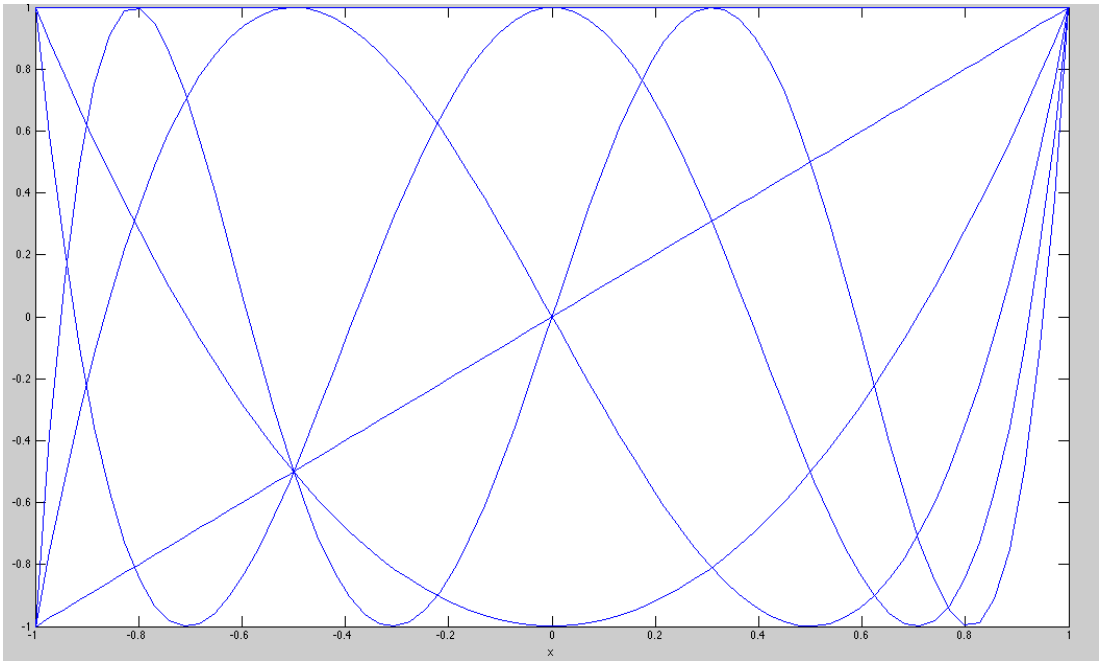

Figure 4.1: The graphs of the CM #1 up to the sixth degree

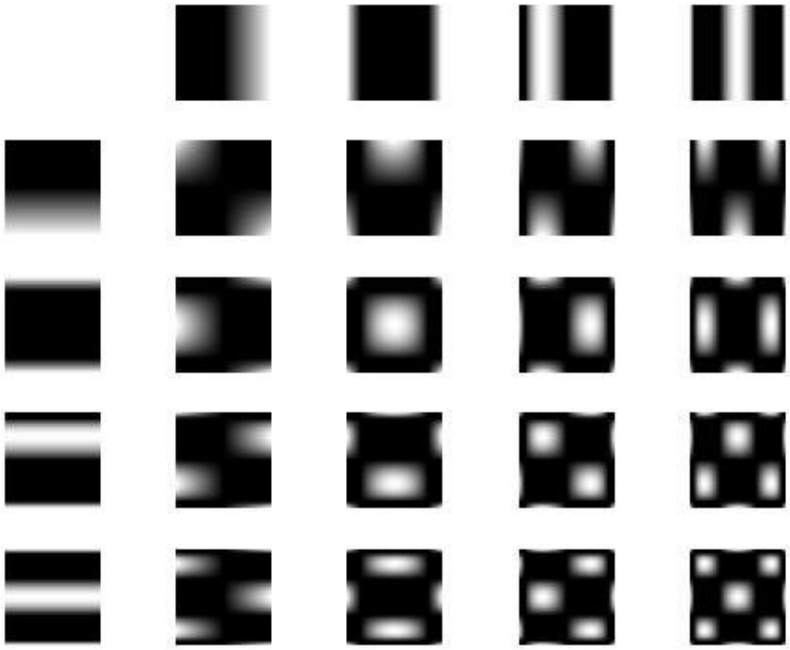

Figure 4.2: The graphs of 2D kernel functions of the CM #1 up to fourth order

A special case occurs when $\lambda = 0.5$. By substituting λ into Equation 4.10, LM is obtained. Another special case is $\lambda = 1$ which gives CM of the second kind. In this

study we choose λ to be 0.75 to illustrate the polynomial that has properties between Legendre Moment and Chebyshev of the second kind.

4.3.1.1.4 Jacobi Moments (JMs)

A more general form of the orthogonal moment in a Cartesian form is JM with two parameters $\alpha \; and \; \beta$ with $\alpha > -1 \; and \; \beta > -1$. Setting $\alpha = \beta \; to \; \lambda - \frac{1}{2}$, 0, $-\frac{1}{2}$, and $\frac{1}{2}$, GM, LM, CM of the first kind and CM of the second kind are generated, respectively. In this study $\alpha = \beta = 1$ is used for extracting features in a SAR Image. The recurrence formula for Jacobi is:

$$P_0^{(\alpha,\beta)}(x) = 1$$

$$P_1^{(\alpha,\beta)}(x) = \frac{1}{2}(\alpha - \beta + \alpha x + \beta x + 2x)$$

$$P_{p+1}^{(\alpha,\beta)}(x) = \frac{((2p+\alpha+\beta+1)(\alpha^2-\beta^2) + (2p+\alpha+\beta)_3 x}{C} P_p^{(\alpha,\beta)}(x) - \frac{2(p+\alpha)(p+\beta)(2p+\alpha+\beta+2)}{C} P_{p-1}^{(\alpha,\beta)}(x) \quad (4.11)$$

where $C = 2(p+1)(p+\alpha+\beta+1)(2p+\alpha+\beta)$

4.3.1.2 Discrete moments in Cartesian coordinate

Many moments are defined in discrete named as Krawtchouk Moments, Racah Moments, Meixner Moments, Charlier Moments, and Hahn Moments. However, the computational complexity of the methods above is too high. In the following subsection, we only consider Krawtchouk Moments.

4.3.1.2.1 Krawtchouck Moments (KWs)

The general PBF form of KM is written as:

$$P_p^{(\varsigma)}(x, N) = {}_2F_1(-p, -x; -N; \frac{1}{\varsigma}) \quad (4.12)$$

and the recurrence formula of KW is as:

$$P_0^{(\varsigma)}(x,N) = 1$$
$$P_1^{(\varsigma)}(x,N) = 1 - \frac{x}{N\varsigma}$$
$$P_{p+1}^{(\varsigma)}(x,N) = \frac{N\varsigma - 2p\varsigma + p - x}{(N-p)} P_p^{(\varsigma)}(x,N) - \frac{p(1-\varsigma)}{(N-p)\varsigma} P_{p-1}^{\varsigma}(x,N) \quad (4.13)$$

where N is the size of $N \times N$ SAR image and ς is the localization factor of moment and is defined between the interval 0 and 1. A common choice for selecting ς is 0.5 [20].

4.3.2 Moments in polar form

Radial moments form a complete orthogonal set on the unit disc $(x^2 + y^2) \leq 1$ as:

$$M_{p,q} = \int_0^{2\pi} \int_0^1 R_{pq}(r)\, e^{-iq\theta} \tilde{f}(r,\theta) r dr d\theta \quad (4.14)$$

where $\tilde{f}(r,\theta) = f(rcos\theta, rsin\theta), R_{pq}(r)$ called radial part of polynomial and $e^{-iq\theta}$ indicates angular part of polynomials. ρ, θ refer to transformation from Cartesian to polar coordinates which is defined as:

$$r = \sqrt{x^2 + y^2}, \qquad and\ \ \theta = \tan^{-1}(\frac{y}{x}) \quad (4.15)$$

Zernike moments (ZMs), Pseudo Zernike moments (PZMs), Fourier Merlin moments (FMMs), Chebyshev Fourier moments (CFM), Radial Harmonic Fourier moments (RHFMs), and Radial Chebyshev moments (RCMs) are the methods that widely used in the polar coordinates. They only differ by the radial part of a polynomial as summarised in Table 4.2. In the following subsection, we look at the behaviour of some moments at a glance.

Table 4.2: Radial part of polynomial basis function of different moments in polar coordinate

Method	Radial part of Polynomial Basis Function
ZM	$R_{pq}(r) = \sum_{s=0}^{(\frac{p-\lvert q\rvert}{2})} \frac{(-1)^s (p-s)!\, r^{p-2s}}{s!\left(\frac{p+\lvert q\rvert}{2}-s\right)!\left(\frac{p-\lvert q\rvert}{2}-s\right)!}$
PZM	$R_{pq}(r) = \sum_{s=0}^{p-\lvert q\rvert} \frac{(-1)^s (2p+1-s)!\, r^{p-s}}{s!\,(p-\lvert q\rvert-s)!\,(p+\lvert q\rvert+1-s)!}$
FMM	$R_p(r) = \sum_{s=0}^{n} (-1)^{p+s} \frac{(p+s+1)!}{(p-s)!\,s!\,(s+1)!} r^s$
CFM	$R_p(r) = \sqrt{\frac{8}{\pi}} (\frac{1-r}{r})^{\frac{1}{4}} \sum_{s=0}^{\frac{(p+2)}{2}} (-1)^s \frac{(p-s)!}{s!(p-s)!} (2(2r-1))^{p-2s}$
RHFM	$R_p(r) = \begin{cases} \frac{1}{r} & \text{if p=0} \\ \sqrt{\frac{2}{r}} \sin((p+1)\pi r) & \text{if p is odd} \\ \sqrt{\frac{2}{r}} \cos(p\pi r) & \text{if p is even} \end{cases}$
RCM	$R_p(\mathrm{r}) = \frac{p!}{\rho(r,N)} \sum_{s=0}^{p} (-1)^{p-s} \binom{N-1-s}{p-s} \binom{p+s}{p} \binom{r}{s}$ where $(r,N) = \frac{N\left(1-\frac{1}{N^2}\right)\left(1-\frac{2^2}{N^2}\right)\ldots\left(1-\frac{p^2}{N^2}\right)}{2p+1}$, $p = 0,1,\ldots,N-1$

4.3.2.1 Zernike Moments (ZMs)

Orthogonal moments in polar are introduced mainly because of their unique property to be rotational invariant. ZMs are the most popular methods that are used in the literature. p = 0,1, 2, ...,18 is the called order of ZM and q is the repetition of ZM with the following condition:

$$p - |q| = even, \qquad |q| \leq p \tag{4.16}$$

4.3.2.2 Pseudo Zernike Moments (PZMs)

PZMs are as an alternative to traditional ZMs with the only difference in their orthogonal radial polynomial. PZMs have a better feature representation capability and are more robust to noise than ZMs.

$$0 \leq |q| \leq p, p = 0,1,2, ..., 10 \tag{4.17}$$

PZMs offer more features than ZMs of the same order because of limitation in Equation 4.16 for ZM. The lower order contains more dominant information.

4.3.2.3 Radial Chebyshev Moments (RCMs)

The RCMs are defined on the discrete domain. RCM of order *p* and repetition *q* for an image of size $N \times N$ with $m = (N/2) + 1$ is one type of the radial moment which is defined in the discrete domain as [106]:

$$R_{pq} = \frac{1}{2\pi\rho(p,m)} \sum_{r=0}^{m-1} \sum_{\theta=0}^{2\pi} t_p(r) * e^{-jq\theta} * f(r,\theta) \tag{4.18}$$

where $t_p(r)$ is an orthogonal polynomial function for an image of size $N \times N$ which can be represented by a recurrence formula as:

$$\begin{gathered} t_0(x) = 1 \\ t_1(x) = \frac{(2x - N + 1)}{N} \\ t_p(x) = \frac{(2p-1)t_1(x)t_{p-1}(x) - (p-1)\left\{1 - \frac{(p-1)^2}{N^2}\right\} t_{p-2}(x)}{p} \end{gathered} \tag{4.19}$$

and $\rho(p,N)$ is the squared-norm as

$$\begin{gathered} \rho(p,N) = \frac{N\left(1 - \frac{1}{N^2}\right)\left(1 - \frac{2^2}{N^2}\right) \ldots \left(1 - \frac{p^2}{N^2}\right)}{2p+1} \\ p = 0,1, \ldots, N-1 \end{gathered} \tag{4.20}$$

Chapter 5

TARGET RECOGNITION IN SAR IMAGES USING RADIAL CHEBYSHEV MOMENTS

5.1 Introduction

In this chapter, a new algorithm for classification of ground vehicles from standard SAR images is proposed. Radial Chebyshev moment (RCM) is a discrete orthogonal moment that has distinct advantages over continuous moments on polar coordinates for feature extraction. Unlike Hue moments, its orthogonal basis leads to having minimum information redundancy, and its discrete characteristics explore some benefits over Zernike moments (ZM) due to having less numerical errors and less computational cost owing to normalisation. In this context, we propose to use RCM as the feature extraction mechanism on the segmented image and to compare results of the fused images with Zernike moments. Firstly, by applying different thresholds, target and shadow regions of each SAR image are extracted separately. Then, segmented images are fused, based on the combination of the extracted area, boundary and texture. Experimental results verify that the accuracy of RCM improves significantly by using fusion of different ROIs. It improves the total accuracy of the classification by 8.57%.

As mentioned earlier moving stationary target acquisition and recognition (MSTAR), a standard SAR-ATR database [9], is used for testing and validation of different algorithms.

Due to the background of SAR images, and to extract the useful information, various preprocessing techniques are introduced in the literature [64], [108-109]. Furthermore, studies explored that shadowing parts have a significant effect on the accuracy of detection in parallel to target information and hence feature fusion based on both parts is recommended in [110].

Different approaches for feature extraction have been introduced for SAR image target recognition. Linear discriminant analysis (LDA), principal component analysis (PCA) and independent component analysis (ICA) techniques have been commonly used in pattern recognition [111–114]. The problem associated with these techniques is that generally they are sensitive to noise [41] and are rotation variant. To overcome these problems, moment-based descriptors can be utilised as an effective region-based shape descriptor. Hue invariant moments are the simplest method for generating shape descriptors [105]. Although they are rotational invariant, they suffer from a high degree of information redundancy since the bases are not orthogonal [107]. Also, higher order moments are noise sensitive. In order to avoid these problems, Zernike moment (ZM) was suggested as a continuous orthogonal moment, which was used in [28]. Zernike polynomials are rotation invariant with its robustness to noise and having a minimum information redundancy since the basis is orthogonal.

However as mentioned earlier, Zernike moments are defined as a continuous function; hence for a digital image, approximation by discrete summation is considered which leads to numerical errors in computation of moments. Moreover, this approximation can affect some properties such as orthogonally and rotational invariance. Zernike moments are expressed inside the unit disc $x^2 + y^2 \leq 1$, which increases the

computational complexity with an appropriate transformation of the image coordinate space [115]. To reduce all the above problems, a discrete orthogonal moment called radial Chebyshev moment (RCM) is introduced to reduce both computational complexities, due to normalisation and computational error caused by approximations [116].

In this chapter, three types of segmentation were applied to generate areas of interests: area, boundary and texture, to be used in the feature extraction process. This approach is adopted for both target and shadow regions of the input image. As feature extractors, ZM and RCM were employed to generate region feature descriptors. Finally, region descriptors are fused by concatenating the feature vectors into longer descriptors to be used in the support vector machine (SVM) classifier. Results showed that in both feature extraction methods, total accuracy of fused segmentation of target and shadow regions improves significantly. Further comparison between ZM and RCM reveals that accuracy of RCM is higher than ZM by 8%. In addition to the improvement gained by using RCM instead of ZM, a fusion of the feature descriptors obtained from segmented areas will also improve the performance by 6%.

This chapter consists of two contributions. The first contribution involves adding the shadow region of the target as an extra source of features improving the SAR recognition. Shadow regions are areas on the ground that are not covered by the radar signal; as a result, no return signal is received, and these areas appear dark in the SAR images. This property is utilised for improving the total accuracy.

The second contribution is about feature fusion. An input SAR image segmented with different techniques can be represented by fusing the region descriptors of these images, which improves the overall accuracy.

5.2 Proposed method for feature fusion using RCM of different ROIs

The details of the proposed method are given in Fig. 5.1. Each SAR image contains a target, shadow and background. Our aim is to remove the background while preserving the target and shadow regions. Histogram equalisation and average filter are used to remove the background. Also, by utilising two different threshold values, target and shadow regions are separated. Furthermore, combining target and shadow corresponds to the third part to be considered. Therefore, a SAR image is categorised into three different parts: target, shadow and combined target-shadow.

Each target, shadow or combined target-shadow is segmented into three different objects: namely, area, which refers to the binary shape region, boundary, which indicates boundary area and texture, which extracts whole texture of the region of interest. Area corresponds to the mask covering the region of interest after background removal as illustrated in Fig. 5.1. Boundary is the processed SAR images after applying Sobel filter followed by dilation to area as it can be seen in Fig. 5.2. Texture is the multiplication of original image by area.

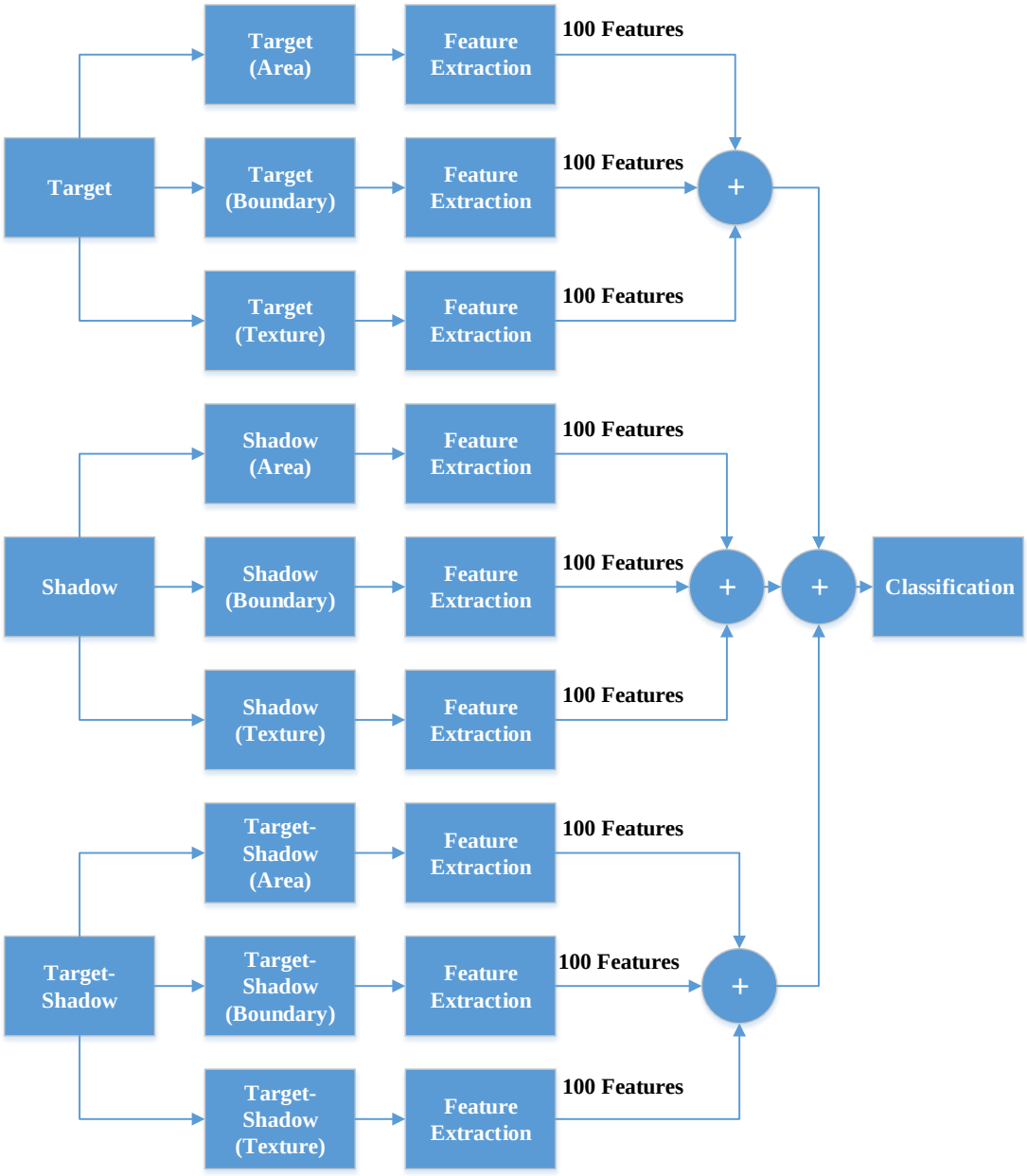

Figure 5.1: Block diagram of the proposed method

RCM is introduced in addition to ZM for feature extraction of the given SAR images. For each segmented object, 100 features are extracted. Feature vectors coming from each of the three-segmented objects are merged to form a vector of 300 features. For a single SAR image, target, shadow and combined target-shadow regions with a vector of 300 features each, is fused by concatenation resulting in a final feature vector of

900 features to be used in classification. We choose library support vector machine (LIBSVM) which is a standard support vector machine (SVM) classifier with tenfold cross validation.

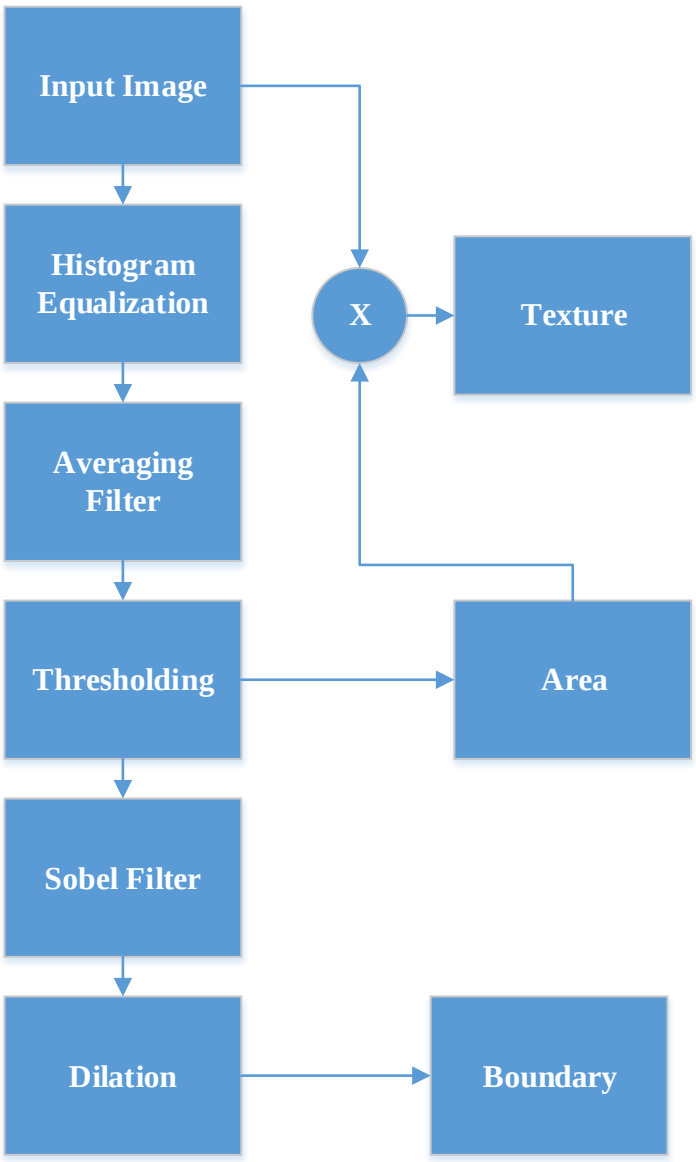

Figure 5.2: Segmentation method for input SAR image

5.2.1 Segmentation

SAR images have a background, which should be removed before further processing. All SAR images in this data-set (MSTAR) are required to have the histogram equalisation, averaging filter, threshold, Sobel filter and dilation to remove background as given in Fig. 5.2.

Histogram equalisation is the first step of the segmentation process. By applying it, the output will have pixel values distributed equally on the interval [0, 1]. An equalised image then is followed by an average filter through which the image is smoothened to reduce noise artifacts. The filter mask size of the average filter was chosen to be 11 × 11.

The thresholding is next applied to the smoothed image. As discussed in the previous section, it is essential to extract the edges of both target and shadow regions; therefore, it is necessary to apply different threshold levels for obtaining both parts. Two thresholds have been adopted in this thesis, τ and ξ for the segmentation of the target and shadow regions, respectively. The grey level threshold is defined as a constant between 0 and 1. To detect the target, which is brighter in the image, it is necessary to choose the constant closer to 1. In [64], τ is chosen to be 0.8. The experimental results validate the effectiveness of τ at 0.8 for efficient segmentation. On the other hand, for detecting shadow regions, which cover the darker area in the image a constant, ξ , closer to zero should be chosen. In this context, ξ is chosen to be 0.2 for effective shadow segmentation. The thresholded images at this stage can be considered to be area/mask corresponding to target and shadow regions, respectively.

Using a mask image, it is multiplied with the input image to generate the texture containing texture of the target as well as that of the shadow.

In the next step, Sobel filter [64] is adopted to perform edge detection on the mask image. Dilation by 2 × 2 structuring element is used to connect the disconnected edges and emphasise the boundaries. In this regard, the edge boundaries (boundaries) of the target and shadow regions are extracted for further processing.

Figure 5.3 explores all segmented parts and regions of a sample image (hb03787.004 image) including area, boundary and texture of target (Fig. 5.3.a-c (respectively)), shadow (Fig. 5.3 d–f (respectively)) and both (Fig. 5.3 g–i (respectively)). For each segmented image, a feature extraction method was applied to extract a distinct number of features. In ZM method, for each segmented image 34 features were extracted; as a result, the total number of extracted features for a single image is 306, while for RCM 100, features are extracted for the single segmented image, which means 900 of features were extracted from every given image.

5.2.2 Feature extraction by using ZM and RCM

Two robust shape-based feature extraction techniques are radial Chebyshev moment [104] and Zernike moment [117].

Zernike moments are orthogonal moments that consist of a set of complex polynomials, known as Zernike polynomials. It forms a complete orthogonal set on the unit disc $(x^2 + y^2) \leq 1$. A complex Zernike moment is defined as [118]:

$$Z_{nm} = \frac{(p+1)}{\pi} \int_x \int_y V_{pq}^*(r,\theta) f(x,y) dxdy \tag{5.1}$$

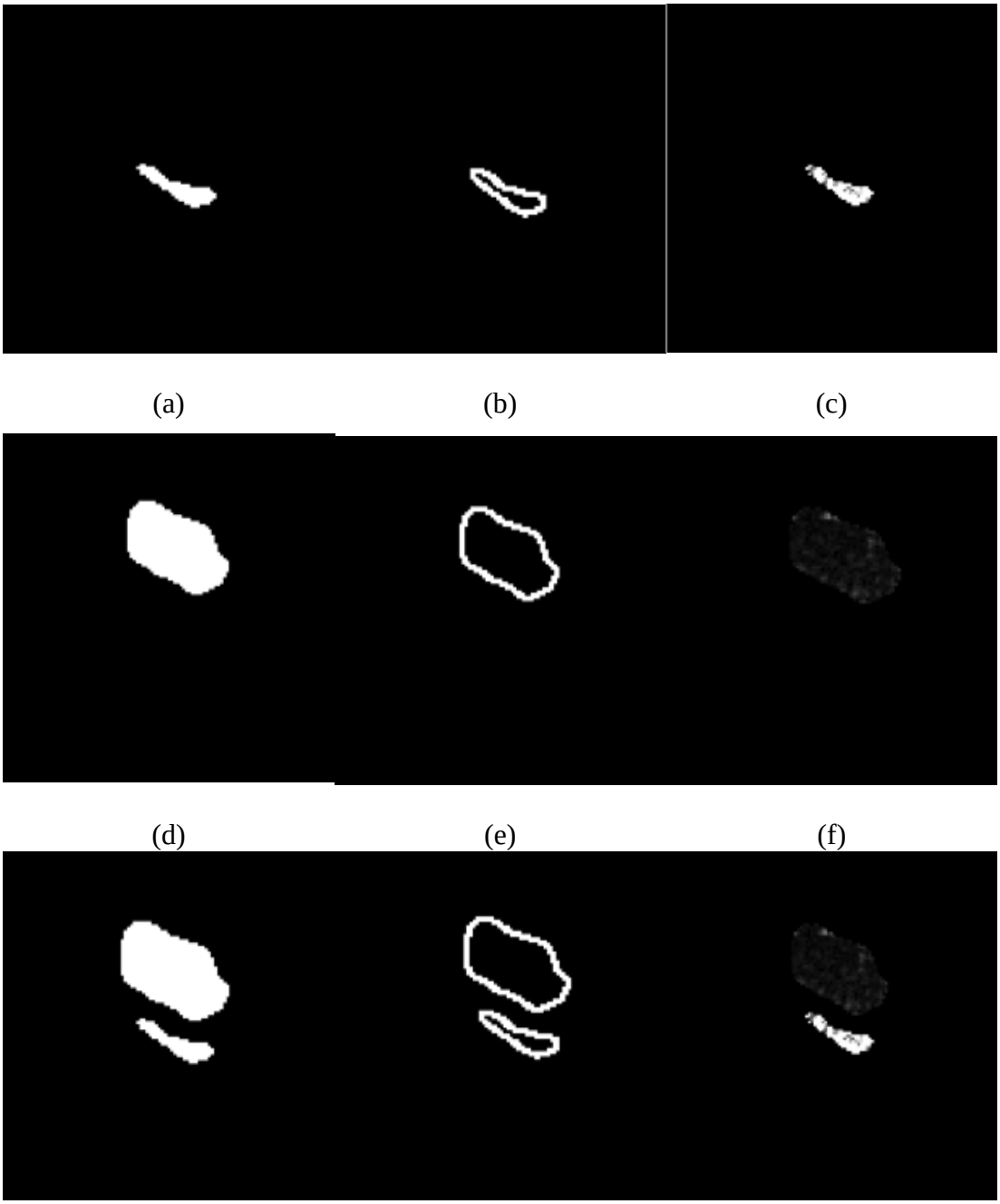

(a) (b) (c)

(d) (e) (f)

(g) (h) (i)

Figure 5.3: First column: Area of target (a), shadow (d) and combined target-shadow (g). Second column: Boundary of target (b), shadow (e) and combined target-shadow (h). Third column: Texture of target (c), shadow (f) and combined target-shadow (i).

For a digital image $f(x, y)$ function with the size of $N \times N$, Equation 5.1 can be approximated as in [119]:

$$Z_{nm} = \frac{(p+1)}{\pi} \sum_{x=1}^{N} \sum_{y=1}^{N} V_{pq}^{*}(r,\theta) f(x,y) \tag{5.2}$$

where $r\ and\ \theta$ in the polar coordinates are defined as:

$$r = (x^2 + y^2)^{\frac{1}{2}}, \qquad and \qquad \theta = tan^{-1}(\frac{y}{x}) \tag{5.3}$$

p = *1, 2, ...* is the order of Zernike polynomial, and q is the repetition of Zernike moment that takes on positive and negative integer subject to the following conditions:

$$p - |q| = even, \qquad |q| \leq p \tag{5.4}$$

The symbol $*$ indicates the complex conjugate. An orthogonal basis function for the Zernike moments is defined by:

$$V_{pq}(r,\theta) = R_{pq}(r) e^{jq\theta} \tag{5.5}$$

where R_{pq} is defined below:

$$R_{pq}(r) = \sum_{s=0}^{(\frac{p-|q|}{2})} \frac{(-1)^s (p-s)!\, r^{p-2s}}{s!\left(\frac{p+|q|}{2} - s\right)!\left(\frac{p-|q|}{2} - s\right)!} \tag{5.6}$$

In [28] 34, Zernike moments are calculated for each image based on Table 5.1. For each segmented image, 34 features are extracted. In this thesis, with an addition of segmented mask, we use the boundary and texture as well for the target images. Furthermore, we use the area, texture and boundary of the shadow regions. Finally, we use three images for combined target and shadow images. In this respect, we use nine images for each object with 34 features for each image, respectively, generating a vector of 306 features in the shape descriptor.

Table 5.1: List of Zernike moments used for each segmented image

Order	Moments	# of Moments	Accumulated Moments
2	$Z_{2,0}$, $Z_{2,2}$	2	2
3	$Z_{3,1}$, $Z_{3,3}$	2	4
⋮	⋮	⋮	⋮
9	$Z_{9,1}$, $Z_{9,3}$, $Z_{9,5}$ $Z_{9,7}$ $Z_{9,9}$	5	28
10	$Z_{10,0}$, $Z_{10,2}$, $Z_{10,4}$, $Z_{10,6}$, $Z_{10,8}$, $Z_{10,10}$	6	34

Table 5.2: List of Radial Chebyshev moments used for each segmented image

Order (p)	Moments	# of Moments	Accumulative #
1	$R_{1,1}$, $R_{1,2}$, $R_{1,3}$, $R_{1,4}$, $R_{1,5}$, $R_{1,6}$, $R_{1,7}$, $R_{1,8}$, $R_{1,9}$, $R_{1,10}$	10	10
2	$R_{2,1}$, $R_{2,2}$, $R_{2,3}$, $R_{2,4}$, $R_{2,5}$, $R_{2,6}$, $R_{2,7}$, $R_{2,8}$, $R_{2,9}$, $R_{2,10}$	10	20
⋮	⋮	⋮	⋮
9	$R_{9,1}$, $R_{9,2}$, $R_{9,3}$, $R_{9,4}$, $R_{9,5}$, $R_{9,6}$, $R_{9,7}$, $R_{9,8}$, $R_{9,9}$, $R_{9,10}$	10	90
10	$R_{10,1}$, $R_{10,2}$, $R_{10,3}$, $R_{10,4}$, $R_{10,5}$, $R_{10,6}$, $R_{10,7}$, $R_{10,8}$, $R_{10,9}$, $R_{10,10}$	10	100

The radial Chebyshev moment of order p and repetition q for an image of size $N \times N$ with m=(N/2)+1 is defined as [115]:

$$R_{pq} = \frac{1}{2\pi\rho(p,m)} \sum_{r=0}^{m-1} \sum_{\theta=0}^{2\pi} t_p(r) * e^{-jq\theta} * f(r,\theta) \tag{5.7}$$

where t_p(r) is an orthogonal basis Chebyshev polynomial function for an image of size $N \times N$:

$$t_0(x) = 1$$

$$t_1(x) = \frac{(2x - N + 1)}{N}$$

$$t_p(x) = \frac{(2p-1)t_1(x)t_{p-1}(x) - (p-1)\left\{1 - \frac{(p-1)^2}{N^2}\right\}t_{p-2}(x)}{p} \tag{5.8}$$

ρ(p,N) is the squared-norm:

$$\rho(p, N) = \frac{N\left(1 - \frac{1}{N^2}\right)\left(1 - \frac{2^2}{N^2}\right)\ldots(1 - \frac{p^2}{N^2})}{2p + 1} \tag{5.9}$$

Like ZM calculation, RCM can be calculated in different order. It is assumed that order p and repetition q are p, q = 1, 2, . . . , 10, which accumulates 100 moment features that are extracted from each segmented image as summarised in Table 5.2. Therefore, the total number of features extracted for a single image is 900 after considering target, shadow and combined target-shadow images in three different segmentation methods.

Features for both ZM and RCM can be computed as many times as is desired. However, considering the dimensionality of an image in the moment space, after a dimension is reached, the extra information that can be gained from a feature is expected to approach zero.

Figure 5.4 demonstrates two graphs. Both graphs indicate the number of features versus total accuracy on the training set using ten-fold cross validation. The first graph shows the accuracy of ZM based on the area of the target. It is clear that after first 40 features (approximately), the accuracy is not varied significantly. Therefore, based on

the study on the training set it can be suggested that the dimension of the moment space can be limited to 40.

Hence, around 40 features are sufficient for evaluating accuracy. Based on this observation and the number of features used for the data-set in [28] which is 34, it was decided to adopt 34 to be the number of features used in ZM approach in this chapter. Figure 5.4 also shows the accuracy of RCM based on the area of the target. Obviously after 100 features, accuracy remains constant. In this context, the decision was taken to use 100 features in the shape descriptor vector in the RCM-based segmented image representation.

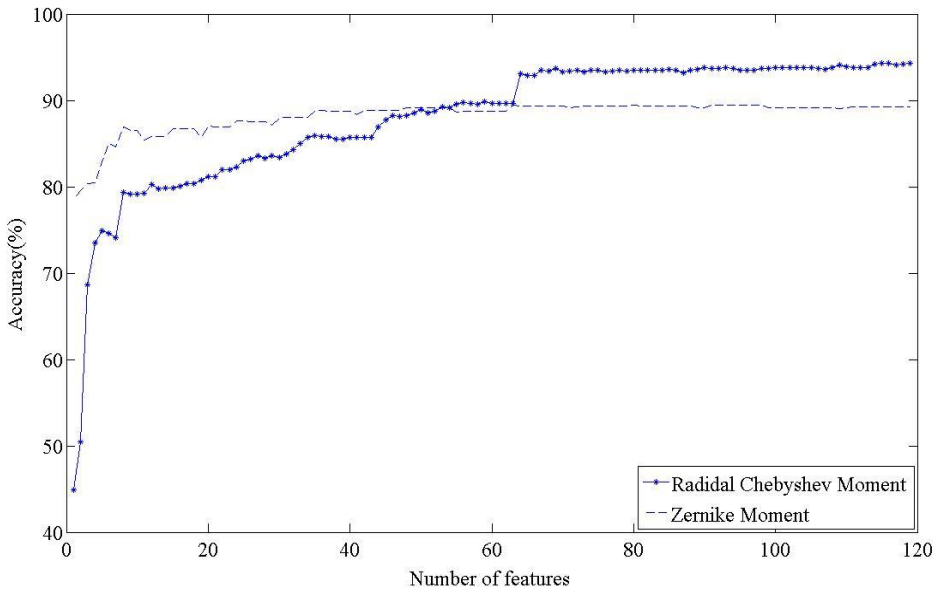

Figure 5.4: Accuracy of area of target in ZM and RCM

5.2.3 Classifier

In the classification stage, *k*-fold class validation technique was applied. We use multi-library support vector machine (multi-LibSVM) [120], which is a standard library for support vector machine (SVM). All codes run under MATLAB pattern recognition

toolbox (PRTools) [121]. The linear kernel is applied in all the experiments in this chapter.

5.3 Experimental results in three-class database

In this section, the experimental results of the proposed method which consists of two contributions are discussed. A comparison based on the feature extraction techniques was made between ZM and RCM. At the same time, effects on feature fusion were examined as the first contribution. Consideration of shadowing parts is the second contribution to the result of this work.

The number of images used as a sample in the whole experiment is 2987. A 10-fold class validation technique is applied in all the experiments.

Table 5.3: ZM and RCM based target recognition without and with preprocessing

Method	# of Features	Accuracy (%)
ZM without Segmentation	34	57.89
RCM without Segmentation	**100**	**75.33**
area of ZM	34	88.85
area of RCM	**100**	**92.03**
boundary of ZM	34	89.25
boundary of RCM	**100**	**92.64**
texture of ZM	34	88.85
texture of RCM	**100**	**90.12**
ZM with concatenating of Targets (area, boundary, texture)	102	88.48
RCM with concatenating of Targets (area, boundary, texture)	**300**	**96.35**

Table 5.3 shows that the accuracy is lower if segmentation is omitted before feature extraction in both techniques. We extract 34 and 100 features for ZM and RCM, respectively. The results on accuracy clearly show that with or without segmentation,

the proposed RCM-based approach is superior to the ZM-based method because Zernike moments are defined as a continuous function; approximation by discrete summation is considered which leads to numerical errors in computation of moments. Moreover, this approximation can affect some properties such as orthogonally and rotational invariance, which in turns decrease the accuracy. However, RCM is a discrete orthogonal moment that reduce numerical errors and computational complexity due to normalisation in ZM, and as a result, we achieve improvement in accuracy. The results also show that area, boundary and texture of RCM based approaches have the higher accuracy than those in ZM. Also boundary has the highest accuracy among each individual ROIs in target regions with 92.64% accuracy. This accuracy is improved to 96.35% when the fusion of the three segmentation methods is performed by concatenating the feature vectors of each method into a single vector.

Table 5.4: Accuracy (%) of segmentation with target and/or shadow based on RCM

RCM	Accuracy (%)
Area (Target)	90.12
Boundary (Target)	92.03
Texture (Target)	92.63
Area (Shadow)	76.03
Boundary (Shadow)	78.67
Texture (Shadow)	77.53
Area(combined target-shadow)	92.43
Boundary (combined target-shadow)	93.74
Texture (combined target-shadow)	91.23

Having RCM superior over the ZM-based target recognition, it was decided to adopt RCM-based feature representation of the targets to SAR images. The dimensionality of the feature vector for each representation is chosen to be 100. One of the major contributions of this study is to include the information extracted from the shadow of the vehicle to be recognised. It should be remembered that this shadowing effect is

based on electromagnetic waves, which is caused by the depression angle of the aerial vehicle acquiring the images rather than the sunlight. In this context, the results obtained from the shape descriptor vectors are given in Table 5.4.

It can be seen that the results obtained from the boundary approach for target and shadow regions are higher than those of area and texture. Furthermore, improvement is provided by fusing the vectors coming from target and shadows, respectively. The highest performance, 93.74%, is obtained from combining boundary shape descriptors of both target and shadow regions.

Table 5.5: Effect on fused data using target shadowing and/or both regions

Method	# of Features	Accuracy (%)
Targets [Area (TA), Boundary (TB), Texture (TT)]	300	96.34
Shadows [Area (SA), Boundary (SB), Texture (ST)]	300	87.78
combined target-shadow [Area (TSA), Boundary (TSB), Texture (TST)]	300	98.15
Concatenating of Targets and Shadows	600	98.25
Concatenating of Target, Shadows and combined target-shadow	900	98.69

In the final setup, the investigation was on the concatenation of feature vectors extracted from target, shadow and combined target-shadow images for area, boundary and texture cases. In other words, feature vectors for targets, shadows and combined target-shadow are extracted for area (100 features), boundary (100 features), and texture (100 features), respectively. After concatenation of the vectors from area, boundary and texture for targets 300 features are generated. Same operation is employed for shadow images; hence, 300 features are used to describe shadow regions.

Finally, 900 features are used to represent target (300), (TA, TB, and TT), shadow (300) (SA, SB, and ST) and combined target-shadow (300) (TSA, TSB, and TST) in a single vector.

Table 5.5 shows the improvement provided by combining area, boundary and texture objects into a single vector. 300 features extracted from combined target-shadow images reached the accuracy to 98.15%. Concatenation of shadows part to targets slightly increased the accuracy, and it reached to 98.25%. However, in comparison with combined target-shadow, more features are extracted (600 features), and accuracy is improved by only 0.1%. The last experiment shows that concatenating of target, shadows and combined target-shadow further improved the accuracy, and it reached its highest value of 98.69%. This result justifies that the feature fusion technique improves the total accuracy. A comparison between Table 5.4 and Table 5.5 indicates that, generally, segmentation based on area, boundary and texture for both target and shadow followed by feature fusion drastically improves the accuracy for RCM. Table 5.6 verifies that the proposed method has the highest performance among the alternative methods in the literature.

Table 5.6: Accuracy of the proposed method versus alternative methods in the literature.

Method	Accuracy (%)
PCA [53]	93.33
LDA [53]	87.33
PCA + LDA + ICA [41]	90.57
Proposed method	98.69

5.4 Experimental results in ten-class database

In this section, we consider ten-class database in SAR images. Target, shadow and combined target-shadow of texture are used as ROIs. RCM is applied to each ROI and then the extracted features are fed to various types of classifiers. SVM with different

kernels (linear, cubic, quadratic and RBF), k-NN, LDA, DT and RF are used for classification. Furthermore, feature fusion is used for improvement in the classification. Table 5.7 summarises all the results. Generally by utilising SVM classifier, the recognition rate of SAR images has the highest performance among all classifiers. Furthermore it is shown that quadratic kernel SVM has the best performance among all SVM classifiers with different kernel functions.

However, regardless of the classifier, which is used for classification, experimental results approve that by concatenating all three ROIs, recognition rate is improved significantly. The highest performance is achieved when cubic kernel SVM followed by feature fusion is used and the accuracy reached to 98.6%. Comparing the 10-class recognition rate with other state-of-the art approaches, the accuracy of proposed method is higher than other methods as it is shown in Table 2.1 in Chapter 2. The comparison shows that proposed method is improved by 3.1%.

Fig. 5.5, Fig. 5.6, Fig. 5.7 and Fig. 5.8 show the confusion matrix of target, shadow, combined target-shadow and fusion method, respectively. The elements on the main diagonals indicate the correct recognition rate. The fusion method has the highest number of elements on its diagonal in comparison to other ROIs. ROC also is another metric that shows how well the recognition rate is. It generated by plotting the sensitivity against 1- specificity. Fig. 5.10.a, Fig. 5.10.b, Fig. 5.10.c and Fig. 5.10.d

show the ROC of target, shadow, combined target-shadow and fusion method, respectively. As the area under the curve (AUC) is larger, then the recognition rate is higher. As it is clear again by comparing ROCs, fusion method has the largest AUC and therefore it has the highest recognition rate. ROC is generally designed for two

class problems. For multi-class problems first sensitivity and specificity of each class versus others are evaluated. Then, the average sensitivity and specificity are reported as the overall sensitivity and specificity. The ROC can be plotted by using the overall sensitivity and specificity. All ROCs and Confusion matrixes in this subsection are achieved by utilizing MATLAB Classifier Application Toolbox.

Table 5.7: Summary of recognition rate of different ROI using RCM among different classifiers using ten-class database (%)

Classifier	Target	Shadow	Combined Target-Shadow	Fusion
SVM (linear)	87.0	82.5	81.9	96.6
SVM (Cubic)	90.5	83.5	90.1	**98.6**
SVM (Quadratic)	**91.9**	88.0	90.2	98.5
SVM (RBF)	88.1	83.4	85.9	97.3
KNN (k=5)	84.7	82.9	87.4	96.5
DT	79.6	72.9	76.7	90.2
RF	80.9	77.2	80.9	93.8
LDA	82.4	77.1	73.7	93.8

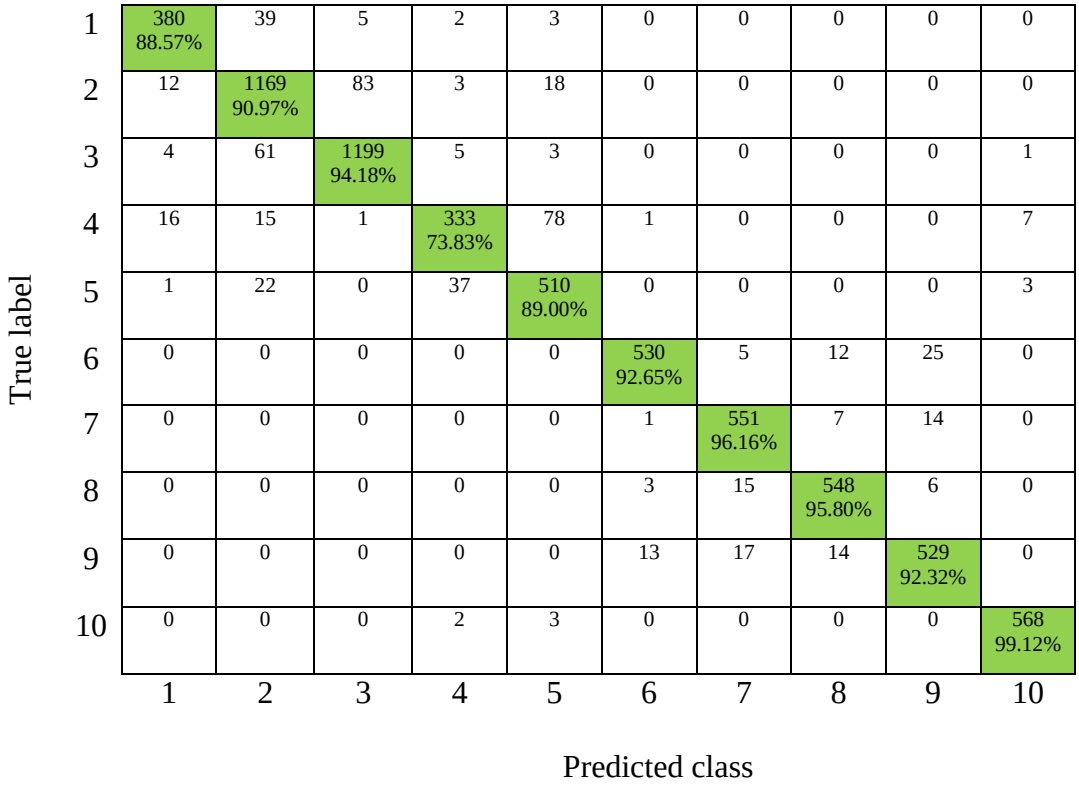

Figure 5.5: Confusion matrix of proposed method for texture of target regions

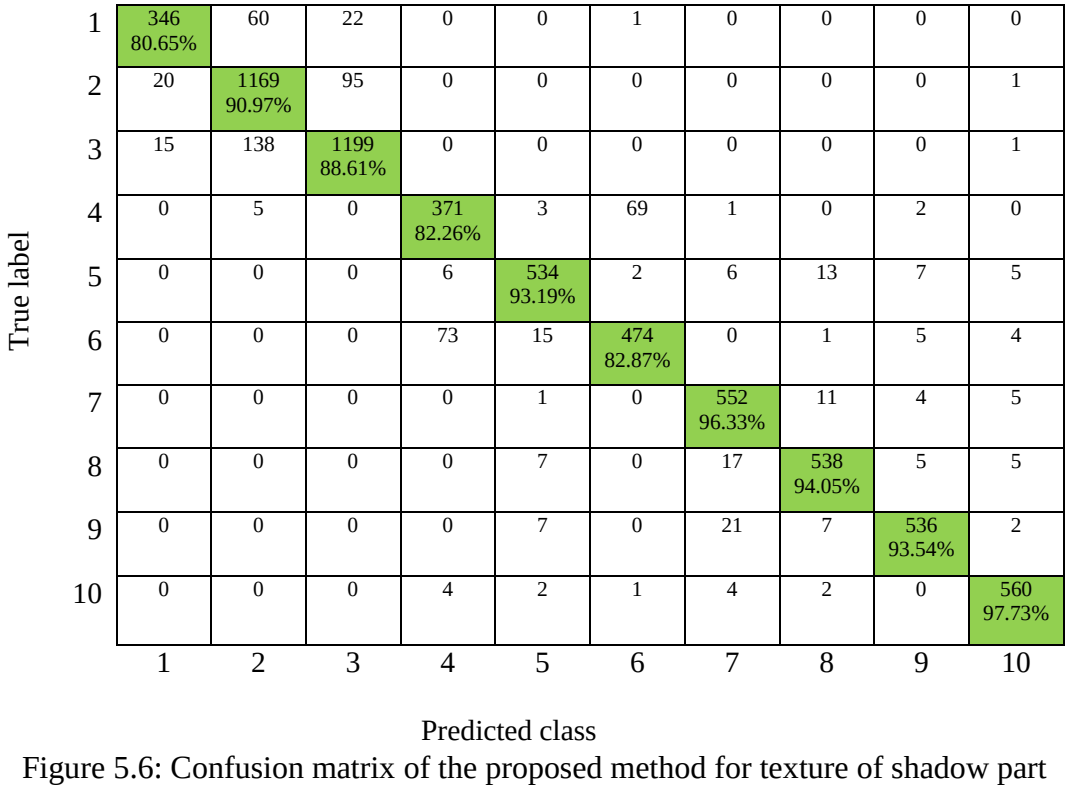

Figure 5.6: Confusion matrix of the proposed method for texture of shadow part

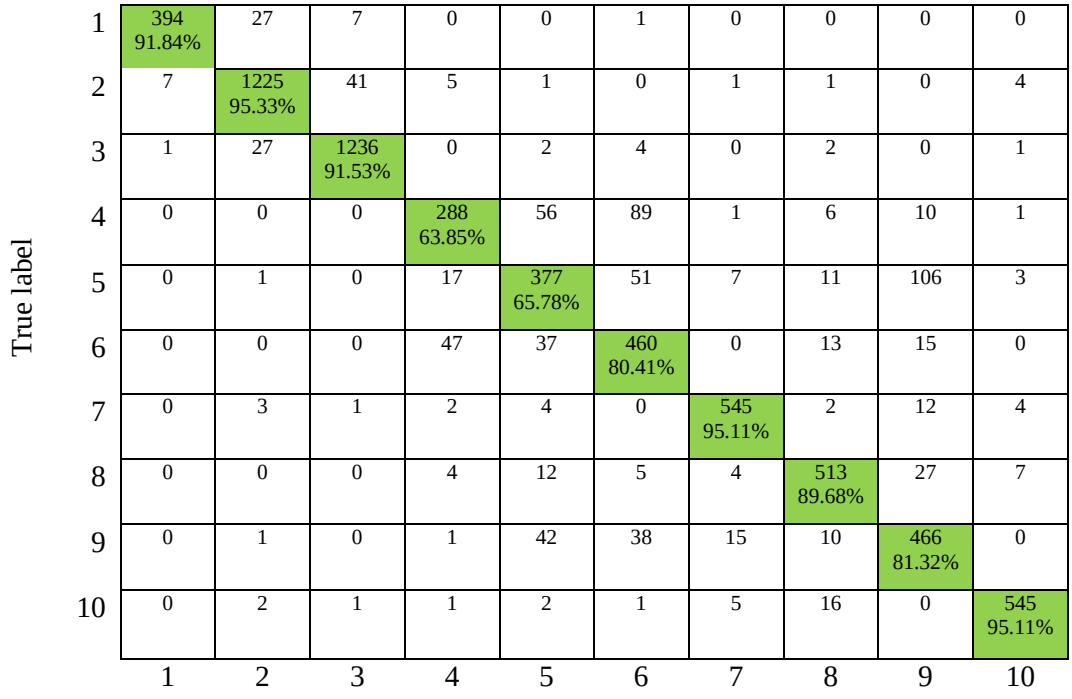

Figure 5.7: Confusion matrix of the proposed method for texture of combined target-shadow

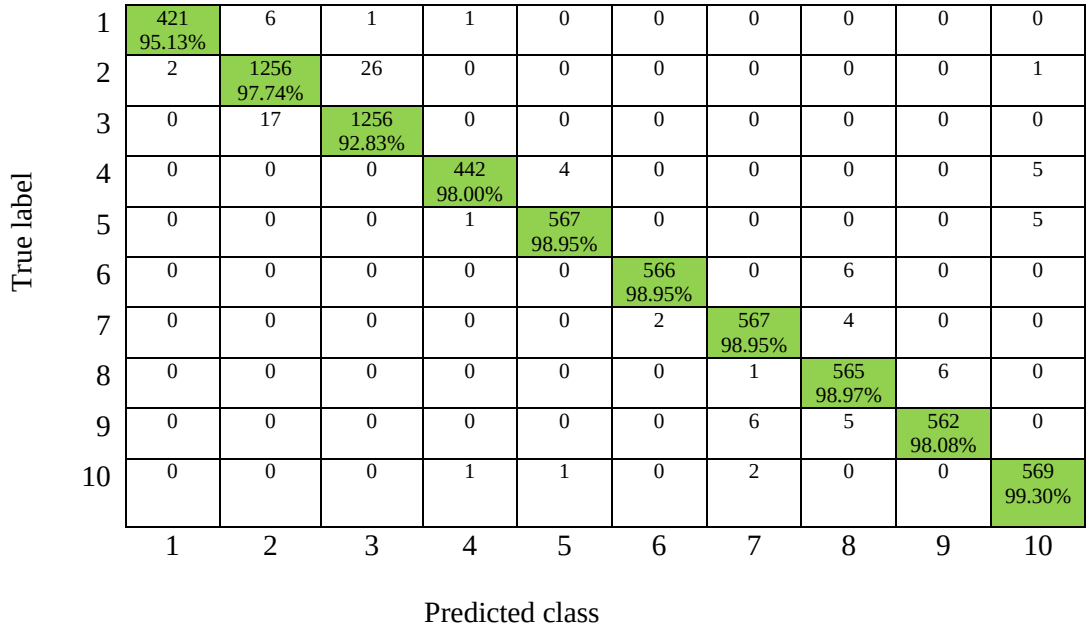

Figure 5.8: Confusion matrix of the proposed method for texture of fusion methods

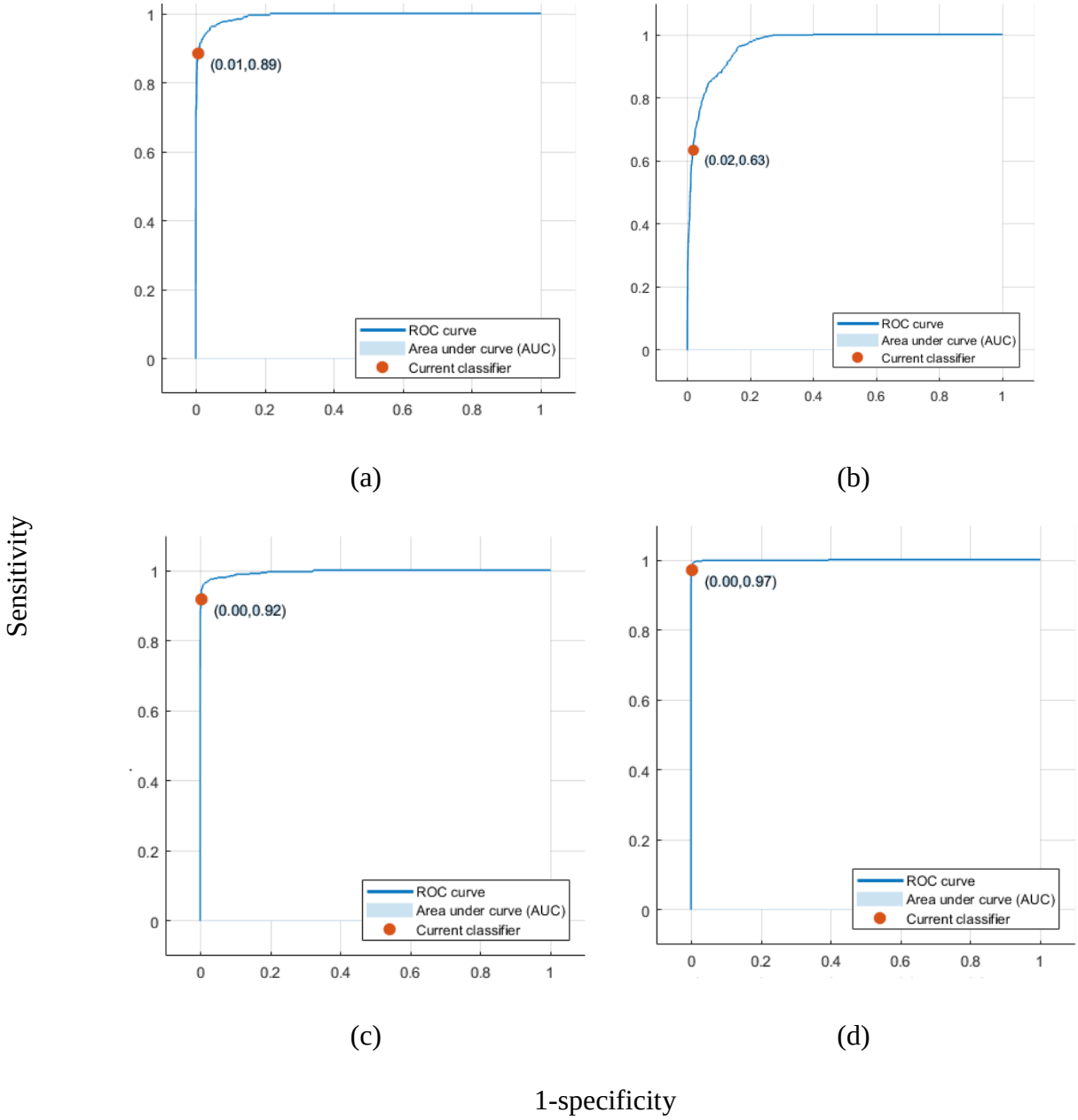

Figure 5.9: ROC of the proposed method. Texture of a. target, b. shadow, c. combined target-shadow, d. feature fusion

5.5 Conclusion

In this chapter, we developed a feature extraction algorithm using radial Chebyshev moments and compared it with a commonly used method called Zernike moments. RCM is a discrete orthogonal moment that reduce numerical errors and computational complexity due to normalisation in ZM, and as a result, we achieve improvement in

accuracy. Experimental results verify that RCM gives a higher performance in accuracy as compared to ZM. Accuracy of RCM without using any segmentation is 75.33%, while the accuracy is 57.89% for ZM.

Additionally, we considered shadow regions as part of feature extraction parallel to target information, and then, we applied feature fusion technique based on different image segmentation process: area, boundary and texture for target and shadow part. Experimental results show that overall accuracy of fused images is improved by both techniques used for feature extraction. The accuracy of fused data for target region is 96.35%, which is around 4% up to 6% improvement over area, boundary and texture. Furthermore, with the addition of shadow effects to fused data, accuracy reached to 98.69%.

We also applied feature fusion based on different ROIs by utilising many classification techniques into the ten-class problem. The aim of using many classification techniques was to verify that regardless of which method is utilised, by including the shadow regions and concatenating different ROIs to the single vector the accuracy will increase significantly.

Chapter 6

IMPROVED SAR TARGET RECOGNITION USING FISHER CRITERION AND DATA FUSION

6.1 Introduction

SAR generates images with high resolution of objects. The principal advantage of SAR images over optical images is, the capability to work independently from any weather condition and solar illumination; however, this enormous amount of information is difficult to handle in making fast decisions. In this chapter we propose a methodology that fuse different information of features to improve the target recognition performance of SAR. To reduce the dimensionality of the images we evaluate 12 traditional moments with 100 features extracted from each one, and select the *k* moments based on the Fisher Criterion. To fuse the *k* moments, we propose to use data fusion techniques: feature level fusion and decision fusion. In the feature level fusion, the *k* more informative moments are concatenated. In the decision fusion, the class probabilities are combined by using sum, median and max rules. The performance of the proposed techniques improve over the individual performances of the moments considered. Furthermore, results support the superiority of these techniques (feature level fusion and decision fusion) over the state-of-the art methods in the literature.

The main contribution of this chapter is feature selection based on Fisher Criterion (FC) followed by two data fusion techniques namely as a feature level fusion and decision fusion. In both techniques, firstly features are extracted from each SAR image

by utilising 12 different moments (for each method 100 features are extracted). Then FC is used to rank all moments by calculating the level of interclass separation of the extracted feature sets, generated by different moments. Moments with Higher FC scores are selected. *k* methods then used for data fusion. The variable *k* is chosen such that it maximises the overall accuracy in the training set. After we determine the value of *k* using the training set, we use it in the test set, which is explained in section 6.4.

In the feature level fusion technique, fusion is established by concatenating the feature vectors coming from the top *k* highest ranked moments, where each method feeds in a vector of 100 features, resulting in a final vector of $k \times 100$. The accuracy in the training set is evaluated by using SVM classifier with the linear kernel function. The overall performance of the feature level fusion has been compared against the performances of the moments without fusion. The highest performance among the 12-moments in the test set was 93.21% for the pseudo-Zernike method whereas the proposed feature level fusion using Fisher Criterion was superior with an overall accuracy of 95.71%.

In the decision fusion technique, similar to the feature level fusion, the top *k* highest ranked moments are selected. Then for each moment, we calculated and assigned class probabilities for each sample. Max rule, sum rule, and median rule are used for making a decision over an ensemble of *k* moments. Experimental results verify that the accuracy of the highest performance among the 12-moments (which is PZM) has increased by 1.9% reaching to 95.11% for some rule-based decision fusion. The results validate the improvement gained by the fusion techniques.

The highest performance is reported by using feature level fusion with Fisher Criterion where the top *6* moments are selected with 95.71% in accuracy. Performance evaluation involved accuracy, sensitivity, specificity and ROC analysis, where the 10-fold cross validation technique was adopted using the Support Vector Machine with linear kernel (SVM).

6.2 Background

In this section, first we briefly explain about the preprocessing. Then we introduce Fisher Criterion, which is applied to rank all moments. Finally, feature level fusion and decision fusion are introduced to improve the accuracy of the target recognition performance of SAR images.

6.2.1 Preprocessing

To get an area, we apply histogram equalisation, smoothing filter and thresholding. Histogram equalisation is applied to an input SAR image. A smoothing filter which uses an 11×11 averaging filter mask is used to reduce the noise artefacts. Then, a segmentation mask, which corresponds to the binary image of ROI is generated by using a threshold value of τ. Experimental analysis verifies the effectiveness of τ to be 0.8 for preserving target. Texture can be achieved by multiplying the original image with its binary mask. Figure 6.1 illustrates the summary of aforementioned technique. This is a visual example of a SAR image (hb03787.004), which belongs to BRT70 class (Armoured Personnel Carrier) with serial number SN-C71.

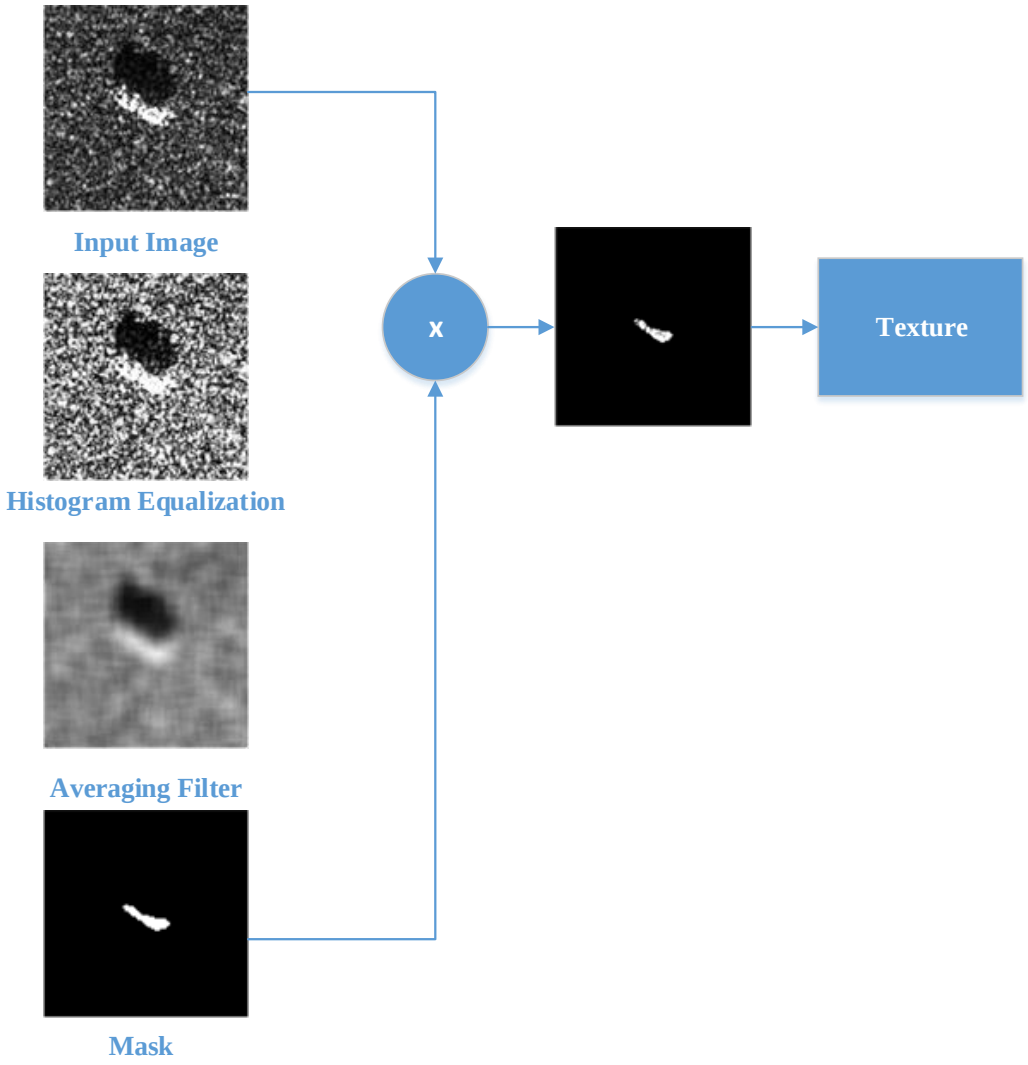

Figure 6.1: Segmentation process of an armoured personnel carrier with serial number SN-C71.

6.2.2 Fisher Criterion

Fisher Criterion (FC) is introduced for ranking, which is free from the role of the classifier. The idea behind it is to determine a scalar feature value that maximises separability of the classes by having a small within-class scatter, and large between-class scatter. For multi-classes pattern, the following feature selection criteria, based on interclass separation, is defined as [122]:

$$J = trace(S_W^{-1} S_B) \tag{6.1}$$

where S_B is between-class scatter and is defined as:

$$S_B = \sum_c (\mu_c - \bar{x})\ (\mu_c - \bar{x})^T \tag{6.2}$$

where μ_c is the mean of class c and $\bar{x}$ is the global mean. S_W is within-class scatter and defined as:

$$S_W = \sum_c \sum_{i \epsilon c} (x_i - \mu_c)(x_i - \mu_c)^T \tag{6.3}$$

6.2.3 Feature level fusion

For each feature extraction technique that we mentioned in the previous session, 100 features are extracted and then by applying Support Vector Machine (SVM) classifier, the accuracy on the training set is evaluated. All of the methods of moments are sorted according to Fisher criterion. Table 6.1 shows the ranks of the respective moments after sorting. Top *k* highest ranked moments are chosen, where *k* is selected such that it maximizes the accuracy in the training set. This value of *k* is then applied to the test set (i.e in test set *k* first moments are selected) and fused to form a data with *k*100* features. Then the accuracy of fused techniques is calculated. The evaluated accuracy shows an improvement in classification.

Table 6.1: Sorting based on FC of each moment for 100 features

		Method Name	FC	Rank FC
Cartesian	1	Legendre Moments	2.56E+03	7
	2	Chebyshev Moments (First Kind)	2.52E+03	11
	3	Chebyshev Moments (Second Kind)	2.53E+03	10
	4	Gegenbauer Moments ($\lambda = 0.75$)	2.55E+03	8
	5	Jacobi Moments ($\alpha = \beta = 1$)	2.54E+03	9
	6	Krawtchouck Moments (p=0.5)	3.06E+03	6
Polar	7	Zernike Moments	3.22E+03	5
	8	Pseudo Zernike Moments	5.07E+03	2
	9	Fourier Merlin Moments	2.31E+03	12
	10	Chebyshev Fourier Moments	5.37E+03	1
	11	Radial Harmonic Fourier Moments	4.61E+03	3
	12	Radial Chebyshev Moments	3.90E+03	4

6.2.4 Decision fusion

In this method, the top *k* highest ranked based-moment feature extractions are selected. Then for each moment, we evaluate class probability for each sample in the test set. Max rule, sum rule, and median rule are used for the decision fusion. More details about decision fusion are provided in section 3.6.2.

6.3 Proposed method of data fusion after ranking features based on FC by utilising different moments

Each SAR image contains a background that should be removed before further processing. Preprocessing provides different stages for segmentation including histogram equalisation, smoothing filtering and thresholding. Numerous moment-based methods are adopted as feature extractors: Legendre Moments (LM), Chebyshev Moments (CM), Gegenbauer Moments (GM), Jacobi Moments (JM), Krawtchouk Moments (KM), Zernike Moments (ZM), Pseudo Zernike Moments (PZM), Fourier Merlin Moments (FMM), Chebyshev-Fourier Moments (CFM), Radial Harmonic Fourier Moments (RHF) and Radial Chebyshev Moments (RCM).

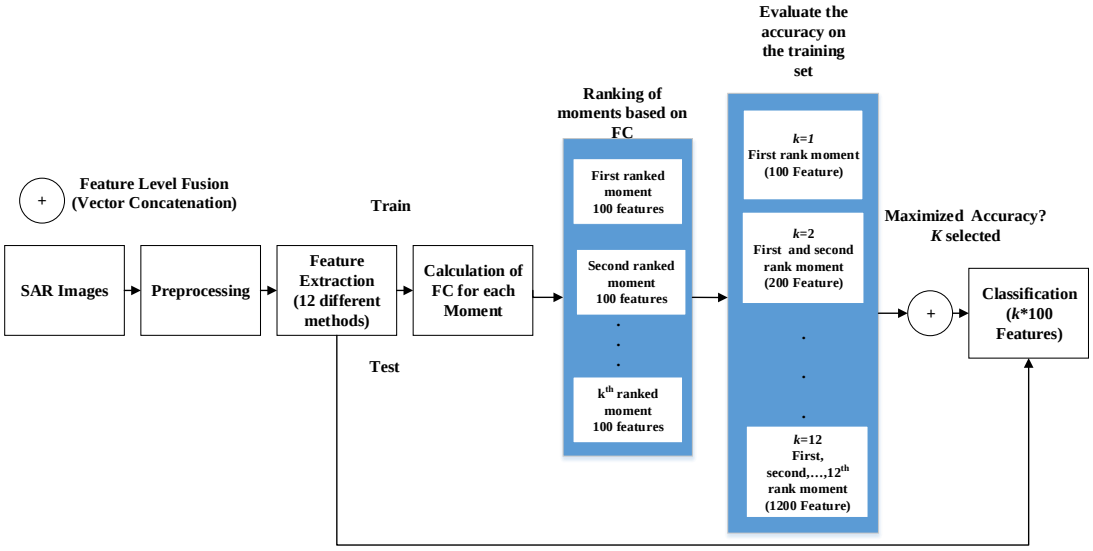

(a)

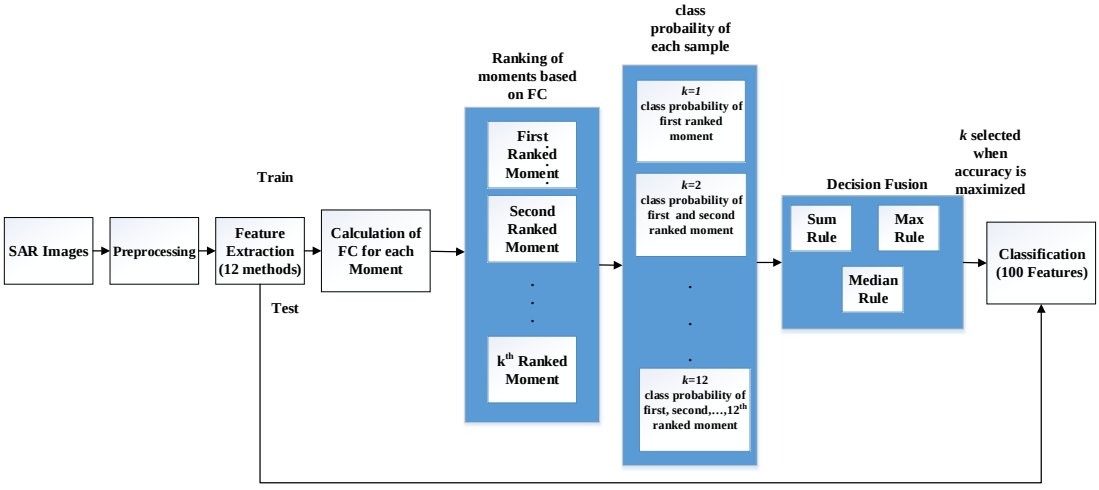

(b)

Figure 6.2: Proposed (a) feature level fusion and (b) decision fusion based frameworks.

Moments are sorted using FC. Top *k* highest ranked moments are selected and used in the proposed fusion frameworks. Two fusion techniques are incorporated. First is the feature level fusion, which concatenates all features of *k* selected moments. Second fusion is the decision fusion framework in which the top *k* highest ranked moments

are chosen, and then class probabilities are evaluated according to different fusion approaches such as, median rule, max rule and sum rule. This process includes the calculation of the median, maximum and total probability of each class respectively and then selecting the class label with the maximum probability. The performance analysis of the proposed frameworks was achieved using the 10-fold cross validation with Support Vector Machine using linear kernel. The proposed data fusion frameworks are illustrated in Fig. 6.2.

6.4 Results and discussions

For each proposed method (feature level and decision fusion), we define a threshold *k,* which is the number of methods used for fusion.

To evaluate the value of *k,* first, we sort the values in Table 6.1, according to the value of Fisher criterion. *k* is progressively increased from 1 to 12 and its value is determined where the accuracy in the training set is maximised. In Table 6.2, *k* for the fusion techniques *is* 6. The bold figure in Table 6.2 indicates the highest performance in the training set and reveals how many methods should be fused in the test set. Similarly, we can find the value of *k* for each rule (max rule, sum rule and median rule) in the decision fusion techniques, as shown in Table 6.3. *k* is chosen to be 3 for sum and max rule, while the highest accuracy based on the median rule is when *k* is 5.

Table 6.2: Finding the value of *k* for feature level fusion

Method Sorted	**Accuracy (%) in training set Based on FC**
Top 1 method *(k=1)*	90.80
Top 2 methods *(k=2)*	95.21
Top 3 methods *(k=3)*	95.28
Top 4 methods *(k=4)*	95.66
Top 5 methods *(k=5)*	95.89
Top 6 methods *(k=6)*	**96.02**
Top 7 methods *(k=7)*	95.61
Top 8 methods *(k=8)*	95.38
Top 9 methods *(k=9)*	95.21
Top 10 methods *(k=10)*	94.91
Top 11 methods *(k=11)*	95.04
Top 12 methods *(k=12)*	95.11

Table 6.4 shows the results of classification using accuracy, sensitivity, specificity and miss rate. The methods of moments are sorted according to the accuracy (%) over the test set. Generally, methods in polar coordinates have higher accuracies, and lower miss rate than those methods of methods in Cartesian coordinates. The main reason for these is that generating rotational invariance in polar form is easier which gives a better performance. Pseudo Zernike Moments have the best performance among all the method of moments.

Table 6.3: Finding the value of *k* for decision fusion (%)

Number of selected methods (*k*)	Sum Rule (Training set)	Median Rule (Training set)	Max Rule (Training set)
Top 1 methods *(k=1)*	93.37	93.37	93.37
Top 2 methods *(k=2)*	94.48	94.48	94.51
Top 3 methods *(k=3)*	**95.38**	94.21	**94.94**
Top 4 methods *(k=4)*	94.61	94.41	94.48
Top 5 methods *(k=5)*	95.00	**94.74**	94.81
Top 6 methods *(k=6)*	94.61	94.24	94.54
Top 7 methods *(k=7)*	94.48	92.96	94.61
Top 8 methods *(k=8)*	93.87	92.66	94.61
Top 9 methods *(k=9)*	93.61	91.76	94.64
Top 10 methods *(k=10)*	93.37	91.06	94.58
Top 11 methods *(k=11)*	92.73	88.52	94.54
Top 12 methods *(k=12)*	92.27	88.52	94.44

Table 6.4: Evaluation of successful classification using accuracy, TPR, TNR and FNR

Method	ACC (%)	TPR	TNR	FNR
PZM	93.21	0.93	0.97	0.07
RHFM	92.79	0.92	0.96	0.07
CFM	90.86	0.91	0.96	0.09
RCM	90.12	0.90	0.95	0.10
ZM	90.3	0.90	0.95	0.10
LM	85.42	0.85	0.92	0.15
GM	85.42	0.85	0.92	0.15
JM	85.00	0.85	0.92	0.15
KM	84.97	0.85	0.93	0.14
CM #1	84.25	0.83	0.91	0.16
CM #2	84.37	0.82	0.91	0.17
FMM	76.53	0.79	0.89	0.21

Table 6.5 summarises all the proposed methods. As we can see, the overall accuracy is improved for each individual fusion technique in comparison to the best method of moment, which is the Pseudo Zernike moment with an accuracy of 93.21%. The highest result is obtained from the feature level fusion based on Fisher Criterion, which increased by 2.5% in accuracy.

Table 6.5: The Accuracy of proposed method by different fusion techniques

Method	# of features	Accuracy (%)
Fusion Based on Fisher Criterion	600	95.71
Sum Rule	100	95.11
Median Rule	100	94.33
Max Rule	100	94.08

A plot of sensitivity against 1-specificity is called Receiver Operating Characteristic (ROC), which illustrates how successful the classification is [97]. From Fig 6.3 it is clear that the ROC of the proposed methods is superior to the highest moment-based method.

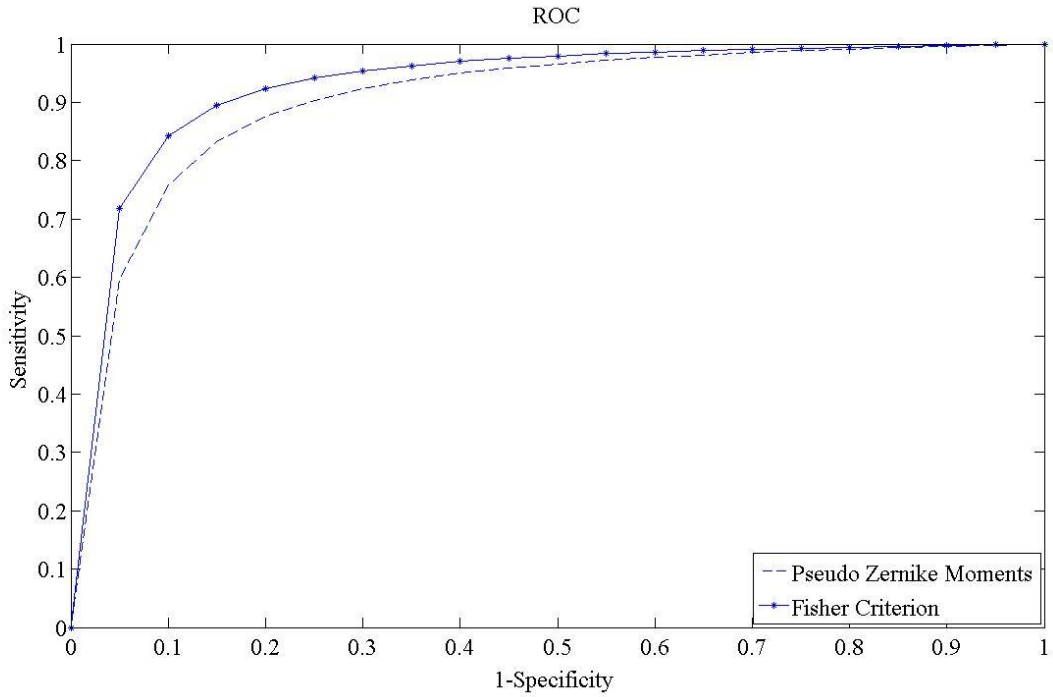

Figure 6.3: ROC Characteristic.

6.4.1 Comparison with other methods

In this section, we compare the proposed method with previous studies on MSTAR. Template matching, perceptron, Optimal Hyperplane [31], LDA, Locality Preserving Projections (LPP) [53], Local Discriminate Embedding (LDE) [52], ICA and PCA [41] are some classical methods considered. As it is summarised in Table 6.6, the

recognition rate of the proposed method is superior to all of the aforementioned classical techniques. Additionally, the proposed method has higher accuracy than a fused classical method such as fusion of PCA, LDA and ICA [41]. Furthermore, state-of-the-art approaches that have been introduced more recently are also considered, which include methods such as Multiscale Local Gradient Ratio Pattern Histogram (MLGRPH) [41], Maximum Interclass Distance (MID) [41], Nonnegative Matrix Factorization (NMF) [49], 2D-slice Zernike moments (2DS-ZMS)[123] and Auto Encoder (AE)[78]. The proposed method has the highest performance among all those algorithms. Even another moment called Zernike Moment used in the literature. An alternative ZM based method [123] which uses SVM classifier is also included in the comparisons.

Table 6.6: Recognition rate of different algorithm

Method	**Accuracy (%)**
Template matching [31]	89.3
Perceptron [31]	92.5
Optimal Hyperplane [31]	93.9
LDA [53]	87.3
LPP [53]	40.1
LDE [52]	92.4
Original image + LSVM [78]	88.64
Original AE + LSVM [78]	88.81
NMF [49]	95.16
ZMS + SVM [123]	82.34
2DS-ZMS + SVM [123]	86.92
MLGRPH [41]	93.88
PCA+SVM [41]	91.61
PCA+LDA+ICA+SVM [41]	90.57
MID+SVM [41]	93.49
Proposed Method	**95.71**

6.5 Conclusions

Previous studies have shown that moments in polar coordinates have better feature representation capabilities with rotation [115], scale and translational invariance. The experimental results also show that accuracies of moments in polar form are much higher than those in Cartesian. In this chapter, we used different method of moments in Cartesian and polar coordinates to extract features to be used for classification. Furthermore, we defined two fusion techniques as feature level fusion and decision fusion. The aim of introducing fusion methods is to help the classifier to improve the classification performance and decrease the false alarm. Fisher Criterion is used to rank the features. The top k highest ranked-based moment feature extractions are selected and fused by the aforementioned techniques. The experimental results verify that both fusion techniques improve the overall accuracy.

Chapter 7

ENTROPY SCORE BASED FEATURE SELECTION FOR MOMENT BASED SAR IMAGE CLASSIFICATION

7.1 Introduction

In this chapter, entropy score based feature selection is utilised to improve the moment based classification performance of Synthetic Aperture Radar Images. To benefit from the diversities introduced by different moments, twelve distinct moments are employed for feature extraction as Legendre Moments (LM), Chebyshev Moments of first (CM#1) and second kind (CM#2), Gegenbauer Moments (GM), Jacobi Moments (JM), Krawchouck Moments (KM), Zernike Moments (ZM), Pseudo Zernike Moments (PZM), Fourier Merlin Moments (FMM), Chebyshev Fourier Moments (CFM), Radial Harmonic Fourier Moments (RHFM) and Radial Chebyshev Moments (RCM). A unique approach is proposed for entropy based feature selection. For all SAR images in the training set, a 3D feature matrix ($\Phi_{i,j,l}$), whose elements are: *i, j, l* (refer to i^{th} moment, j^{th} feature and l^{th} sample) is created. For each feature, an entropy score for each element of feature is calculated and entropy score matrix $H_{i,j}$ is created. After calculating the entropy score based on each aforementioned approach, the moments in each feature (column of the matrix (H)) are ranked in the descending order. Finally, feature selection is performed by choosing top *k* moments of feature matrix associated with highest ranked entropies of all methods. Experimental result shows up to 2.91% improvement in accuracy with the proposed approach.

7.2 Proposed entropy score for feature selection

We propose the new approach for improvement of automatic target recognition in SAR images by applying 12 moments to increase the feature information of SAR images. Although adding more features, improves the recognition rate, it causes redundancy of information brought by the correlation of features and arousal of computational complexity. Therefore, it is a need for selecting specific features and hence feature selection should be applied to minimize the classification error [135]. In previous studies the focus was to find of subset form given input data D with M features. Regarding to those problems, a feature vector of M features are created and the best subsets (S) of M (where S≤M) was chosen for effective dimensionality reduction.

However, in this study, a 3D matrix Φ with size $i \times j \times l$ is created where *i* refers to each moment, *j* refers to each feature and *l* refer to each sample. For each feature, *j*, entropy of sub-feature matrix ($F_{i,l}$) is evaluated. Once entropy for all features is performed, the entropy score matrix ($H_{i,j}$) is created. Entropy score is defined to be the measure to evaluate the class separability by the ratio of total sample population and average within-class population. Entropy score matrix H is ranked according to the entropy on each column. The top *k* corresponding moments for each feature is used to evaluate the recognition rate of SAR images. The summary of the proposed approach is illustrated in Fig.7.1.

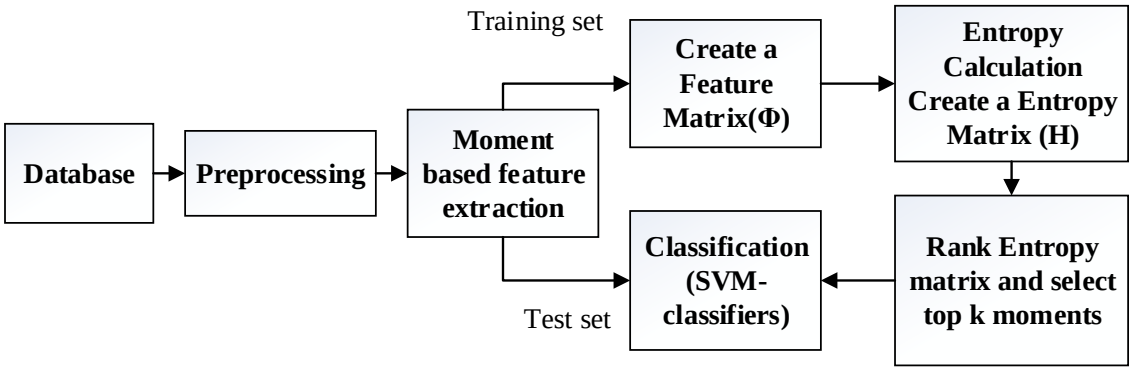

Figure 7.1: Frameworks of the proposed approach. Selection by *k* highest entropy associated features by feature level fusion

Input SAR images go through preprocessing for noise removal. A preprocessing is required to remove the background of SAR images before any feature extraction techniques. Preprocessing consists of different stages of histogram equalisation, smoothing filter and thresholding. Next, two types of moments are used to extract features. The first type of moments are defined by Cartesian coordinates: Legendre Moments, Chebyshev Moments of a first and second kind, Gegenbauer Moments, Jacobi Moments and Krawtchouk Moments. The second type of moments are defined in polar coordinates: Zernike Moments, Pseudo Zernike Moments, Fourier Merlin Moments, Chebyshev Fourier Moments, Radial Harmonic Fourier Moments and Radial Chebyshev Moments. For each moment, 100 features are extracted. Entropy calculation is performed and entropy score matrix H is created, elements of each column of matrix H are ranked in the descending order and top *k* moments of each feature are selected. Finally, support vector machine (SVM) classifier with a linear kernel function is used for classification.

7.2.1 Preprocessing

An example of preprocessing stage for an MSTAR image of an armoured personnel carrier (BTR70) is shown in Fig 7.2. Details of preprocessing stage are provided in section 3.3.

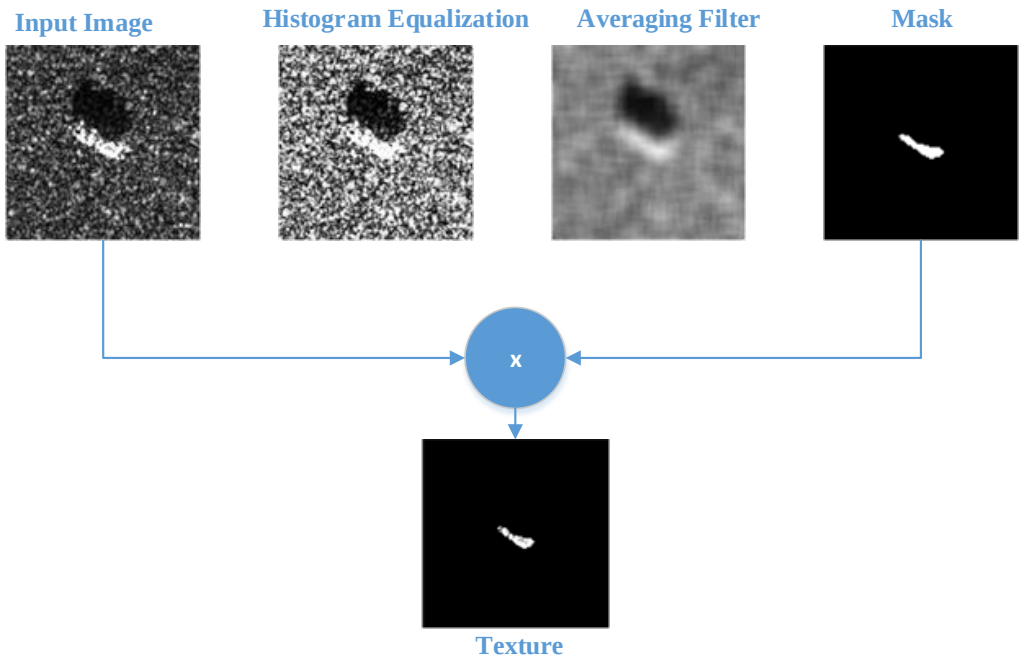

Figure 7.2: Preprocessing of an MSTAR image.

7.2.2 Feature extraction

Moments are projections of a function to the polynomial basis that are used to capture significant features and are widely used in many applications. In this study, two types of moments are used to extract features: moments in Cartesian and moments in polar. With different polynomial basis, different moments are generated for both types. Further details of feature extraction are given in Chapter 4.

7.2.3 Entropy calculation

The higher entropy for a feature is an indicator of higher information content and the corresponding feature should be selected. Arguing that higher entropies include the features with more scattered data, we propose a novel approach to maximize the ratio of total and within-class entropies to generate the entropy score.

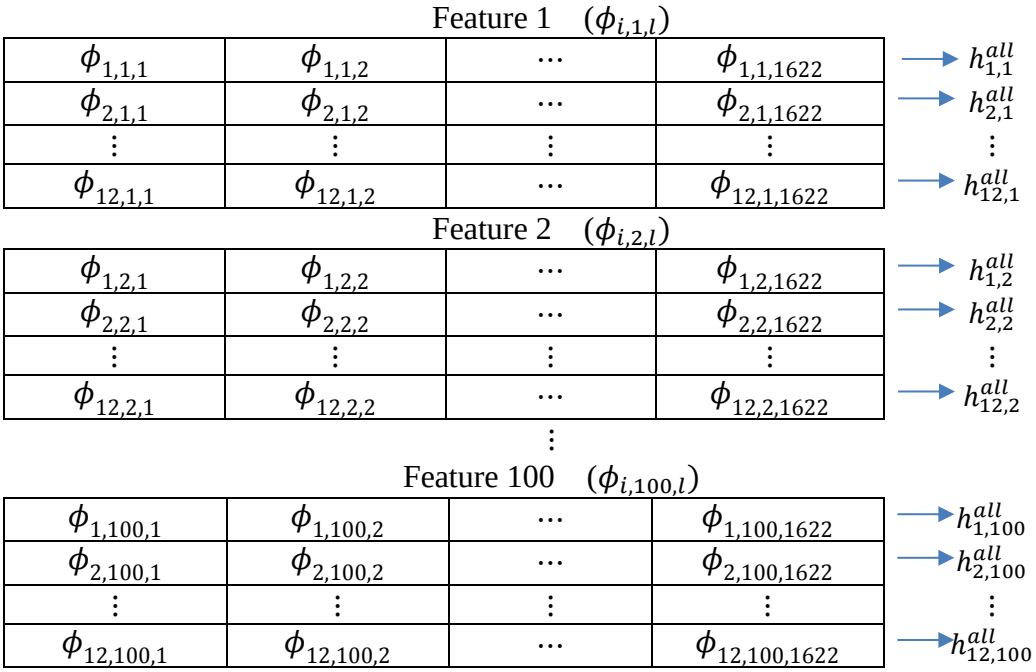

Figure 7.3: 3D feature matrix Φ and Entropy evaluation

As it is shown in Fig 7.3 a 3D feature matrix ($\Phi_{i,j,l}$), is created after extracting *100* features of *1622* training samples for *12* moments. where i=1,2,3,…,12 refer to Pseudo Zernike moment, radial harmonic Fourier moment, Chebyseshv Fourier moment, radial Chebyshev moment, Zernike moment, Legendre moment, Gegenbauer moment, Jacobi moment, Krawchouk moment, Chebyshev moment of first kind, Chebyshev moment of second kind and Fourier merlin moment respectively. j=1,2,…,100 refer to j^{th} feature of moment i. For each feature j, entropy of all samples l in the training set ($h_{i,j}^{all}$) of moment i is calculated as:

$$h_{i,j}^{all} = -\sum_{l=1}^{1622} p_{i,j,l}\left(log_2 p_{i,j,l}\right) \tag{7.1}$$

where $p_{i,j,l}$ corresponds to the probabilities extracted from the distribution of the respective samples in the training set.

Entropy score tries to maximize the ratio of total sample population to within-class population by calculating respective entropies. For C class problem the within-class entropy is calculated as:

$$h_{i,j}^{w} = \frac{1}{C}\sum_{m=1}^{C} h_{i,j}^{c} \tag{7.2}$$

where $h_{i,j}^{c}$ is the entropy of each class. Then the entropy score is calculated as:

$$h_{i,j}^{s} = \frac{h_{i,j}^{all}}{h_{i,j}^{w}} \tag{7.3}$$

After evaluation the entropy of each feature the entropy score matrix *H* (12×100), is formed for further processing as:

$$H_{i,j} = \begin{bmatrix} h_{1,1}^{s} & \cdots & h_{1,100}^{s} \\ \vdots & \ddots & \vdots \\ h_{12,1}^{s} & \cdots & h_{12,100}^{s} \end{bmatrix} \tag{7.4}$$

where each element of the matrix refer to the entropy score of moment *i* and feature j. Then for each feature *j* the matrix *H* is ranked in the descending order. The top *k* rows of the ranked *H* matrix is selected representing top *k* moments.

7.2.4 Selection by *k* highest entropy associated features by feature level fusion

The data-set is divided into training set and the test set. In this study, all samples captured at 17° depression angle considered as training set and all samples which are collected at 15 ° depression angle considered to be a test set. An entropy score matrix (*H*) of size 12× 100 is created where $h_{i,j}^{s}$ refers to the entropy of method *i* and feature

j as shown in Table 7.1. The columns on matrix *H* is ranked and the corresponding moment for each feature is selected. H_{rank} is the column ranked of the matrix *H* as it is shown in Table 7.2. The corresponding moments for each feature are shown in Table 7.3.

Table 7.1: Entropy score matrix, (*H*) for the first five features

		Feature1	**Feature2**	**Feature3**	**Feature4**	**Feature5**
1	**PZM**	0.007	0.022	0.134	1.004	4.743
2	**RHFM**	5.369	5.923	6.490	6.865	7.074
3	**CFM**	6.815	6.601	6.671	6.637	6.645
4	**RCM**	5.948	5.652	5.660	6.069	6.287
5	**ZM**	4.021	0.744	0.127	0.013	0.014
6	**LM**	0.764	2.016	0.583	0.438	1.977
7	**GM**	0.307	0.618	0.435	0.337	0.822
8	**JM**	0.665	1.122	0.704	0.462	1.469
9	**KM**	4.815	6.087	3.972	1.551	3.696
10	**CM #1**	0.275	0.343	0.475	0.313	0.694
11	**CM #2**	0.079	0.302	0.249	0.223	0.519
12	**FMM**	3.865	3.829	3.230	3.025	2.925

For each column of H_{rank} the corresponding top *k* moments are selected. *k* is progressively increased from 1 to 12 making a total of 100 to 1200 features. The selection for *k* is such that the overall accuracy (ACC) in the training set is maximised as follows:

$$k_{selected} = arg_k \max \left(ACC(1{:}\,k) \right) \tag{7.6}$$

Table 7.2: Column ranked of the matrix *H*

Feature 1	Feature 2	Feature 3	Feature 4	Feature 5
6.815	6.601	6.671	6.865	7.074
5.948	6.087	6.490	6.637	6.645
5.369	5.923	5.660	6.069	6.287
4.815	5.652	3.972	3.025	4.743
4.021	3.829	3.230	1.551	3.696
3.865	2.016	0.704	1.004	2.925
0.764	1.122	0.583	0.462	1.977
0.665	0.744	0.475	0.438	1.469
0.307	0.618	0.435	0.337	0.822
0.275	0.343	0.249	0.313	0.694
0.079	0.302	0.134	0.223	0.519
0.007	0.022	0.127	0.013	0.014

Table 7.3: Corresponding Moment of ranked entropies H_{rank}

Feature 1	Feature 2	Feature 3	Feature 4	Feature 5
3	3	3	2	2
4	9	2	3	3
2	2	4	4	4
9	4	9	12	1
5	12	12	9	9
12	6	8	1	12
6	8	6	8	6
8	5	10	6	8
7	7	7	7	7
10	10	11	10	10
11	11	1	11	11
1	1	5	5	5

Fig. 7.4 indicates that the number of *k* to be selected in the training is 5. We use *k* to be 5 in the test set, where the first *k* moments of each feature should be selected. For example, in feature 1 the moment 3, 4, 2, 9 and 5 should be selected.

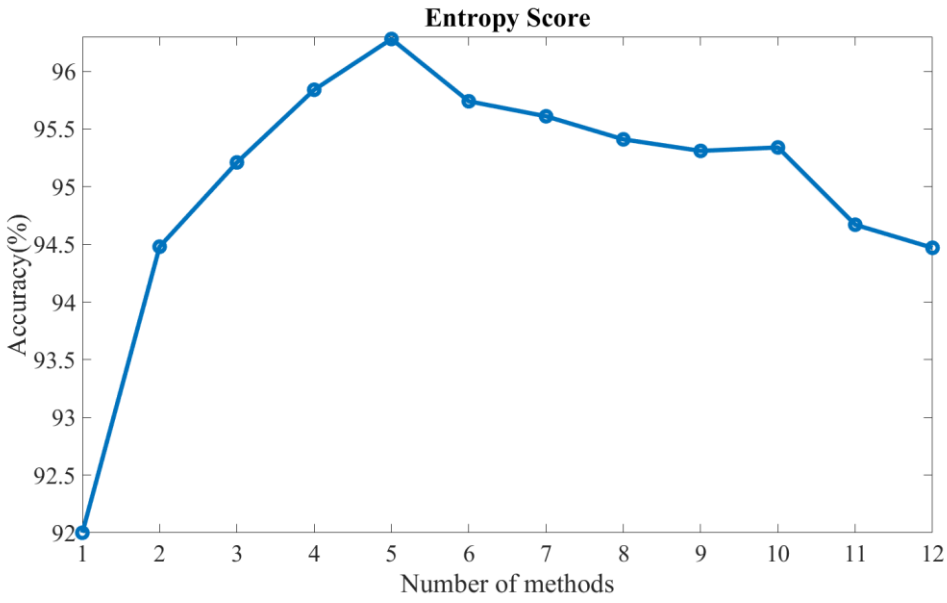

Figure 7.4: Number of fused methods

7.3 Results and discussions

As we discussed earlier we defined stopping criteria to determine the value of *k*. This parameter is chosen to maximise the accuracy by using 10-fold cross validation over the training set. The highest-ranking *k* methods are determined which maximises the accuracy. We independently employ 12 different moments, which are ranked according to their associated entropy levels. The addition of the moments is according to the respective entropies. Hence, in iteration *k*, k^{th} highest methods are combined by including the highest performing $k\times$ 100 features. The results show that the accuracy is maximised at *k as* 5, with 96.28%. Further increase of *k* decreases the accuracy. This is due to the possible inclusion of redundancies and the features that are not as discriminative as those associated with the higher entropies. Note that when *k* is 5 we include 500 features in the feature vector to be classified.

Table 7.4 shows the accuracy of each individual moment, and 100 features are extracted for each moment. Generally, moments on the polar form have a better

performance in comparison to those in Cartesian. This is because the moments in polar coordinates feature representation have capabilities with rotation, scale and translational invariance. Pseudo Zernike Moment has the highest accuracy among all moments.

Table 7.4: Accuracy of each individual Moment with 100 features

		Method	Accuracy (%)
Cartesian	1	Legendre Moments	85.42
	2	Chebyshev Moments (First Kind)	84.25
	3	Chebyshev Moments (Second Kind)	84.37
	4	Gegenbauer Moments ($\lambda = 0.75$)	85.42
	5	Jacobi Moments ($\alpha = \beta = 1$)	85.00
	6	Krawtchouck Moments (p=0.5)	85.97
Polar	7	Zernike Moments	90.30
	8	**Pseudo Zernike Moments**	**93.21**
	9	Fourier Merlin Moments	76.53
	10	Chebyshev Fourier Moments	90.86
	11	Radial Harmonic Fourier Moments	92.79
	12	Radial Chebyshev Moments	90.12

Table 7.5 compares proposed approach with the Pseudo Zernike Moments (which has the highest accuracy among each individual moment). Proposed method requires selection of 500 features and the accuracy is improved by 2.91%.

Table 7.5: Accuracies of proposed methods

Method	Number of features	Accuracy (%)
Highest Performance Among Moments	100	93.21
Proposed Method	**500**	**96.12**

The proposed method is also compared with previous studies on MSTAR. Linear discriminant analysis (LDA), locality preserving projections (LPP) [53], local discriminate embedding (LDE) [52], independent component analysis (ICA), principle

component analysis (PCA) local binary pattern (LBP) and Multiscale local gradient ratio pattern histogram (MLGRPH) [41] are some classical methods considered. As it is summarized in Table 7.6, the recognition rate of proposed method is superior to all of the aforementioned classical techniques. Additionally, the proposed method has higher accuracy than fused classical methods such as fusion of PCA, LDA and ICA.

Table 7.6: Recognition rate of different algorithms

Method	Accuracy (%)
LDA [53]	87.3
LPP [53]	40.1
LDE [52]	92.4
Original image + LSVM [78]	88.64
Original AE + LSVM [78]	88.81
NMF [49]	95.16
MLGRPH [41]	93.88
PCA+SVM [41]	91.61
PCA+LDA+ICA+SVM [41]	90.57
MID+SVM [41]	93.49
LBP+SVM [32]	72.1
Proposed Method	**96.12**

7.4 Conclusions

In this chapter, we applied entropy score based feature selection for improvement of classification performance in target recognition for SAR images. Different moments including LM, CM #1, CM #2, GM, JM, KM, ZM, PZM, CFM, FMM, RHFM and RCM are used to benefit from the diversities introduced by different moments. Twelve feature vectors are extracted using 12 different moments. Entropy score are used for ranking the moments of each feature. Feature selection is performed by choosing the

top *k* moments. The results obtained by the proposed approach outperforms the state-of-the-art alternative techniques in the literature. The results generated by the proposed approach reaches an improvement of level up to 2.91% in accuracy.

Chapter 8

ENSEMBLE OF CLASSIFIERS FOR IMPROVED SAR IMAGE RECOGNITION

8.1 Introduction

In this section, a new approach for classification of three and ten kinds of ground vehicles from Moving Stationary Target Acquisition and Recognition images is proposed. Each SAR image includes background, target and shadow regions. First, backgrounds are removed by pre-processing. Then Pseudo Zernike moment features are extracted from target and shadow regions. Extracted features from target, shadow and combined target-shadow regions are then fused using feature fusion and are fed to different classifiers. Five classifiers are adopted including support vector machine, decision tree, linear discriminant analysis, *k*- nearest neighbour and random forest. Finally, the performance of the proposed method is calculated by majority voting based on all output labels corresponding to each classifier. The experimental results justify the combining features coming from the target, shadow and target-shadow improve the performance. Additional improvement in the overall accuracy is also obtained by using an ensemble of classifiers through majority voting (MV). Experimental results show that feature fusion followed by majority voting increases the recognition rate up to 99.5%.

8.2 Proposed method on ensemble of classifiers

A summary of the proposed method is illustrated in Fig. 8.1. First, preprocessing is applied to each input SAR image extracting three different regions of interests as target, shadow and combined target-shadow region. These regions go through extraction of three different parts, which includes area, boundary and texture. For each region and parts, 100 features are extracted using Pseudo Zernike Moments. A feature vector then is created by concatenation of all extracted feature vectors of each region and part to form a feature fusion of 900 features.

Different classifiers such as support vector machine, decision tree, a linear discriminant analysis, k-nearest neighbour and random forest are adopted as part of the feature fusion process generating the overall performance of each classifier. Finally, by utilising majority voting among five classifiers, class label of each sample is evaluated, and overall performance is calculated. Experimental results indicate an improvement using both feature fusion and majority voting, with the recognition rate increasing to 99.5%.

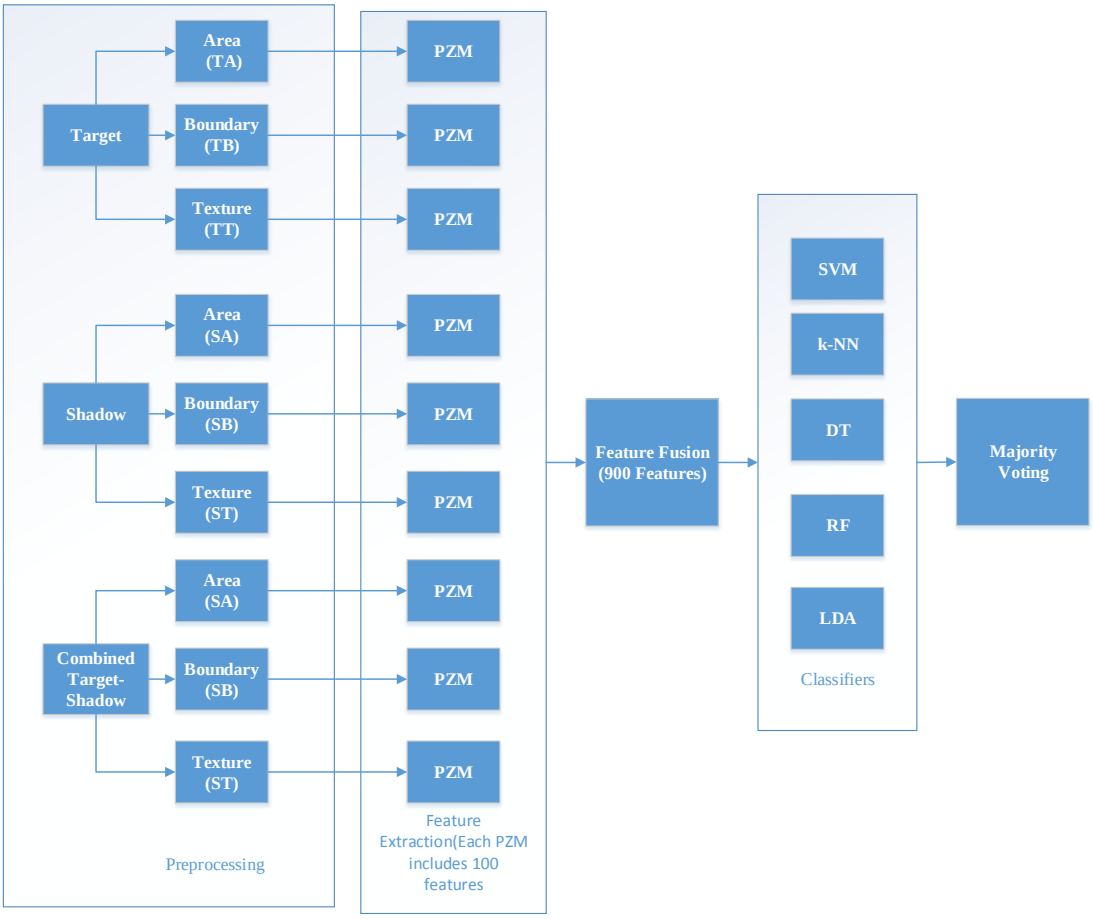

Figure 8.1: Ensembles of classifiers for improved SAR

8.2.1 Preprocessing

SAR images consist of background that should be first removed before any further processing. The proposed preprocessing employs, histogram equalisation followed by averaging filtering through which the image is smoothened to reduce noise artefacts. The well-explained procedure is given in section 3.3.

Fig. 8.2 shows the summary of preprocessing of a SAR image in the target region only. For each region, three segmented parts are generated as area, boundary and texture. Therefore, for each sample SAR image, a total of nine regions are generated as it is illustrated in Fig. 5.3.

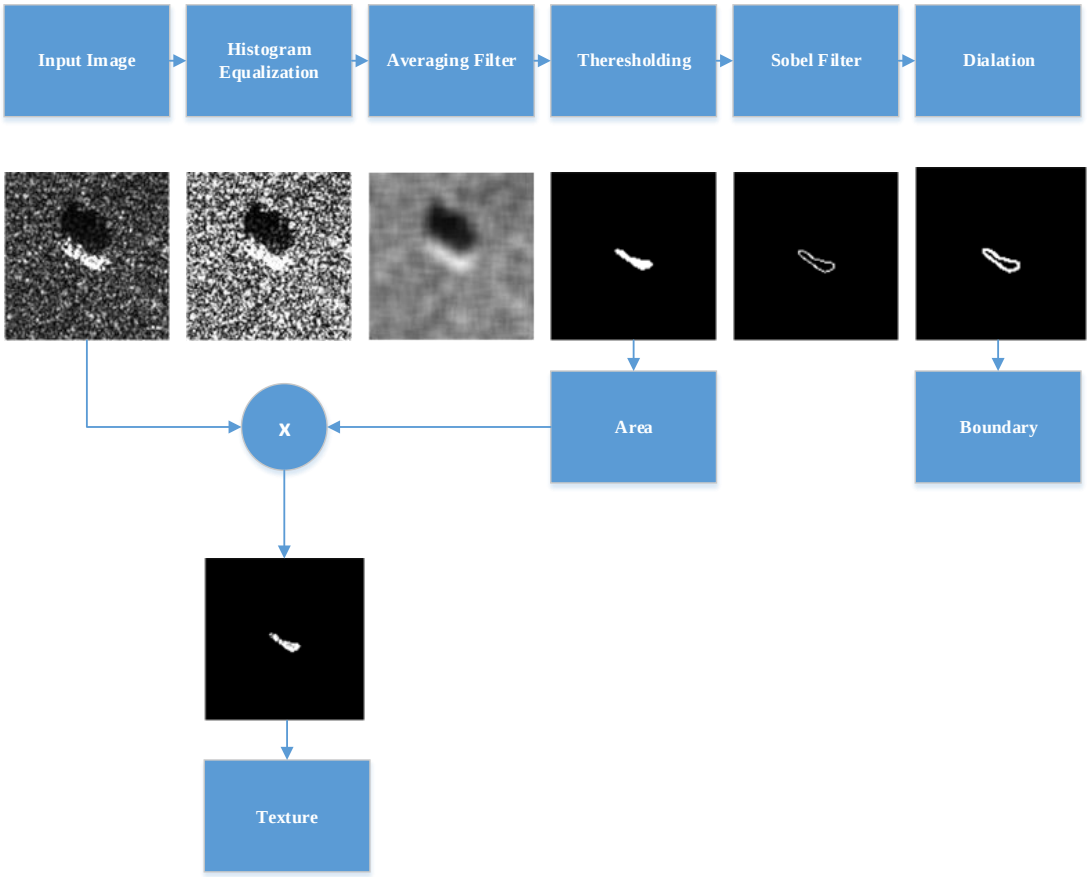

Figure 8.2: Preprocessing of target region

8.2.2 Feature extraction

Moments used to extract significant features from nine-regions (area, boundary and texture of the target, shadow and combined target-shadow) of SAR images. More details of Moments methods are provided in Chapter 4.

8.2.3 Feature fusion

As mentioned earlier, for each segmented image (area, boundary and texture for the target, shadow, and combined target-shadow) 100 features are extracted by utilising PZMs. By concatenating each segmentation technique, a feature fusion vector with 900 features is generated for each sample. This fused vector then is fed to different classifiers.

8.2.4 Ensemble of classifiers and majority voting

Five different classifiers are introduced for target recognition of SAR images. Support vector machine (SVM) with the Quadratic kernel, decision tree (DT), linear discriminant analysis (LDA), k- nearest neighbour (KNN) with *k=3* and random forest (RF) are used for evaluating accuracy. A 10-fold cross validation technique is applied in all experiments.

Finally, voting is applied among all five classifiers above for finding the output class label of each sample. Five different classifications rules *c1(x), c2(x), c3(x), c4(x)* and *c5(x)* are combined to produce a classifier that is superior to any individual classifier. Majority voting among five classifiers can be evaluated as:

$$C(X) = arg_i max \sum_{j=1}^{5} (c_j(X) = i) \quad (8.1)$$

where *X* is the test set, and *i* is the class label. In the case of having the same vote for two classes, a random selection is performed between these classes.

8.3 Experimental results and discussions

Each region (target, shadow, and combined target-shadow) includes three different segmentation parts as area, boundary and texture. Table 8.1 shows the accuracy of different segmented parts in the target regions only. For each segmented part, 100 features are extracted and the accuracy is calculated by five different classifiers. The texture of target region followed by SVM classifier has the highest accuracy.

The same approach is adopted for the shadow regions. Shadow regions are areas on the ground that are not covered by the radar signal; as a result, no return signal is

received, and these areas appear dark in the SAR images. As shown in Table 8.2, accuracies of shadow regions are less than those in the target region. However due to having high accuracies they can be considered as one part of target recognition.

Table 8.1: Accuracy (%) by different classifier (target region)

Classifier	Texture	Boundary	Area
SVM	**96.2**	**95.7**	**95.5**
LDA	91.9	90.8	92.1
KNN	95.6	94.0	95.0
DT	86.9	89.2	87.5
RF	92.1	93.4	93.4

In Table 8.3, we evaluate the recognition rate of combined target-shadow regions of different segmented parts. The results show improvements drastically on each classifier and each individual segmented part. Further improvements are achieved by applying majority voting for each part. In the final consideration, we fused all features by concatenation of target (area, boundary and texture), shadow (area, boundary and texture) and combined target-shadow (area, boundary and texture) regions to form a vector with 900 features. Experimental results indicate that fusion slightly improves the recognition rate. As it is shown in Table 8.4, after applying majority voting on the classifiers using fused feature vectors, the performance reflected by the accuracy hits to the highest level of 99.5%.

Table 8.2: Accuracy (%) by different classifier (shadow region)

Classifier	Texture	Boundary	Area
SVM	**85.5**	**91.7**	90.4
LDA	78.3	78.9	76.2
KNN	83.6	88.3	86.0
DT	72.5	72.2	74.3
RF	79.5	85.5	85.2

Table 8.3: Accuracy (%) by different classifiers (combined target-shadow region)

Classifier	Texture	Boundary	Area
SVM	**97.8**	**97.9**	**97.9**
LDA	94.1	95.1	94.2
KNN	96.5	96.8	97.1
DT	86.0	89.0	86.6
RF	93.8	96.3	95.2
MV	98.2	98.4	98.1

Table 8.4: Accuracy (%) -Ensembles of classifiers

Method	All (900 Features)
SVM	99.2
LDA	96.7
KNN	95.0
DT	86.8
RF	96.2
MV (Ensemble of five classifiers)	**99.5**

In the final setup, we used 10-class database. We only used texture of target, shadow and combined target shadow. In this regard, for each region 100 features are extracted. The features of each individual ROI are fed to different classifiers as it is shown in Table 8.5. Experimental result shows that the highest performance achieved by feature fusion followed by SVM classifier and the recognition rate reaches to 98.52%. Further improvement is achieved by feature fusion followed by majority voting among classifiers and is reached to 99.25% in the accuracy.

Table 8.5: Accuracy (%) by different classifiers in 10-class problem

Region	KNN	DT	SVM	RF	LDA
Target	84.65	79.71	91.85	74.11	82.31
Target-Shadow	82.96	74.05	87.69	70.15	76.99
Shadow	87.27	78.51	90.22	72.69	74.09
Feature level fusion	96.33	89.47	98.52	89.29	93.86
Feature level fusion+ MV	99.25				

Table 8.6 shows the comparison of the performance of the proposed technique with other techniques in the literature. Linear discriminant analysis (LDA), principle component analysis (PCA) and independent component analysis (ICA) are a rotational variant, and therefore the recognition rate is poor, even though all methods are fused. Temple matching requires huge amounts of data to be analysed. A better choice of feature extraction technique is the moment enforced by fusion. In [32] radial harmonic Fourier moment (RHFM) followed by local binary pattern (LBP), Haar wavelet transform (HWT), radon transform (RT), PCA and SVM and in [27] radial Chebyshev moment (RCM) followed by fusion techniques are successfully applied. However, the proposed method outperforms all other techniques in the literature.

Table 8.6: Comparison of proposed method with other techniques

Method	Accuracy (%)
LDA [53]	87.4
ZM [30]	89.4
Template Matching [31]	90.4
PCA+LDA+ICA [41]	90.6
MINACE [124]	90.6
PCA [53]	93.3
Seven EFS Coefficient [41]	93.5
QP normalized Image [28]	94.1
RHFM+LBP+HWT+RT+PCA+SVM [32]	98.1
RCM + Feature Fusion [27]	98.7
Proposed Method (in 3-class)	**99.5**
Proposed Method (in 10-class)	**99.25**

8.4 Comparison of all proposed methods

In this section, we compare all four proposed methods. Table 8.7 shows the accuracy of each proposed method. In the first proposed method, in 3-class problem and 10-class problem, for each SAR image, 9 region of interests are extracted as: area of target (TA), boundary of target (TB), texture of target (TT), area of shadow (SA), boundary of shadow (SB), texture of shadow (ST), area of target-shadow (TSA), boundary of target-shadow (TSB) and texture of target-shadow (TST). For each ROI, 100 features are extracted using RCM to form a feature vector with 900. The same approach is performed for proposed method # 4, except that instead of using RCM we applied PZM. In addition, we evaluate the output class label of each sample by majority voting among five different classifiers as SVM, DT, RF, LDA and k-NN. Both proposed methods are superior to other two proposed methods because of two reasons. Firstly, shadow regions are involved for the feature extraction that increase the useful information of each SAR image. Secondary different ROIs are introduced. Each ROI carries specific information. For example TB emphasize on the boundary of target. Extracting features form each ROI and combining them side by side, form a single

feature vector, that has the most informative and useful information that is superior to proposed method #2 and proposed method #3 in which only a single ROI is used. Also propose method # 4 is superior to proposed method #1 mainly because we adopted 5 different classifiers. Arguing that the accuracy of each method may considered to be biased depending on one classifier, we consider the majority voting among classifiers, in which the class label of each sample is the one with highest vote among these 5 classifiers. Majority voting helps to improve the accuracy while avoiding redundancies. It is also reduced the dependency from one classifier which in turns may lead to a biased decision. Experimentally we also see that the accuracy of proposed method # 4 is superior to others both in 3-class and 10-class problems. However, in proposed method #2 and propose method #3, although the accuracy is less than other proposed methods, we only considered one ROI which is TT. For this ROI, 12 moment methods are used to extract the features as Legendre Moments (LM), Chebyshev Moments of first kind (CM #1), Chebyshev Moments of second kind (CM #2),Jacobi Moments (JM), Gegenbauer Moments (GM), Krawtchouk Moments (KM), Zernike Moments (ZM), Pseudo Zernike Moments (PZM), Fourier Merlin Moments (FMM), Chebyshev Fourier Moments (CFM), Radial Harmonic Fourier Moments (RHFM) and Radial Chebyshev Moments (RCM). The aim of introducing many moment methods was to improve the target recognition performance. For each moment, 100 features is then extracted. If we fuse all methods, then we would have a single feature vectors with 1200 features. However having many features arise the redundancy between correlated features. In order to overcome this problem we introduce 2 unique techniques to increase the recognition performance and class separability and decreases the dimensionality of features by ranking. In proposed method #2 we calculate the class separability of each moment method based on Fisher Criterion (FC),

and moments with highest class separability are selected. We found that if we select the first 6 moments with highest class separability, the accuracy would be maximised in the training set. Therefore selection is perform by choosing 600 features (100 feature for each selected moment). The accuracy is improved over a single ROI. Consider only TT of RCM and TT of PZM, the accuracy over test set was 93.21% and 90.12% respectively in 3-class problem as shown in Table 6.4. Selection and fusion of most separable moments based on FC increases the accuracy up to 95.71%. Further improvement was achieved by introducing the novel approach based on Entropy Score. In this proposed method, instead of limit ourselves with selecting the most separable moments and the fusing all features associated with selected moments, for each feature we select more informative moment based on entropy score. Since each feature has a specific characteristic, then for each feature the moments with highest-class separation would be selected and in this regard, we expected the accuracy to be improved. Experimentally we justify that the accuracy is improved since we selected more dominant features rather than selecting all features associated with a specific moment. In addition, we observe that only 500 features are used to improve the accuracy up to 96.12% in 3-class problem. The same approach is done for 10- class problem.

Table 8.7: Summary of all proposed methods

Method	Number of features	Number of classes	Accuracy (%)
Target Recognition In SAR Images Using Radial Chebyshev Moments (proposed method #1)	900	3	98.69
		10	96.63
Improved SAR Target Recognition Using Fisher Criterion And Data Fusion (proposed method #2)	600	3	95.71
		10	91.08
Entropy Score Based Feature Selection For Moment Based SAR Image Classification (proposed method #3)	500	3	96.12
		10	92.88
Ensemble Of Classifiers For Improved SAR Image Recognition (proposed method #4)	**900**	**3**	**99.50**
		10	**99.4**

8.5 Computational complexities of proposed methods

One aim of adopting moments is to decrease the computational complexity. We observed that by extracting only few moments, we achieved an acceptable accuracy. In Chapter 5 for example, by extracting only 34 features using ZM, the accuracy reaches to 89.25%. However, there is tradeoff between accuracy and computational cost. Since in SAR-ATR high recognition rate is the most important factor, in all proposed methods we had to increase the computational cost to improve the recognition rate. In Chapter 5 and Chapter 8, extracting 9 ROIs caused the computational cost to be increased, but the accuracy of extracted regions improved up to 98.69%. Ensemble of classifiers after feature level fusion in Chapter 8 further are increased the complexity, however the accuracy improved to 99.55%. In Chapter 6 and Chapter 7 complexity increased by applying 12 different moment methods to improve the target recognition performance, further increasing of computational complexity is due to introduce two ranking methods for reducing dimensionality as FC

and Entropy Score. While the cost of computation arises, the accuracies of aforementioned proposed method also improved to 95.71% and 96.12% respectively. In summary at some stage for improving the performance, we increase the computational cost, but still the computational cost of all proposed methods are comparable with those mentioned in Table 2.1.

8.6 Conclusion

In this chapter, first, we segmented both target and shadow regions of SAR images by using preprocessing approaches. For each region, we defined different segmentation parts. Then we extracted all segmented parts in the target, shadow and combined target-shadow regions by utilising Pseudo Zernike Moments. All segmented parts are combined with each other to form a fusion vector. Experimental results show an improvement in accuracy by using fusion techniques in respect of different classifiers. Furthermore, even higher accuracy is achieved using majority voting after obtaining the class labels from five classifiers on each sample. Experimentally it is proved that the ensemble of classifiers using majority voting increases the accuracy. Finally, overall accuracy has the highest performance when feature fusion followed by majority voting is applied and it reaches to 99.5%. This result means a 3.3% improvement over the standard approach with texture segmentation only, which is 96.2% for three-class problem. In addition, we used ten-class problem in which the accuracy improved up to 99.25%.

Chapter 9

CONCLUSIONS AND FUTURE WORK

The aim of this thesis is to introduce novel approaches for feature extraction and features selection to improve the recognition rate while utilising fewer numbers of features.

9.1 Conclusion

We developed a feature extraction algorithm using RCM and compared with the commonly used method in the literature as ZM. RCM is a discrete orthogonal moment that reduces numerical errors and computational complexity due to normalisation in ZM. Additionally, we considered shadow regions as part of feature extraction parallel to target information, and then we applied feature fusion technique based on a different image segmentation process: area, boundary and texture. These approaches together improved the total accuracy by 8%.

We used different method of moments in Cartesian and polar coordinates to extract features to be used for classification. Fisher Criterion is used to rank the performances of each moment. Moments in polar coordinates have better feature representation capabilities with rotation scale and translational invariance. Then we defined two fusion techniques as feature level fusion and decision fusion. Fusion technique used to help the classifier to improve the classification performance and decrease the false alarm.

We applied entropy based feature selection for improvement of classification performance in target recognition for SAR images. Different moments including LM, CM #1, CM #2, GM, JM, KM, ZM, PZM, CFM, FMM, RHFM and RCM are used to benefit from the diversities introduced by different moments. The results obtained by entropy score feature selection approach outperforms the state-of-the-art alternative techniques in the literature.

We also segmented both target and shadow regions of SAR images by using preprocessing approaches. For each region, we defined different segmentation parts. Then we extracted all segmented parts in the target, shadow and combined target-shadow regions by utilising PZM. All extracted parts are combined with each other to form a fusion vector. Higher accuracy is achieved using majority voting after obtaining the class labels from five classifiers on each sample. Experimentally it is approved that the ensemble of classifiers using majority voting increases the accuracy. Finally, the overall accuracy has the highest performance when feature fusion followed by majority voting is applied and reaching to 99.5%.

9.2 Future work

Recently, application of SAR images that involved three-dimensional images of objects are increased drastically and the feature extraction is the challenging problem. One technique is to adopt and develop the moments for extracting features from three-dimensional SAR images.

Many techniques such as genetic algorithms [136] and random forest [137] are successfully adopted in many applications such as Alzheimer or cancer detection for feature selection . As a future work, these algorithms can be used for effective selection

of features in SAR images. Finally, in the classification stage, deep learning algorithms [139] achieve high performance in classification in many applications and many researchers address to use deep learning as a classifier in higher dimensional space rather than traditional classifiers such as SVM.

REFERENCES

[1] Siegert, F., & Hoffmann, A. A . (2000). The 1998 forest fires in East Kalimantan (Indonesia): A quantitative evaluation using high resolution, multitemporal ERS-2 SAR images and NOAA-AVHRR hotspot data. *Remote Sensing of Environment, 72(1), 64-77.*

[2] Cohen, J., Riihimäki, H., Pulliainen, J., Lemmetyinen, J., & Heilimo, J. (2016). Implications of boreal forest stand characteristics for X-band SAR flood mapping accuracy. *Remote Sensing of Environment*, 186, 47-63.

[3] Chini, M., Pierdicca, N., & Emery, W. J. (2009). Exploiting SAR and VHR optical images to quantify damage caused by the 2003 Bam earthquake. *IEEE Transactions on Geoscience and Remote Sensing*, 47(1), 145-152.

[4] Wang, S., Wang, M., Yang, S., & Jiao, L. (2017). New hierarchical saliency filtering for fast ship detection in high-resolution SAR images. *IEEE Transactions on Geoscience and Remote Sensing*, 55(1), 351-362.

[5] Fustes, D., Cantorna, D., Dafonte, C., Arcay, B., Iglesias, A., & Manteiga, M. (2014). A cloud-integrated web platform for marine monitoring using GIS and remote sensing. Application to oil spill detection through SAR images. *Future Generation Computer Systems*, 34, 155-160.

[6] Erten, E., Lopez-Sanchez, J. M., Yuzugullu, O., & Hajnsek, I. (2016). Retrieval of agricultural crop height from space: A comparison of SAR techniques. *Remote Sensing of Environment*, 187, 130-144.

[7] Baranoski, E. J. (2008). Through-wall imaging: Historical perspective and future directions. *Journal of the Franklin Institute*, 345(6), 556-569

[8] Uğur, S., & Arıkan, O. (2012). SAR image reconstruction and autofocus by compressed sensing. *Digital Signal Processing*, 22(6), 923-932.

[9] Sensor Data Management System (SDMS) Public website. (2017, June 22). Retrieved from https://www.sdms.afrl.af.mil.

[10] Slide share (2017, September 17). Retrieved from https://www.slideshare.net/Forward2025/radar-2009-a-18-synthetic-aperture-radar

[11] Nicoli, L. P. (2007). Automatic Target Recognition of Synthetic Aperture Radar Images Using Elliptical Fourier Desciptors (*Doctoral dissertation*, *Florida Institute of Technology).*

[12] Hosny, K. M. (2007). Exact Legendre moment computation for gray level images. *Pattern Recognition*, 40(12), 3597-3605.

[13] Hosny, K. M. (2011). Image representation using accurate orthogonal Gegenbauer moments. *Pattern Recognition Letters*, 32(6), 795-804.

[14] Yap, P. T., & Paramesran, R. (2004, November). Jacobi moments as image features. In TENCON 2004. 2004 *IEEE Region 10 Conference* (pp. 594-597). IEEE.

[15] Yap, P. T., Paramesran, R., & Ong, S. H. (2003). Image analysis by Krawtchouk moments. *IEEE Transactions on image processing*, 12(11), 1367-1377.

[16] Zhu, H., Shu, H., Liang, J., Luo, L., & Coatrieux, J. L. (2007). Image analysis by discrete orthogonal Racah moments. *Signal Processing*, 87(4), 687-708.

[17] Sayyouri, M., Hmimid, A., & Qjidaa, H. (2015). A fast computation of novel set of Meixner invariant moments for image analysis. *Circuits, Systems, and Signal*

[18] See, K. W., Loke, K. S., Lee, P. A., & Loe, K. F. (2007). Image reconstruction using various discrete orthogonal polynomials in comparison with DCT. *Applied Mathematics and Computation*, 193(2), 346-359.

[19] Yap, P. T., Paramesran, R., & Ong, S. H. (2007). Image analysis using Hahn moments. *IEEE transactions on pattern analysis and machine intelligence*, 29(11).

[20] Flusser, J., Zitova, B., & Suk, T. (2009). Moments and moment invariants in pattern recognition. John Wiley & Sons.

[21] Khotanzad, A., & Hong, Y. H. (1990). Invariant image recognition by Zernike moments. *IEEE Transactions on pattern analysis and machine intelligence*, 12(5), 489-497.

[22] Singh, C., & Upneja, R. (2014). Accurate calculation of high order pseudo-Zernike moments and their numerical stability. *Digital Signal Processing*, 27, 95-106.

[23] Singh, C., & Ranade, S. K. (2013). A high capacity image adaptive watermarking scheme with radial harmonic Fourier moments. *Digital signal processing*, 23(5), 1470-1482.

[24] Zhu, H., Yang, Y., Gui, Z., Zhu, Y., & Chen, Z. (2016). Image analysis by generalized Chebyshev–Fourier and generalized pseudo-Jacobi–Fourier moments. *Pattern Recognition*, 51, 1-11.

[25] Sheng, Y., & Shen, L. (1994). Orthogonal Fourier–Mellin moments for invariant *pattern recognition*. JOSA A, 11(6), 1748-1757.

[26] Ping, Z., Ren, H., Zou, J., Sheng, Y., & Bo, W. (2007). Generic orthogonal moments: Jacobi–Fourier moments for invariant image description. Pattern Recognition, 40(4), 1245-1254.

[27] Bolourchi, P., Demirel, H., & Uysal, S. (2017). Target recognition in SAR images using radial Chebyshev moments. *Signal, Image and Video Processing*, 11(6), 1033-1040.

[28] Amoon, M., & Rezai-Rad, G. A. (2013). Automatic target recognition of synthetic aperture radar (SAR) images based on optimal selection of Zernike moments features. *IET Computer Vision*, 8(2), 77-85.

[29] Clemente, C., Pallotta, L., Gaglione, D., De Maio, A., & Soraghan, J. J. (2017). Automatic Target Recognition of Military Vehicles With Krawtchouk Moments. *IEEE Transactions on Aerospace and Electronic Systems*, 53(1), 493-500.

[30] Bolourchi, P., Demirel, H., & Uysal, S. (2016, November). Continuous Moment-Based Features for Classification of Ground Vehicle SAR Images. *In Modelling Symposium (EMS)*, 2016, European (pp. 53-57). IEEE.

[31] Zhao, Q., & Principe, J. C. (2001). Support vector machines for SAR automatic target recognition. *IEEE Transactions on Aerospace and Electronic Systems*, 37(2), 643-654.

[32] Bolourchi, P., Moradi, M., Demirel, H., & Uysal, S. (2017, April). Feature Fusion for Classification Enhancement of Ground Vehicle SAR Images. *UKSim-AMSS 19th International Conference on Modelling & Simulation.* European (pp. 111-115). IEEE.

[33] Srinivas, U., Monga, V., & Raj, R. G. (2014). SAR automatic target recognition using discriminative graphical models. *IEEE transactions on aerospace and electronic systems*, 50(1), 591-606.

[34] Dong, G., Kuang, G., Wang, N., Zhao, L., & Lu, J. (2015). SAR target recognition via joint sparse representation of monogenic signal. IEEE Journal of Selected Topics in Applied Earth Observations and Remote Sensing, 8(7), 3316-3328.

[35] Mahalanobis, A., Carlson, D. W., & Kumar, B. V. (1998). Evaluation of MACH and DCCF correlation filters for SAR ATR using MSTAR public data base. *Algorithms for Synthetic Aperture Radar Imagery, 3370*, 460-468.

[36] Singh, R., & Kumar, V. (2002, August). Performance of the extended maximum average correlation height(EMACH) filter and the polynomial distance classifier correlation filter(PDCCF) for multiclass SAR detection and classification. *In Proceedings of SPIE*, 4727, 265-276.

[37] Patnaik, R., & Casasent, D. (2005, March). MINACE filter classification algorithms for ATR using MSTAR data. *In Proc. SPIE* 5807, pp. 100-111.

[38] DeVore, M. D., & O'Sullivan, J. A. (2002). A performance-complexity study of several approaches to automatic target recognition from synthetic aperture radar images. *IEEE Transactions on Aerospace and Electronic Systems*.

[39] Kaplan, L. M. (2001). Analysis of multiplicative speckle models for template-based SAR ATR. *IEEE Transactions on Aerospace and Electronic Systems*, 37(4), 1424-1432.

[40] DeVore, M. D., & O'Sullivan, J. A. (2004). Quantitative statistical assessment of conditional models for synthetic aperture radar. *IEEE Transactions on Image Processing*, 13(2), 113-125.

[41] Yuan, X., Tang, T., Xiang, D., Li, Y., & Su, Y. (2014). Target recognition in SAR imagery based on local gradient ratio pattern. *International journal of remote sensing*, 35(3), 857-870.

[42] Song, S., Xu, B., & Yang, J. (2016). SAR target recognition via supervised discriminative dictionary learning and sparse representation of the SAR-HOG feature. *Remote Sensing*, 8(8), 683.

[43] Anagnostopoulos, G. C. (2009). SVM-based target recognition from synthetic aperture radar images using target region outline descriptors. *Nonlinear Analysis: Theory, Methods & Applications*, 71(12), 2934-2939.

[44] Yang, Y., Qiu, Y., & Lu, C. (2005, May). Automatic target classification—experiments on the MSTAR SAR images. *In Software Engineering, Artificial Intelligence, Networking and Parallel/Distributed Computing, 2005 and First ACIS International Workshop on Self-Assembling Wireless Networks. SNPD/SAWN 2005. Sixth International Conference on (pp. 2-7). IEEE.*

[45] Saghri, J. A., & Guilas, C. (2005). Hausdorff probabilistic feature analysis in SAR image recognition. *In Proc. of SPIE* Vol (Vol. 5909, pp. 590903-1).

[46] Pink, T. H., & Ramanathan, U. (2000). Intelligent selection of useful features for optimal feature-based classification. *In Geoscience and Remote Sensing Symposium, 2000. Proceedings. IGARSS 2000. IEEE 2000 International* (Vol. 7, pp. 3012-3014). IEEE.

[47] Mishra, A. K. (2008, November). Validation of PCA and LDA for SAR ATR. *In TENCON 2008-2008 IEEE Region 10 Conference* (pp. 1-6). IEEE.

[48] Maokuan, L., Jian, G., Hui, D., & Xin, G. (2006, October). SAR ATR based on support vector machines and independent component analysis. *In Radar, 2006. CIE'06. International Conference on* (pp. 1-3). IEEE.

[49] Cui, Z., Cao, Z., Yang, J., Feng, J., & Ren, H. (2015). Target recognition in synthetic aperture radar images via non-negative matrix factorisation. *IET Radar, Sonar & Navigation*, 9(9), 1376-1385.

[50] Han, P., Wu, R., Wang, Y., & Wang, Z. (2003, April). An efficient SAR ATR approach. *In Acoustics, Speech, and Signal Processing, 2003. Proceedings.(ICASSP'03). 2003 IEEE International Conference* on (Vol. 2, pp. II-429). IEEE.

[51] Mishra, A. K., & Motaung, T. (2015). Application of linear and nonlinear PCA to SAR ATR. *In Radioelektronika (RADIOELEKTRONIKA), 2015 25th International Conference* (pp. 349-354). IEEE.

[52] Liu, M., Wu, Y., Zhang, P., Zhang, Q., Li, Y., & Li, M. (2013). SAR target configuration recognition using locality preserving property and Gaussian mixture distribution. *IEEE Geoscience and Remote Sensing Letters*, 10(2), 268-272.

[53] Wang, B., Huang, Y., Yang, J., & Wu, J. (2011). A feature extraction method for synthetic aperture radar (SAR) automatic target recognition based on maximum interclass distance. *Science China Technological Sciences*, 54(9), 2520-2524.

[54] Sophian, A., Tian, G. Y., Taylor, D., & Rudlin, J. (2003). A feature extraction technique based on principal component analysis for pulsed eddy current NDT. *NDT & e International*, 36(1), 37-41.

[55] Yang, F., Gao, W., Xu, B., & Yang, J. (2015). Multi-frequency polarimetric SAR classification based on Riemannian manifold and simultaneous sparse representation. *Remote Sensing*, 7(7), 8469-8488.

[56] Sun, X., Nasrabadi, N. M., & Tran, T. D. (2015). Task-driven dictionary learning for hyperspectral image classification with structured sparsity constraints. *IEEE Transactions on Geoscience and Remote Sensing*, 53(8), 4457-4471.

[57] Aharon, M., Elad, M., & Bruckstein, A. (2006). K-SVD: An algorithm for designing overcomplete dictionaries for sparse representation. *IEEE Transactions on signal processing*, *54*(11), 4311-4322.

[58] Mairal, J., Bach, F., Ponce, J., & Sapiro, G. (2009, June). Online dictionary learning for sparse coding. *In Proceedings of the 26th annual international conference on machine learning* (pp. 689-696). ACM.

[59] Gangeh, M. J., Farahat, A. K., Ghodsi, A., & Kamel, M. S. (2015). Supervised dictionary learning and sparse representation-a review. *arXiv preprint arXiv*:1502.05928.

[60] Bryant, M. L., & Garber, F. D. (1999, August). SVM classifier applied to the MSTAR public data-set. In AeroSense'99 (pp. 355-360). *International Society for Optics and Photonics.*

[61] Soh, L. K., & Tsatsoulis, C. (1999). Adaptive multiresolution quantization for contextual information gain in SAR sea ice images. *In Geoscience and Remote Sensing Symposium, 1999. IGARSS'99 Proceedings. IEEE 1999 International* (Vol. 3, pp. 1567-1569). IEEE.

[62] Schumacher, R., & Schiller, J. (2005, May). Non-cooperative target identification of battlefield targets-classification results based on SAR images. *In Radar Conference*, 2005 IEEE International (pp. 167-172). IEEE.

[63] Haker, S., Sapiro, G., & Tannenbaum, A. (2000). Knowledge-based segmentation of SAR data with learned priors. *IEEE Transactions on Image Processing,* 9(2), 299-301.

[64] Sun, Y., Liu, Z., Todorovic, S., & Li, J. (2007). Adaptive boosting for SAR automatic target recognition. *IEEE Transactions on Aerospace and Electronic Systems,* 43(1).

[65] Yang, M., Kpalma, K., & Ronsin, J. (2008). A survey of shape feature extraction techniques.

[66] Chang, Y. W., & Lin, C. J. (2008, December). Feature ranking using linear SVM. *In Causation and Prediction Challenge* (pp. 53-64).

[67] Duch, W., Wieczorek, T., Biesiada, J., & Blachnik, M. (2004, July). Comparison of feature ranking methods based on information entropy. *In Neural Networks, 2004. Proceedings. 2004 IEEE International Joint Conference on* (Vol. 2, pp. 1415-1419). IEEE.

[68] Geng, X., Liu, T. Y., Qin, T., & Li, H. (2007, July). Feature selection for ranking. *In Proceedings of the 30th annual international ACM SIGIR conference on Research and development in information retrieval* (pp. 407-414). ACM.

[69] Pohjalainen, J., Räsänen, O., & Kadioglu, S. (2015). Feature selection methods and their combinations in high-dimensional classification of speaker likability, intelligibility and personality traits. *Computer Speech & Language*, 29(1), 145-171.

[70] Yan, W. (2007, July). Fusion in multi-criterion feature ranking. *In Information Fusion, 2007 10th International Conference on* (pp. 1-6). IEEE.

[71] Prati, R. C. (2012, June). Combining feature ranking algorithms through rank aggregation. *In Neural Networks (IJCNN), The 2012 International Joint Conference on* (pp. 1-8). IEEE.

[72] Mangai, U. G., Samanta, S., Das, S., & Chowdhury, P. R. (2010). A survey of decision fusion and feature fusion strategies for pattern classification. *IET Technical review*, 27(4), 293-307.

[73] Dong-dong, G., Tang, T., Zhao, L., & Lu, J. (2015, July). A feature combining spatial and structural information for SAR image classification. *In Geoscience and Remote Sensing Symposium (IGARSS*), 2015 *IEEE International* (pp. 4396-4399). IEEE.

[74] Kim, S., Song, W. J., & Kim, S. H. (2016). Robust Ground Target Detection by SAR and IR Sensor Fusion Using Adaboost-Based Feature Selection. *Sensors*, 16(7), 1117.

[75] Narasimhamurthy, A. (2005). Theoretical bounds of majority voting performance for a binary classification problem. *IEEE Transactions on Pattern Analysis and Machine Intelligence*, 27(12), 1988-1995.

[76] Kittler, J., Hatef, M., Duin, R. P., & Matas, J. (1998). On combining classifiers. *IEEE transactions on pattern analysis and machine intelligence*, 20(3), 226-239.

[77] Amrani, M., Chaib, S., Omara, I., & Jiang, F. (2017, July). Bag-of-visual-words based feature extraction for SAR target classification. *In Ninth International Conference on Digital Image Processing (ICDIP 2017)* (pp. 104201J-104201J). International Society for Optics and Photonics.

[78] Guo, D., & Chen, B. (2017, May). SAR image target recognition via deep Bayesian generative network. *In Remote Sensing with Intelligent Processing* (RSIP), 2017 International Workshop on (pp. 1-4). IEEE.

[79] Arivazhagan, S., Priyadharshini, R. A., & Sangeetha, L. (2017). Automatic target recognition in SAR images using quaternion wavelet transform and principal component analysis. *International Journal of Computational Vision and Robotics*, 7(3), 314-334.

[80] Deng, S., Du, L., Li, C., Ding, J., & Liu, H. (2017). SAR Automatic Target Recognition Based on Euclidean Distance Restricted Autoencoder. *IEEE Journal of Selected Topics in Applied Earth Observations and Remote Sensing*.

[81] Zhang, R., & Zhang, M. (2017). SAR target recognition based on active contour without edges. *Journal of Systems Engineering and Electronics*, 28(2), 276-281.

[82] Osuna, E., Freund, R., & Girosi, F. (1997). Support vector machines: Training and applications.

[83] Perseus Documantation . (2017, July 30). Retrived from http://www.coxdocs.org/doku.php?id=perseus:user:activities:matrixprocessing:learning:classificationparameteroptimization

[84] Ding, B., Wen, G., Huang, X., Ma, C., & Yang, X. (2017). Data Augmentation by Multilevel Reconstruction Using Attributed Scattering Center for SAR Target Recognition. *IEEE Geoscience and Remote Sensing Letters*.

[85] Dong, G., & Kuang, G. (2016). SAR target recognition via sparse representation of monogenic signal on Grassmann manifolds. *IEEE Journal of Selected Topics in Applied Earth Observations and Remote Sensing*, 9(3), 1308-1319.

[86] Lin, C., Wang, B., Zhao, X., & Pang, M. (2013). Optimizing kernel PCA using sparse representation-based classifier for MSTAR SAR image target recognition. *Mathematical Problems in Engineering*, 2013.

[87] Yu, X., Li, Y., & Jiao, L. C. (2011, January). SAR automatic target recognition based on classifiers fusion. *In Multi-Platform/Multi-Sensor Remote Sensing and Mapping (M2RSM)*, 2011 International Workshop on (pp. 1-5). IEEE.

[88] Huang, X., Wang, J., Shang, J., Liao, C., & Liu, J. (2017). Application of polarization signature to land cover scattering mechanism analysis and classification using multi-temporal C-band polarimetric RADARSAT-2 imagery. *Remote Sensing of Environment*, 193, 11-28.

[89] Malik, C., & Malhotra, R. (2016). A Survey on Various Classification Methods for SAR Images. *Journal of Network Communications and Emerging Technologies (JNCET)* www. jncet. org, 6(5).

[90] A Complete Tutorial on Tree Based Modeling from Scratch (in R & Python). (2017, August 02). Retrived from https://www.analyticsvidhya.com/blog/2016/04/complete-tutorial-tree-based-modeling-scratch-in-python/

[91] How Decision Algorithems Works, (2017, August 02). Retrived from http://dataaspirant.com/2017/01/30/how-decision-tree-algorithm-works/

[92] Belgiu, M., & Drăguţ, L. (2016). Random forest in remote sensing: A review of applications and future directions. *ISPRS Journal of Photogrammetry and Remote Sensing*, 114, 24-31.

[93] Random Forest Template for TIBCO Spotfire (2017, August 02). Retrived from https://towardsdatascience.com/random-forest-learning-essential-understanding-1ca856a963cb

[94] Ding, B., Wen, G., Ye, F., Huang, X., & Yang, X. (2017, March). Feature extraction based on 2D compressive sensing for SAR automatic target recognition. *In Antennas and Propagation (EUCAP), 2017 11th European Conference on* (pp. 1219-1223). IEEE.

[95] Ding, B., Wen, G., Ma, C., & Yang, X. (2016). Decision fusion based on physically relevant features for SAR ATR. *IET Radar, Sonar & Navigation*, 11(4), 682-690.

[96] Du, C., Zhou, S., Sun, J., & Zhao, J. (2014). Feature extraction for SAR target recognition based on supervised manifold learning. *In IOP Conference Series: Earth and Environmental Science* (Vol. 17, No. 1, p. 012241). IOP Publishing.

[97] Farag, A. A., & Elhabian, S. Y. (2008). A Tutorial on Data Reduction Linear Discriminant Analysis (LDA). *University of Louisville*.

[98] Lei, B., van der Heijden, F., Xu, G., Feng, M., Zou, Y., de Ridder, D., & Tax, D. M. (2017). Classification, parameter estimation and state estimation: an engineering approach using MATLAB. John Wiley & Sons.

[99] Tahmasbi, A., Saki, F., & Shokouhi, S. B. (2011). Classification of benign and malignant masses based on Zernike moments. *Computers in biology and medicine,* 41(8), 726-735.

[100] ROC Curves in NCSS (2017, October 23). Retrived from https://ncss-wpengine.netdna-ssl.com/wp-content/uploads/2016/06/

[101] Liu, Q., Zhu, H., & Li, Q. (2011, December). Object recognition by combined invariants of orthogonal Fourier-Mellin moments. *In Information, Communications and Signal Processing (ICICS) 2011 8th International Conference on* (pp. 1-5). IEEE.

[102] Ying-Dong, Q., Cheng-Song, C., San-Ben, C., & Jin-Quan, L. (2005). A fast subpixel edge detection method using Sobel–Zernike moments operator. *Image and Vision Computing,* 23(1), 11-17.

[103] Zhang, J., & Tan, T. (2002). Brief review of invariant texture analysis methods. *Pattern recognition,* 35(3), 735-747.

[104] Mukundan, R. (2004). Some computational aspects of discrete orthonormal moments. *IEEE Transactions on Image Processing,* 13(8), 1055-1059.

[105] Hu, M. K. (1962). Visual pattern recognition by moment invariants. *IRE transactions on information theory*, 8(2), 179-187.

[106] Athilakshm, R., & Wahi, A. (2014). Improving Object Classification Using Zernike Moment, Radial Cheybyshev Moment Based on Square Transform Features: A Comparative Study. *World Applied Sciences Journal*, 32(7), 1226-1234.

[107] Mukundan, R., & Ramakrishnan, K. R. (1998). Moment functions in image analysis—*theory and applications.* World Scientific.

[108] Gao, G., Zhao, L., Zhang, J., Zhou, D., & Huang, J. (2008). A segmentation algorithm for SAR images based on the anisotropic heat diffusion equation. *Pattern Recognition*, 41(10), 3035-3043.

[109] Choi, H., & Baraniuk, R. G. (2001). Multiscale image segmentation using wavelet-domain hidden Markov models. *IEEE Transactions on Image Processing*, 10(9), 1309-1321.

[110] Lombardo, P., Sciotti, M., & Kaplan, L. M. (2001). SAR prescreening using both target and shadow information. *In Radar Conference, 2001. Proceedings of the 2001 IEEE* (pp. 147-152). IEEE.

[111] Liang, J., Wang, M., Chai, Z., & Wu, Q. (2014). Different lighting processing and feature extraction methods for efficient face recognition. *IET Image Processing*, 8(9), 528-538.

[112] Lu, J., Plataniotis, K. N., & Venetsanopoulos, A. N. (2003). Face recognition using LDA-based algorithms. *IEEE Transactions on Neural networks*, 14(1), 195-200.

[113] Rosipal, R., Girolami, M., Trejo, L. J., & Cichocki, A. (2001). Kernel PCA for feature extraction and de-noising in nonlinear regression. *Neural Computing & Applications*, 10(3), 231-243.

[114] Bartlett, M. S., Movellan, J. R., & Sejnowski, T. J. (2002). Face recognition by independent component analysis. *IEEE Transactions on neural networks*, 13(6), 1450-1464.

[115] Mukundan, R., Ong, S. H., & Lee, P. A. (2001). Image analysis by Tchebichef moments. *IEEE Transactions on image Processing*, 10(9), 1357-1364.

[116] Xiao, B., Ma, J. F., & Cui, J. T. (2012). Radial Tchebichef moment invariants for image recognition. *Journal of Visual Communication and Image Representation*, 23(2), 381-386.

[117] Xin, Y., Pawlak, M., & Liao, S. (2007). Accurate computation of Zernike moments in polar coordinates. *IEEE Transactions on Image Processing*, 16(2), 581-587.

[118] Hwang, S. K., & Kim, W. Y. (2006). A novel approach to the fast computation of Zernike moments. *Pattern Recognition*, 39(11), 2065-2076.

[119] Walia, E., Goyal, A., & Brar, Y. S. (2014). Zernike moments and LDP-weighted patches for content-based image retrieval. *Signal, Image and Video Processing*, *8*(3), 577-594

[120] A library for support vectorm machines. (2016, June 12). Retrived from https://www.csie.ntu.edu.tw/cjlin/libsvm

[121] PRTools a matlab toolbox for pattern recognition. (2016, June 12). Retrived from http://prtools.org

[122] Berry, M. W., & Castellanos, M. (2008). Survey of text mining II (Vol. 6). New York: *Springer*.

[123] Zhang, X., Liu, Z., Liu, S., Li, D., Jia, Y., & Huang, P. (2017). Sparse coding of 2D-slice Zernike moments for SAR ATR. *International Journal of Remote Sensing*, 38(2), 412-431.

[124] Patnaik, R., & Casasent, D. (2007, April). SAR classification and confuser and clutter rejection tests on MSTAR ten-class data using Minace filters. *In Proc. SPIE* (Vol. 6574, p. 657402).

[125] Shu, H., Luo, L., & Caatrieux, J. L. (2007). Moment-based approaches in imaging. Part 1, basic features. *IEEE Engineering in Medicine and Biology Magazine*, 26(5), 70-74

[126] Zhu, H., Shu, H., Xia, T., Luo, L., & Coatrieux, J. L. (2007). Translation and scale invariants of Tchebichef moments. *Pattern Recognition*, 40(9), 2530-2542.

[127] Flusser, J. (2000). On the independence of rotation moment invariants. *Pattern recognition*, 33(9), 1405-1410.

[128] Ping, Z., Wu, R., & Sheng, Y. (2002). Image description with Chebyshev–Fourier moments. *JOSA A*, 19(9), 1748-1754.

[129] Xia, T., Zhu, H., Shu, H., Haigron, P., & Luo, L. (2007). Image description with generalized pseudo-Zernike moments. *JOSA A*, 24(1), 50-59.

[130] Sheng, Y., & Shen, L. (1994). Orthogonal Fourier–Mellin moments for invariant pattern recognition. *JOSA A*, 11(6), 1748-1757.

[131] Ren, H., Ping, Z., Bo, W., Wu, W., & Sheng, Y. (2003). Multidistortion-invariant image recognition with radial harmonic Fourier moments. *JOSA A*, 20(4), 631-637.

[132] Devi, R., & Kumar, A. (2014, February). A region based SAR images classification using improved moment analysis (IMA*). In Optimization, Reliabilty, and Information Technology (ICROIT), 2014 International Conference on* (pp. 341-346). IEEE.

[133] Flusser, J., & Suk, T. (1993). Pattern recognition by affine moment invariants. *Pattern recognition*, 26(1), 167-174.

[134] Peng, X., Wang, Y., Hong, W., Tan, W., & Wu, Y. (2013). Autonomous navigation airborne forward-looking SAR high precision imaging with combination of pseudo-polar formatting and overlapped sub-aperture algorithm. *Remote Sensing*, 5(11), 6063-6078.

[135] Fahad, A., Tari, Z., Khalil, I., Almalawi, A., & Zomaya, A. Y. (2014). An optimal and stable feature selection approach for traffic classification based on multi-criterion fusion. *Future Generation Computer Systems*, 36, 156-169.

[136] Kharrat, A., Gasmi, K., Messaoud, M. B., Benamrane, N., & Abid, M. (2010). A hybrid approach for automatic classification of brain MRI using genetic algorithm and support vector machine. *Leonardo Journal of Sciences*, 17(1), 71-82.

[137] Menze, B. H., Kelm, B. M., Masuch, R., Himmelreich, U., Bachert, P., Petrich, W., & Hamprecht, F. A. (2009). A comparison of random forest and its Gini importance with standard chemometric methods for the feature selection and classification of spectral data. *BMC bioinformatics*, 10(1), 213.

[138] Hu, L., Liu, J., Liu, H., Chen, B., & Wu, S. (2007, November). Automatic target recognition based on SAR images and two-stage 2DPCA features. *In Synthetic Aperture Radar, 2007. APSAR 2007. 1st Asian and Pacific Conference on* (pp. 801-805). IEEE.

[139] Furukawa, H. (2017). Deep Learning for Target Classification from SAR Imagery: Data Augmentation and Translation Invariance. *arXiv preprint arXiv*:1708.07920.